EUROPEAN COMMISSION

Community research

Long-term Performance of Engineered Barrier Systems

PEBS

Long-term Performance of Engineered Barrier Systems PEBS

Engineered Barrier Emplacement Experiment in Opalinus Clay: "EB" Experiment

EDZ seismic results - seismic transmission measurements

(DELIVERABLE-N°: D2.1-6)

Contract (grant agreement) number: FP7 249681

Author:

Kristof Schuster

BGR, Germany

Date of issue of this report: 30/06/2014

Start date of project: 01/03/10 Duration : 48 Months

Project co-funded by the European Commission under the Seventh Euratom Framework Programme for Nuclear Research &Training Activities (2007-2011)		
Dissemination Level		
PU	Public	**PU**
RE	Restricted to a group specified by the partners of the [acronym] project	
CO	Confidential, only for partners of the [acronym] project	

EURATOM

Table of Contents

List of Figures

List of Tables

1 Introduction

The Engineered Barrier Emplacement Experiment in Opalinus Clay (EB) is a long running experiment which started in 2000 and was incorporated in 2010 into the PEBS Project (Long-term performance of Engineered Barrier Systems) and was finished beginning of 2013 with a full dismantling. In the run-up to the dismantling activities, planned for autumn and winter 2012, in August 2012 a seismic array which was installed in 2002 and was operated over 576 days (Schuster, 2004) was reactivated and seismic transmission measurements were resumed in order to characterize with the help of seismic parameters the evolution of the Opalinus Clay as well as the bentonite during the dismantling.

The history and some of the background information on both projects (EB and PEBS) was compiled already in the PEBS Deliverable D2.1-4 by Palacios et al. (2013, sections 1.1 and 1.2.1) and is resumed here and extended with the information concerning the geophysical and geotechnical activities which were at the responsibility of BGR.

1.1 The EB project

The Engineered Barrier Emplacement Experiment in Opalinus Clay (EB Experiment) aimed at demonstrating a new concept for the construction of HLW repositories in horizontal drifts, in competent clay formations. The principle of the new construction method was based on the combined use of a lower bed made of compacted bentonite blocks, and an upper buffer made of granular bentonite material (GBM). The project consisted on a real scale isothermal simulation of this construction method in the Opalinus Clay formation at the Mont Terri underground laboratory in Switzerland. A steel dummy canister, with the same dimensions and weight as the Spanish reference canister, was placed on top of a bed of bentonite blocks, and then the upper part of the drift was buffered with the GBM made of bentonite pellets (Figure 1.1). The drift was sealed with a concrete plug having a concrete retaining wall between the plug and the GBM. Since the end of the test installation the evolution of the different hydro-mechanical parameters were monitored, both in the barrier and the rock (especially in the Excavation Disturbed Zone (EDZ)). Relative humidity and temperature in the rock and in the bentonite buffer, rock and canister displacement, pore pressure and total pressure were registered by means of different types of sensors. Due to the short amount of free water available in this formation, an artificial hydration system was installed to accelerate the hydration process in the bentonite.

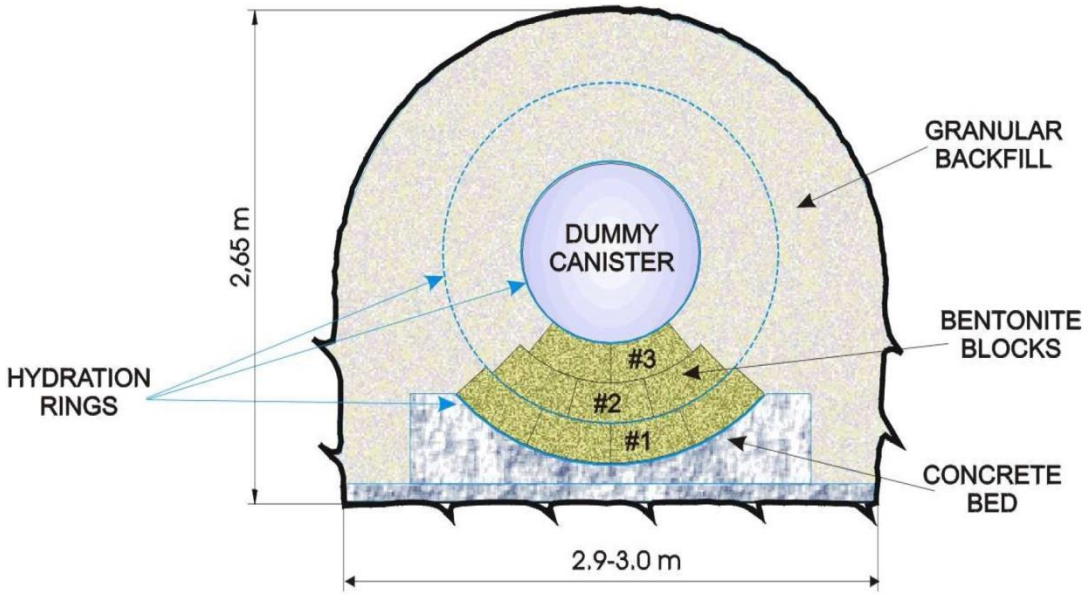

Fig. 1.1 EB experimental layout.

The basic objectives of the project were the following:

- Definition of backfill material (composition, grain size distribution ...). Demonstration of the manufacturing process at semi-industrial scale.
- Characterization of the hydro-mechanical properties of the backfill material.
- Design and demonstration of the emplacement and backfilling technique.
- Quality Assessment of the clay barrier in terms of the achieved geomechanical parameters (homogeneity, dry density, voids distribution ...) after emplacement.
- Characterization of the EDZ in the Opalinus Clay, and determination of its influence in the overall performance of the system.
- Investigation of the evolution of the hydro-mechanical parameters in the clay barrier and the EDZ as a function of the progress of the hydration process.
- Development of a hydro-mechanical model of the complete system adjusted and calibrated with the data resulting from the experiment.

After 10.5 years of operation, the experiment has been dismantled between the 19th of October 2012 and the 1st of February 2013. The main aim of this document is to describe the design and to present data, results and conclusions of the seismic long-term monitoring experiment started on the 12th of July 2012.

1.2 Background

1.2.1 Funding

The first phase of the EB experiment - years 2000 to 2003 - devoted to the test design, installation and start-up of the operation, was co-financed by the European Commission (contract nº FIKW-CT-2000-00017), under the framework of the research and training programme (Euratom) in the field of nuclear energy, and ENRESA (Spain). Besides ENRESA, BGR (Germany) and NAGRA (Switzerland) were the principal contractors and AITEMIN (Spain) and CIMNE (Spain) the assistant contractors.

Between 2003 and 2009 the project operation continued under the support of the Mont Terri Consortium, project 32.015: EB, phases 10 to 14.

From 2010, the experiment is part of the PEBS project, Work Package 2 Experimentation. The PEBS project is one of the “Small and Medium Projects” forming part of the FP7 Euratom programme. It is a multinational European research project that investigates processes affecting the engineered barrier performance of geological repositories for high-level waste disposal. The PEBS consortium consists of 17 leading nuclear research organizations, radioactive waste management agencies/implementing organizations, universities and companies.

1.2.2 Experimental sequence

After the preparation of the design document (Aitemin, 2001) and the components procurement, the installation of the experiment was carried out in several steps. The instrumentation was installed from November 2001 to February 2002: in-rock pore pressure sensors, rock displacement sensors and some rock relative humidity sensors, canister displacement sensors, relative humidity sensors in bentonite and total pressure cells. The artificial hydration system was installed in March 2002. The installation of the experiment was finished in April 2002, including the retaining wall, the concrete plug and the data acquisition system.

The artificial hydration of the bentonite started in May 2002 and ended in June 2007. There was an initial hydration phase with a significant amount of water injected (6,700 litres in two days) that was stopped after several water stains appeared on the wall. After that, the

hydration was restarted and from September 2002 to June 2007, there were different hydration phases with continuous water injection. The detailed record of effective water inflow for bentonite hydration is included in report SDR EB N19 (Aitemin, 2007).

After the end of the hydration phase, the monitoring of the experiment continued in order to follow the evolution of the bentonite.

The Engineered Barrier Emplacement Experiment is described in detail in the “EB Experiment Test Plan”, Project Deliverable 1, EC contract FIKW-CT2000-00017 (Aitemin, 2001), which includes the preliminary design, the emplacement and the operation.

BGR was in charge of performing at different stages of the EB experiment several geophysical and geotechnical oriented measurements for the characterization of the EBS, partly with subcontractors (TU Berlin, GMuG and Solexperts). For the initial characterization of the EB niche, immediately after the excavation, ultrasonic / seismic and geoelectrical measurements were performed in boreholes as well as along profiles (June 2001 – November 2001). After the closure of the niche (end of April 2002) and the start of the hydration phase (beginning of May 2002) a seismic long-term monitoring started (April 2002 – November 2003), including an acoustic emission experiment (April 2002 – April 2003). In November 2002 and one year later, in November 2003, geoelectrical measurements in the backfilled niche were conducted. The hydraulic characterization was executed in five stages between October 2001 and October 2003. These activities are documented in Schuster et al., 2004a. In August 2011, more than nine years after the closure, BGR drilled two horizontal pilot boreholes for the characterization of the bentonite. Geophysical measurements (geoelectrical and ultrasonic), sampling of bentonite at different depths and preparations for a hydro test were done in August 2011 (Schuster et al. 2014). In July 2012 the seismic long-term monitoring was resumed in order to monitor the expected changes in rock and bentonite parameters during the dismantling process in autumn and winter 2012 (this report). This monitoring is ongoing. For the same reason a geoelectrical circular profile was reactivated and was used for daily measurements between September 2012 and May 2013 (Furche and Schuster, 2014).

2 Seismic transmission measurements

The seismic transmission measurements, drafted as a seismic long-term monitoring experiment, aimed at the characterization of the evolution of the back fill material bentonite and the Opalinus Clay within the Engineered Barrier Emplacement Experiment (EB, Mayor et al., 2007). It is a follow-up experiment of a similar experiment which was performed between April 2002 and November 2003 (Schuster, 2004). Because the results of this first campaign were very promising it was decided to resume the seismic experiment several months before the planned dismantling. After several adaptions and tests the measurements could be resumed in July 2012 and measurements are still ongoing. For the new experiment most of the devices installed in 2002 could be reused. In the following we therefore distinguish between the old data and results (April 2002 - November 2003, phase 1) and the data gained since July 20012, including the recently achieved results (phase 2). The location of the EB Experiment is shown in Figure 2.1. Please note, that during phase 1 not all galleries in the Mont Terri Rock Laboratory existed.

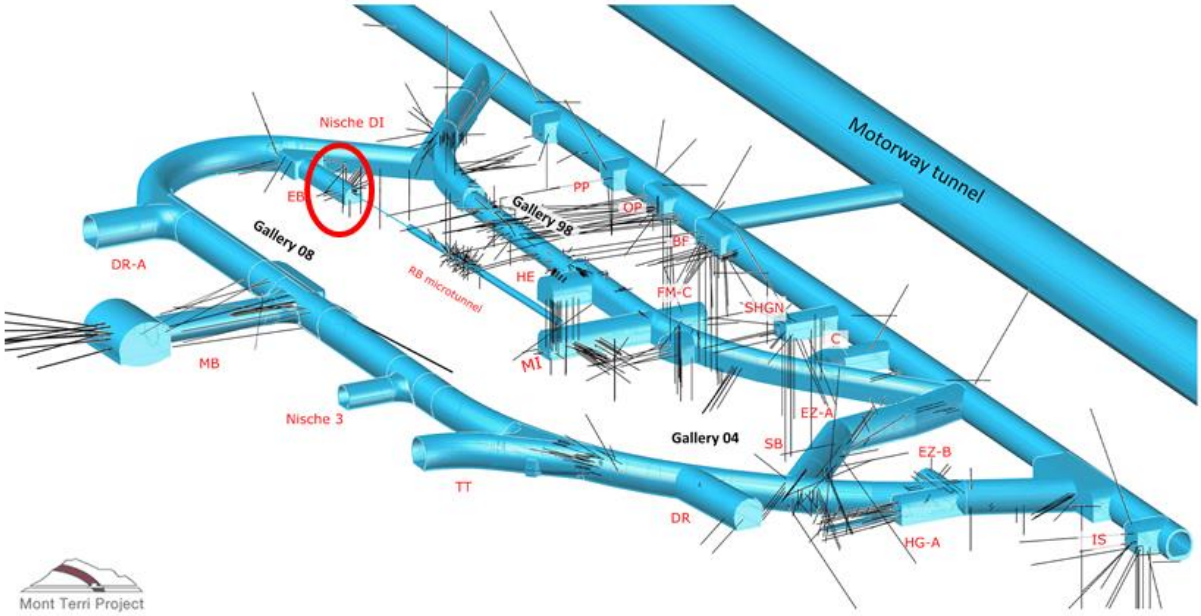

Fig. 2.1 Location of the EB-niche in the Mont Terri RL. The plan shows the situation in 2011.

2.1 Layout of the seismic transmission precursor experiment

The first seismic experiment (phase 1), including all seismic data and the major results, is described in detail by Schuster (2004). Because the new experiment (phase 2) uses the installation done in 2002 some of the most important facts from this report are repeated here. The 6 m long precisely excavated EB niche which was closed in 2002 with a 2.2 m thick concrete plug is shown schematically in Figure 2.2.

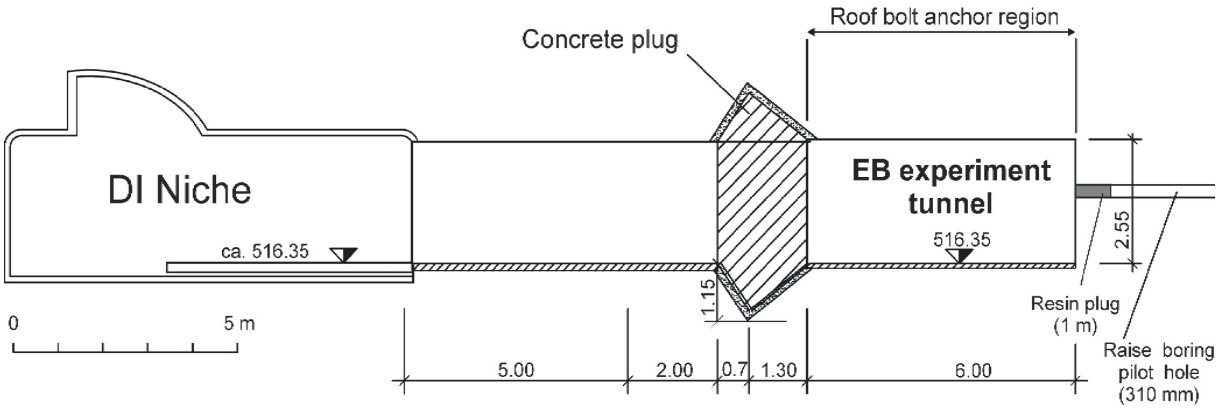

Fig. 2.2 EB niche in the Mont Terri RL (Mayor et al., 2007).

In Figure 2.3 the layout of the seismic array is presented. In total 24 piezoelectric transducers were used, 20 located in four two meter long boreholes and 4 transducers are located in the gap between the canister and the rock. The radially oriented boreholes are located on the eastern part of the EB niche wall, between 10 and 11:30 o'clock and the center of the array is approximately 3.5 m from the former entrance (later the back side of the concrete plug). Ten transducers serve as emitters and 14 as receivers. Unfortunately, the marks used in this and some other figures and the shortcuts used for the phase 2 data differ. The reason is changing from German to English from phase 1 to phase 2 data. Please note, the emitter transducers are marked in Figure 2.3 with S (German Sender, now English emitter (E)) and the receiver transducers are marked with E (German Empfänger, now English receiver (R)). Furthermore, already in phase 1 the receiver E12 was renamed to E06.

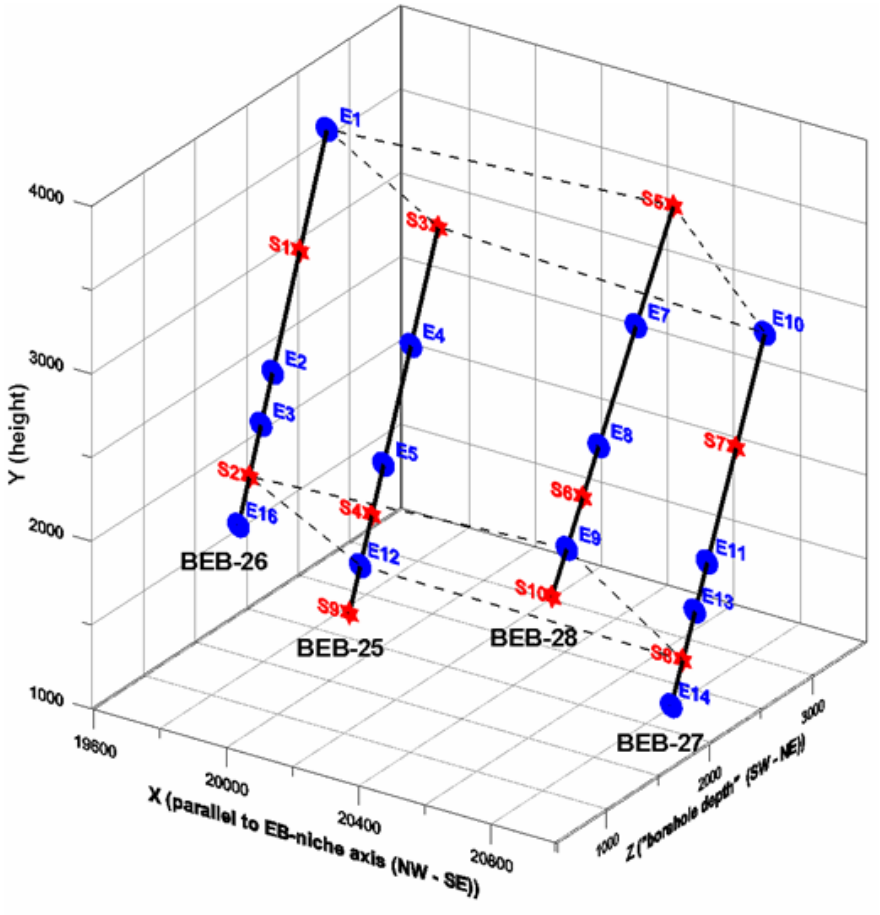

Fig. 2.3 Layout of the seismic array located in the EB niche. Transducers S9, S10, E14 and E16 located in the gap between canister and rock, 20 cm from the interface. Notation: emitters, red (S, German Sender), receivers, blue (E, German Empfänger).

Figure 2.4 shows the situation in the EB niche shortly before the closure. Two of the four piezoelectric transducers which are placed in the space between the canister and the rock are marked with red arrows. This region was later filled up with granular bentonite.

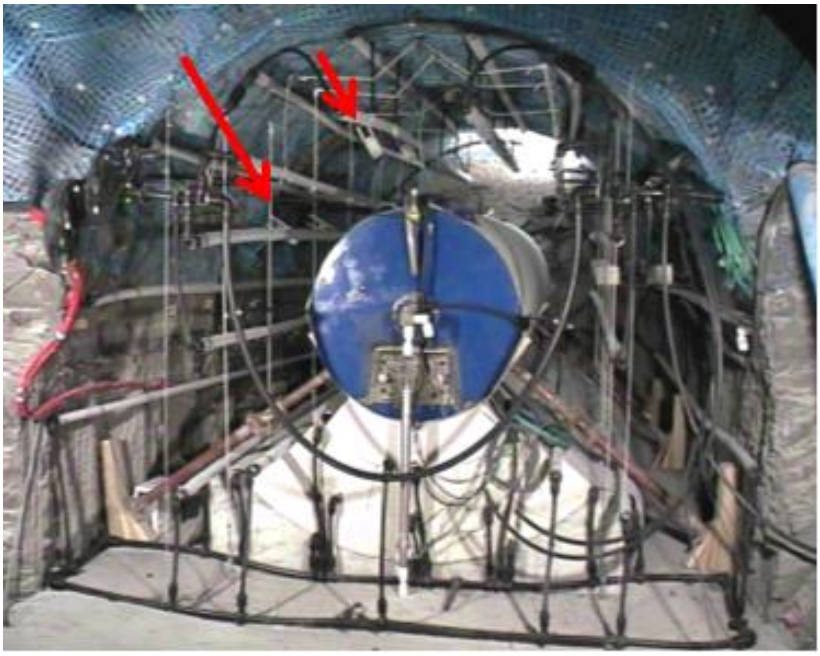

Fig. 2.4 EB niche in 2002 with emplaced dummy canister, hydration pipes and instrumentation cables. Two piezoelectric transducers marked with arrows.

More details of these four transducers are presented in Figure 2.5. The four piezoelectric transducers which are covered later by granular bentonite are placed 20 cm away from the Opalinus Clay, the later interface between the bentonite and the rock. The synthetic plastic plates at the same time indicate the location of the borehole mouths of the radially oriented boreholes.

Fig. 2.5 Details of the seismic instrumentation. Four transducers located in the later backfill.

2.2 Results from seismic transmission precursor experiments

Shortly after the excavation of the EB niche a geophysical characterization of the initial stage of the niche started in June 2001. The results from seismic measurements are compiled in Schuster (2002). One of the main results from these seismic investigations was a detailed analysis of the seismic in-situ anisotropy behavior of the Opalinus Clay with a high resolution mini sonic probe developed by BGR. Figure 2.6 shows a result from detailed cross hole measurements between two boreholes (BEB-B09 and BEB-B19) located at the eastern wall of the niche, at about 9:30 o'clock. The later installed seismic array for the long-term monitoring is located close by at the same side of the niche, but between 9:30 and 11 o'clock.

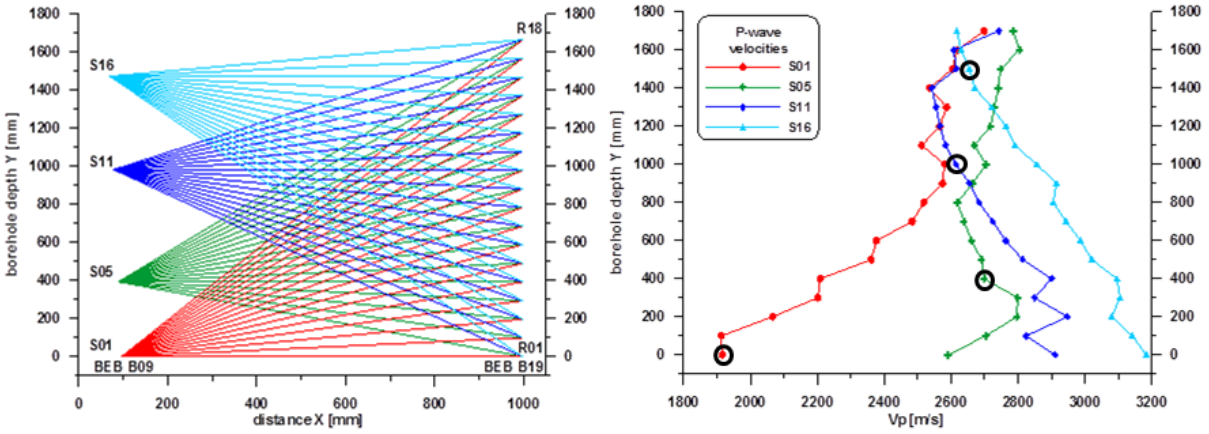

Fig. 2.6 Details of a seismic cross hole measurement between two sub horizontal boreholes at a distance of 1 m. Left: Ray paths from 4 emitter positions. Right: Derived v_p. Black circles indicate v_p derived from ray paths oriented 45° to the bedding and running parallel to the wall.

In Figure 2.6 exemplarily the derived P-wave velocities from 4 out of 16 emitter locations between 0 and 1.6 m borehole depth are selected. They already show the broad v_p variation. With black circles the v_p values marked which result from travel paths running parallel to the wall, an orientation which will be picked up in the later discussion of phase 2 data. It is astonishing that v_p at 40 cm is higher than for greater borehole depth, a fact that was seen even more pronounced in the interval velocity measurements performed in both boreholes. Figure 2.7 show results from two interval velocity measurements in borehole BEB-B09 performed in June and October 2001. For three emitter – receiver distances used in the mini sonic probe the apparent P-wave velocities are plotted (green: 10 cm, red: 20 cm, blue: 30 cm). Differences between the v_p point to the existence of a borehole wall disturbed zone.

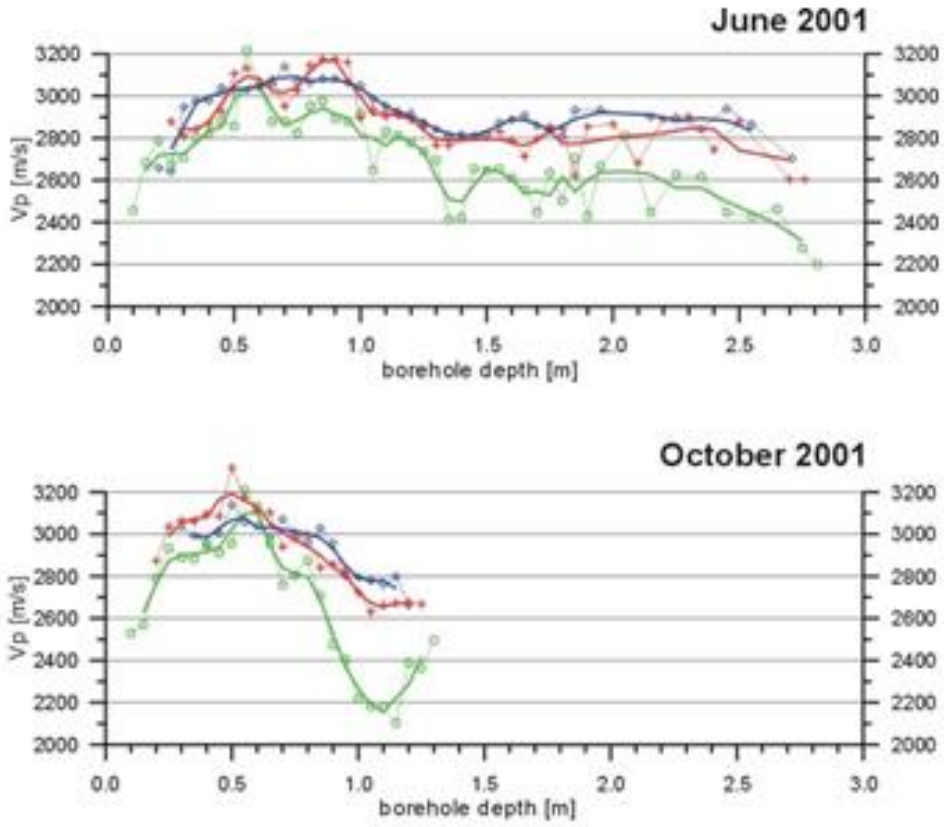

Fig. 2.7 Results from interval velocity measurements in borehole BEB-B09. Three apparent P-wave velocities, whereas the blue v_p is closest to the 'real' v_p.

The P-wave velocity derived from the greatest distance between emitter and receiver (30 cm) generally is closest to the 'real' velocity. The higher velocities between 0.4 m and 1 m could be explained with sandy layers and nodules found in drill cores.

Taking all emitter locations and also the reverse emitter-receiver combinations from the cross hole measurements into account, it results in 576 different ray paths. In Figure 2.8 all derived v_p are compiled. According to the indicated fit curve the seismic p-wave velocities vary at this location between 2600 m/s and 3100 m/s what originates basically from the orientation of the ray paths towards the bedding planes. This has to be taken into account for the later analyses. Velocities in the range between 1800 m/s and 2500 m/s result most probably from EDZ features.

As an overall result we can conclude that already in such a small part of the Opalinus Clay a very complex velocity distribution has to be taken into account. Because seismic parameters are closely linked to several rock mechanical parameters, for example Young's Modulus, it has to be regarded.

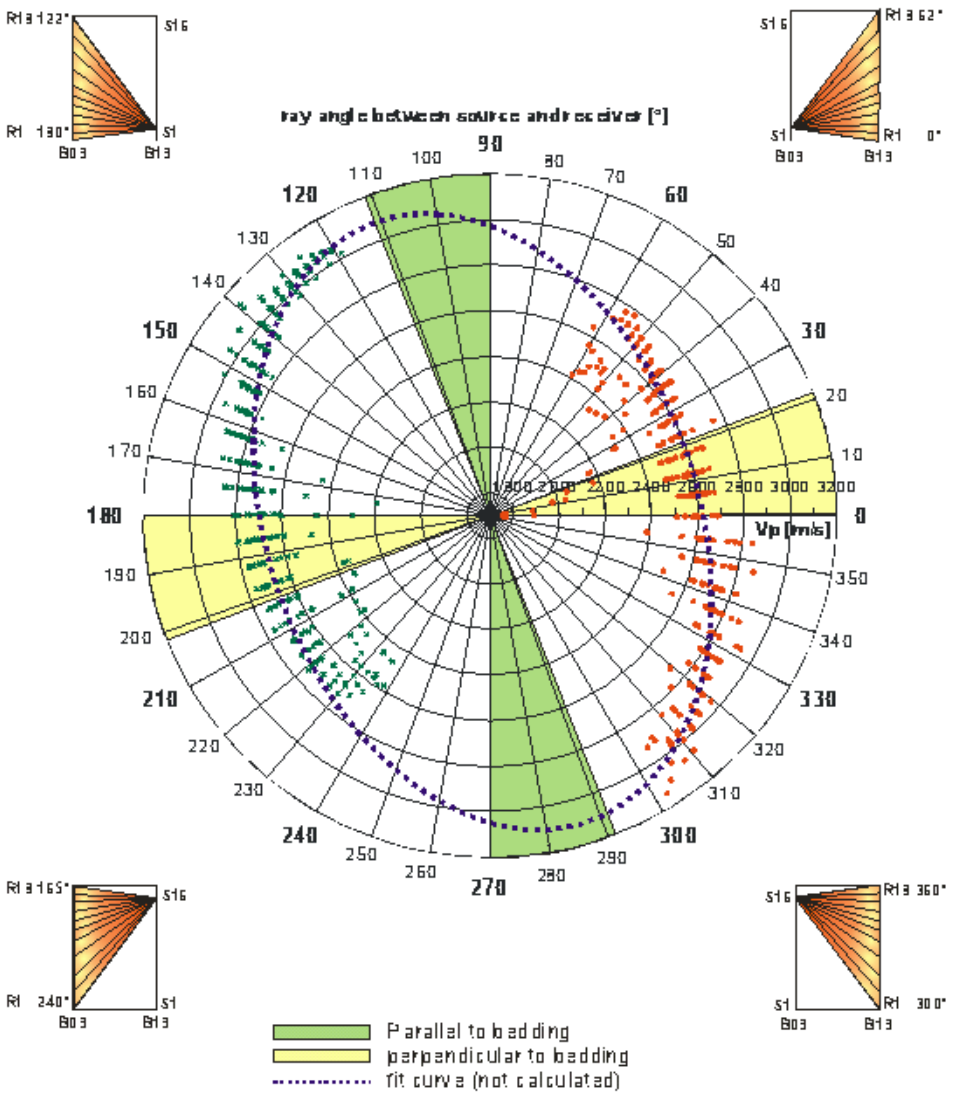

Fig. 2.8 Results from a seismic anisotropy study with 576 emitter-receiver combinations.

The main result from the seismic transmission long-term monitoring experiment, performed between April 2002 and November 2003, is compiled in Figure 2.9 (Schuster, 2004). Data from five representative depth levels are compiled. For seismic travel paths running parallel to the wall of the niche at depths of 8 cm, 38 cm, 138 cm and 208 cm from the interface bentonite – Opalinus Clay and for ray paths in the bentonite at 20 cm from the interface the seismic traces in an ensemble normalized wiggle mode are displayed. Each trace plot s, which was ensemble normalized individually, shows the evolution over 576 days whereas only every 2nd trace is plotted.

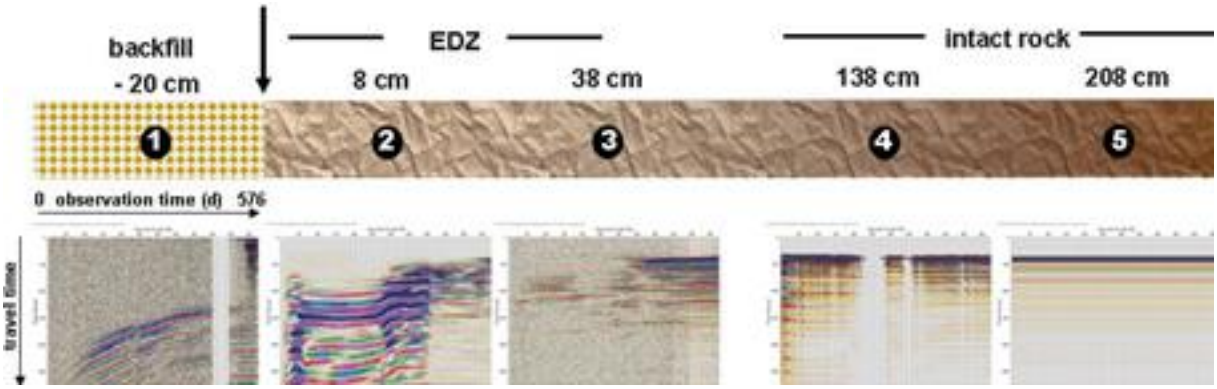

Fig. 2.9 Main results from phase 1 seismic transmission experiment. Seismic sections at four depth levels in OPA and one in the backfill show remarkable trends.

The main results which were derived from these seismic plots in a rather qualitative form were summarized as follows.

- **1 backfill**: decreasing travel times and increase of amplitudes are clear indications of an ongoing compaction process.
- **2-3 EDZ**: Decreased travel times and weaker amplitudes at the beginning and the continuous development towards shorter travel times and stronger amplitudes imply a recovering process going on in the EDZ.
- **4-5 intact rock**: travel times and amplitudes seem to be unaffected by the developments going on over 576 days.

Already in this data a close link between seismic parameters and geomechanical properties of rock is visible. This relationship will be underlined in more detail for some exemplary data sets in the next chapter.

2.3 Comparison of results from geotechnical and seismic monitoring

For one data set exemplarily the relationship between geotechnical parameters gained within the first 576 days of the EB experiment and geophysical parameters from the seismic long-term monitoring data set, measured in parallel, are assembled in Figure 2.10. The seismic data were measured between emitter E04/S4 and receiver R13/E13. The travel path runs parallel to the tunnel wall at a distance of 38 cm. Details of the total pressure measurements are described in SDR EB N19 (Aitemin, 2007) and the data were provided by Aitemin. The three locations of sensors are marked in Figure 2.10a with red points ((1) – (3)) and they are

regarded as representative for these depths. The following locations in the backfill and in the OPA are taken for a detailed analysis into account:

(1) Total pressure sensor at the interface bentonite - OPA
(2) Seismic section of measurements in the bentonite, 20 cm from the interface
(3) Seismic section of measurements in the OPA, 38 cm from the interface

Even if not all relationships between changing geophysical and geotechnical parameters are fully understood up to now a clear correlation in many cases are obvious. This particular extensive discussion should moreover support the awareness and acceptance of geophysical methods in the field of geomechanical problems. An advantage of seismic measurements is the fact that, depending on the desired resolution, greater or smaller parts of the rock mass can be scanned. In this example the wave propagation path is 0.88 m.

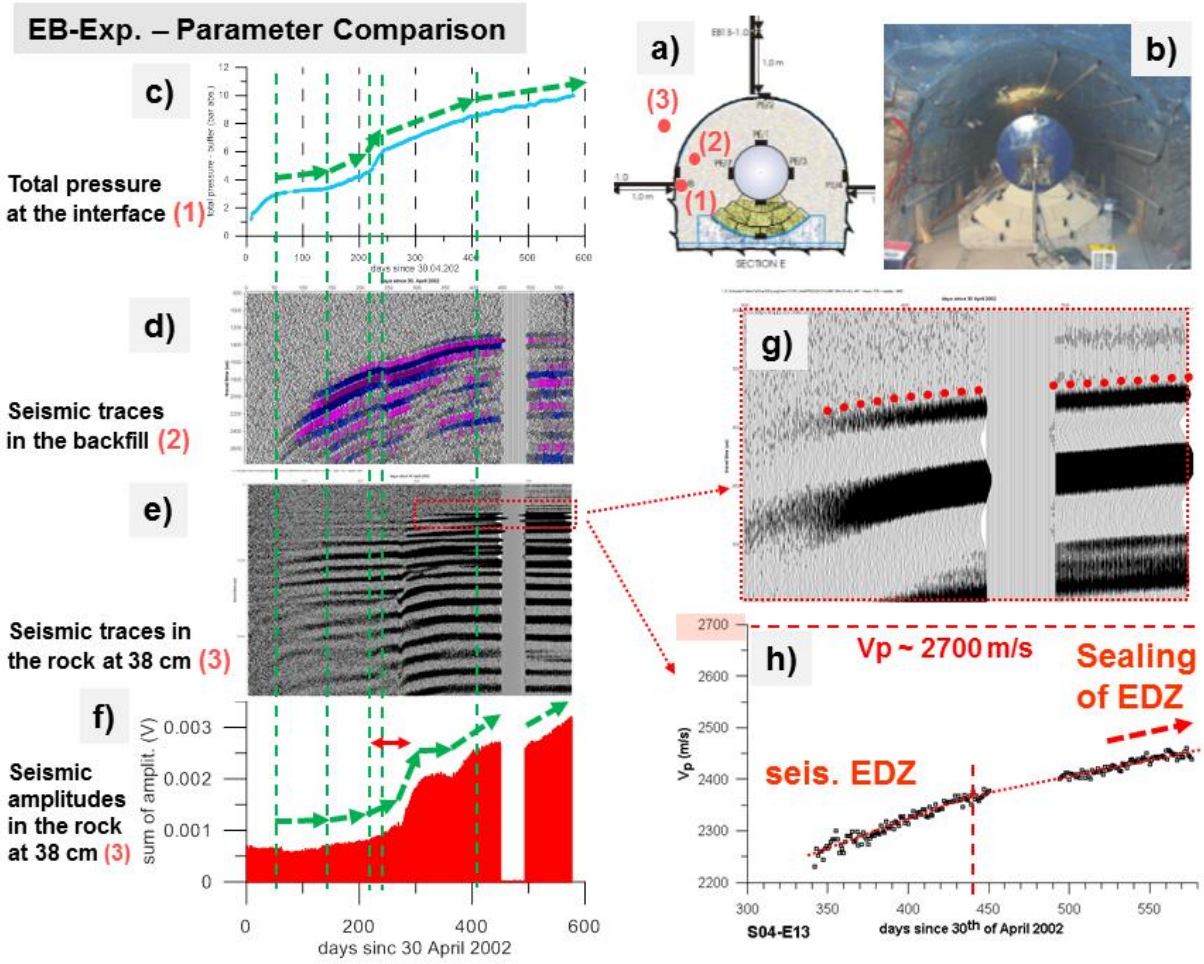

Fig. 2.10 Comparison of geotechnical and seismic parameters derived in the EB experiment. Details are discussed in the text.

The eight sub plots (2.10a - 2.10h) depicted in Figure 2.10 provide the following information and allow for a qualitative interpretation. Due to a technical problem seismic data between day 450 and 490 are lost.

- **(a)** Distribution of geotechnical and seismic sensors as described above.
- **(b)** Photograph of the dummy canister and some hydration pipes in the EB niche.
- **(c)** A gradual increase of total pressure from 1 kbar to 10 kbar at the interface bentonite-OPA with two pronounced steps are recorded within 576 days after the closure of the niche and the start of hydration.
- **(d)** Evolution of seismic signals in the bentonite, 20 cm from the interface. Decreasing travel times and strengthening of amplitudes are clear indications for a consolidation of the bentonite.
- **(e)** Complete seismic section derived in OPA at a distance of 38 cm from the interface.
- **(f)** Derived amplitudes (mean value of sum for each trace) from the seismic section shown in (e). A jump starting around day 280 dominates.
- **(g)** Enlargement of the P-wave phase with picked travel times used for the P-wave velocity determination. Phase identification before day 340 was not possible due to the high attenuation of seismic signals caused by the still unconsolidated bentonite.
- **(h)** Evolution of the derived P-wave velocity (second part of the P-wave phase) in the OPA 38 cm from the interface (black dots). Two gradients (red dashed lines) can be distinguished (days 350 – 450 and 500 – 570).

A very clear correlation between the total pressure build-up at the interface bentonite – OPA and the evolution of different seismic parameters can be seen. At all identified bending points in the total pressure graph a green dashed line is plotted in order to support the interpretation.

- After the first steep increase of pressure build-up (day 50 in (a)) seismic phases can be correlated slightly in (d) and (e).Before that time the amplitudes and correlative phases are weak due to the high attenuation of seismic wave energy in the by far not consolidated bentonite (d) and the still well formed EDZ (e).
- Until day 220 the total pressure build-up takes place in two steps with weak gradients. In the seismic sections (bentonite (d) and OPA (e)) a strengthening of later phases are visible.

- Between days 220 and 240 a very steep pressure increase takes place. Appropriate reactions in both seismic sections seem to be delayed by several tens of days. The red arrow in (f) underlines this for the amplitudes. But also the later seismic phases in both sections ((d) and (e)) change accordingly.
- Around day 400 a change of the slope in the pressure graph can be seen. Delayed by about 40 days the amplitudes change (f) and especially the slope of the P-wave velocity (h) changes to a degraded slope.
- In (h) a clear trend in the P-wave velocity is visible. As a result of several own investigations a v_p of 2700 m/s for a travel paths orientation 45° to bedding was regarded as an indicator for an intact rock. The evolution of v_p seem to trend towards this velocity. Until day 440 faster and then according to the weaker slope with a slower speed. The EDZ seem to seal continuously.

Further attention is needed to clarify such relationships.

3 Objectives and motivation for the resumption of the seismic long-term monitoring

Since December 2003, after the phase 1 of the seismic monitoring ended, a continuation of changes in rock properties in the vicinity of the EB niche and especially in the bentonite was expected due to the ongoing resaturation processes and the stress redistribution around the EB niche. Even the excavation of the new Gallery 2008 could contribute to a certain extend to a stress redistribution. Furthermore, the planned dismantling process would offer an unique opportunity to observe a recreation of an EDZ with the help of seismic parameters. As outlined in the previous chapter, the phase 1 seismic data gave strong indications that according to seismic parameters the EDZ which was created during the excavation of the niche was on the way to recover. Figure 3.1 shows the evolution of the total pressure in the backfill material (Aitemin, 2012) which supports the assumption of ongoing processes. Additionally the period of phase 1 and the time window (around day 3403) where the pilot boreholes were drilled through the concrete plug into the bentonite (Schuster et al., 2014) are indicated. The data plot ends five month before the beginning of dismantling (around day 3830).

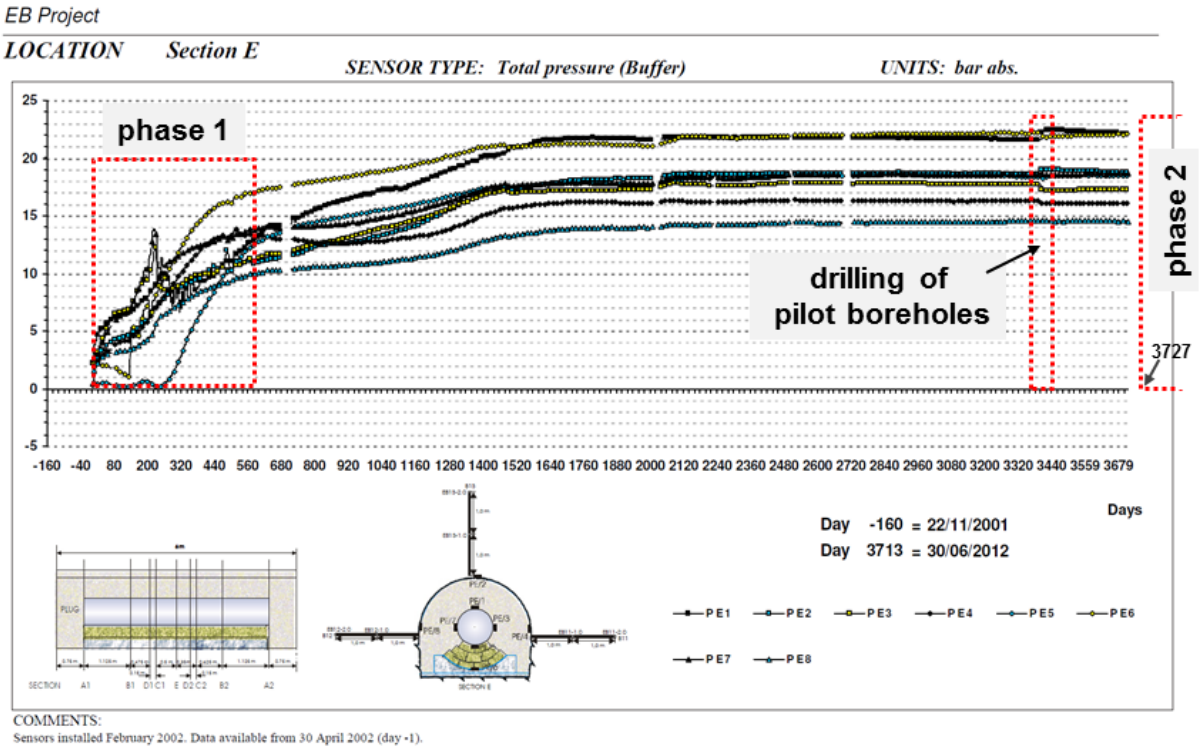

Fig. 3.1 Total pressure evolution in the back fill of the EB experiment (modified from Aitemin, 2012). Day 1 corresponds to April 30, 2002.

Furthermore, a second seismic long-term monitoring experiment which was conducted by BGR within the PEBS project in the micro-tunnel (HE-E Experiment), showed very clear correlations between changing rock properties and derived seismic parameters (Schuster, 2014).

In general, seismic parameters like P-wave velocity (v_p) and the amplitudes of first arrival phases react very sensitive to appropriate changes. Along the seismic array in the EB niche these parameters characterize the rock in an integral way over distances between 0.3 m and 3.1 m depending on the emitter-receiver locations. Not all correlations and dependencies between varying seismic parameters and related rock property changes are completely understood until now. In Figure 3.2 a simplified sketch for a seismic wave field traveling 90 cm between emitter and receiver in OPA with a travel path orientation 45° towards the bedding illustrates the sensitivity of P-wave velocities to alterations in rock. Several options for anomalies are given on the left side: creation of an Excavation Damaged Zone (EDZ), micro cracks, increased porosity, fractures and a lithological change. For an intact OPA with a v_{p0} of 2700 m/s an integral anomaly of 20 mm, what corresponds to 2.2 % of the total travel path length, would reduce the velocity to 2653 m/s (case 1: micro cracks, filled with “fluids” equals 98.3 % of v_{p0}) or even to 2332 m/s (case 2: pure micro cracks, “gas filled” equals 86.4 % of v_{p0}).

In terms of travel times the described variations for a 20 mm wide anomaly would range between 333.3 µs for the intact OPA, 386.0 µs for case 2 (pure micro cracks, “gas filled”) and 339.3 µs for case 1: micro cracks, filled with “fluids”. Consequently these are differences in travel time of 6 µs for case 1 and 52.7 µs for case 2.

Due to the very good data quality in general a small difference of 1 to 2 µs for a first arrival phase can be resolved. In this very simplified approach no scattering effects and/or relations between seismic wave length and size and aspect ratio of anomalies (e.g. pore size) are taken into account. Both cases, all voids filled with air/gas or with fluids are extreme cases. A combination of partly gas and fluid filled pores is also conceivable and rather realistic, especially when short term developments in argillaceous rock are investigated.

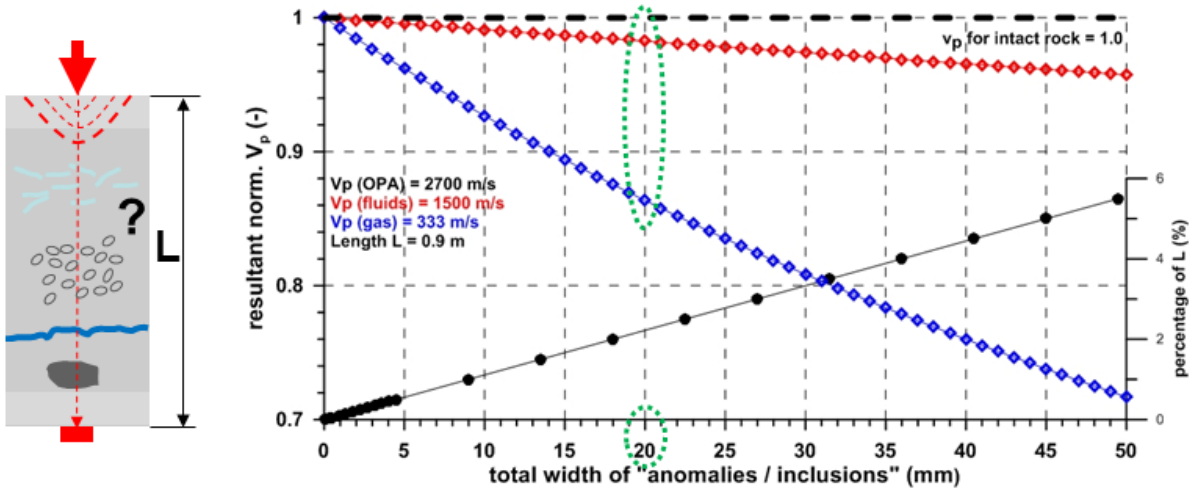

Fig. 3.2 Simplified illustration of v_p variations depending on anomalies encountered along the travel path. Left: Seismic wave field represented by a seismic ray path traveling through different anomalies in OPA. Right: Resultant normalized v_p graphs for two extreme cases, all voids filled either with gas or with fluids.

Figure 3.3 shows exemplarily a seismic section from phase 2 of the long-term monitoring. An emitter – receiver combination (E04-R13) covering 598 days of daily observation / recording (July 12, 2012 – March 1, 2014) was chosen. All traces are plotted in a trace normalized display. The thin dashed line corresponds to the arrival time for the first arrival phase (P-waves) at day 1. The distance between emitter and receiver is 88 cm, comparable to the situation discussed in Figure 3.2 (L = 90 cm). Data were only slightly processed (subtraction of DC shift, move start time, mean filter/3 point window, time cut). Note the very good data quality, except of some drop outs between days 135 and 205. These deficiencies are related to partly wanted and some unwanted disconnections (cable cuts) of the seismic array from the recording unit during the dismantling activities. Already in this plot the tendency of increasing travel times for all seismic phases are visible. It starts around day 100 with the beginning of the dismantling operation. Figure 3.4 shows this evolution more clearly. For the same data set only every 20th trace is plotted in an ensemble normalized display with a higher resolution in time.

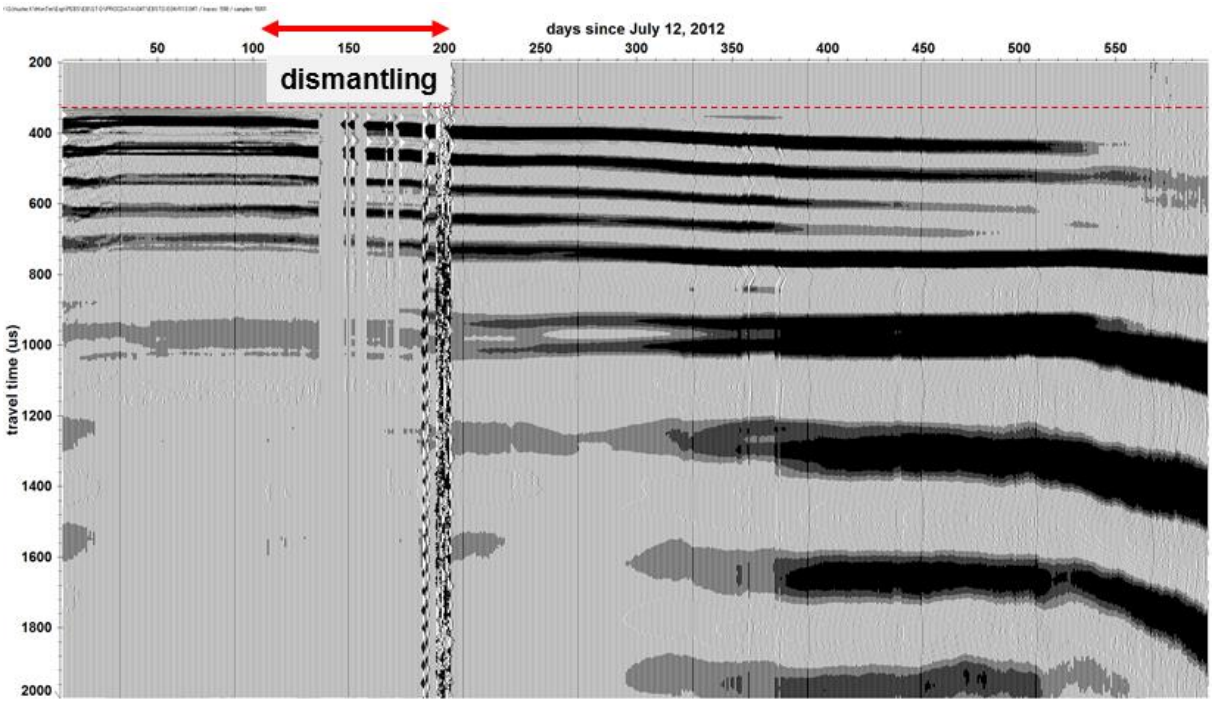

Fig. 3.3 Seismic section (E04→R13) covering 598 days of observation (July 12, 2012 – March 1, 2014). All traces, trace normalized display.

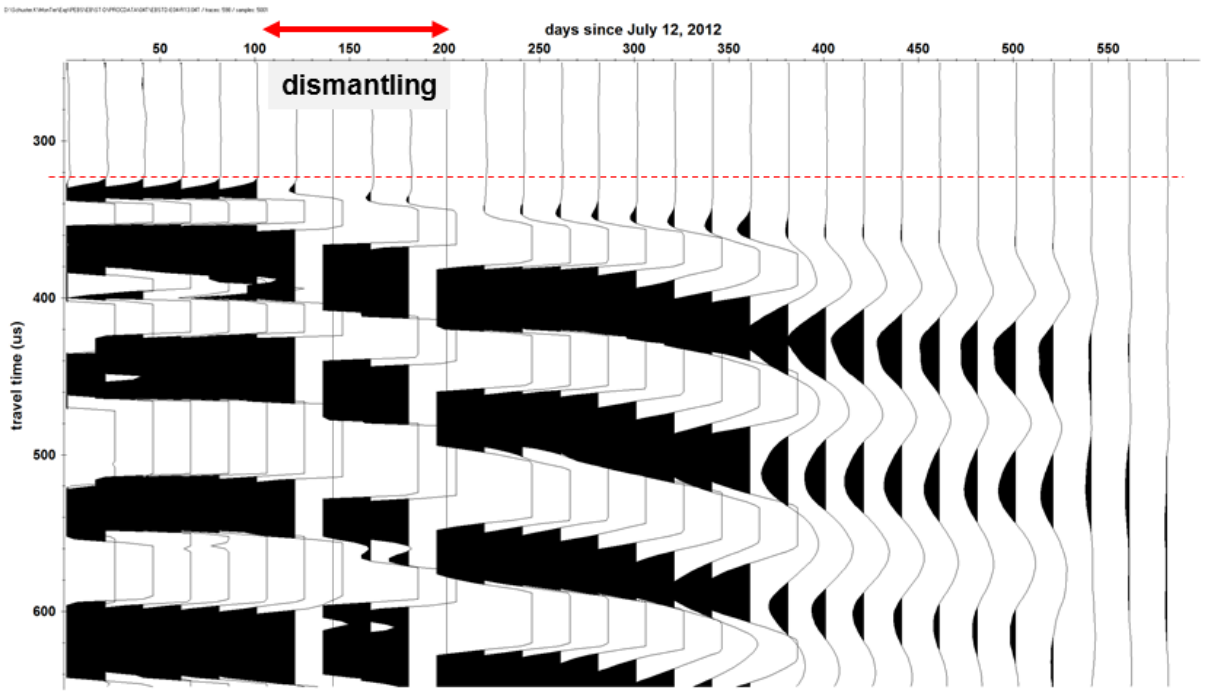

Fig. 3.4 More detailed display of section E04→R13 data (comp. Fig. 3.3), but only every 20th trace is plotted in an ensemble normalized display.

The seismic section represents a seismic travel path in the OPA at a distance of 38 cm from the interface bentonite – OPA. This is an area where the Excavation Damaged Zone (EDZ)

and/or Excavation disturbed Zone (EdZ) was developed during the excavation and seemed to be on the way to sealing during the hydration phase of the bentonite at the end of phase 1 monitoring (cf. Fig. 2.10).

For this emitter-receiver combination travel paths are roughly oriented 45° to bedding. P-wave phases change remarkably. Within the first 100 days for the P-wave arrival phase a slight increase of travel times and amplitudes are visible, followed by a remarkable decrease of travel times and amplitudes until day 598. In terms of first arrival times up to 60 µs which results in different p-wave velocities with a pronounced v_p decrease of up to 83 % of v_{p0} (cf. also Fig. 7.6). Furthermore, the amplitudes varies, they change in magnitude and in frequency content. A change of the frequency content can be seen, indicated by the changing shapes of first arrival phases. All together these are very clear indications that remarkable changes in rock properties occur with ongoing time.

A very interesting point is to rate the evolution of the Opalinus Clay and the backfill material in the time between the end of the first and the beginning of the second monitoring phase. A comparison of first arrival travel times from the end of phase 1 recording (around day 576, T-P0 = 362 µs) and the beginning of phase 2 (around day 3730, T-P0 = 318.5 µs), nearly 8.6 years later, shows a decrease of nearly 43.5 µs. In this case the very good correlative positive part of the first arrival phase was taken. This results in a v_p increase of about 300 m/s, which points to a consolidation of the rock mass. For the negative part of the first arrival phase, which is worse correlative, we measure 338.5 µs around day 570 (end of phase 1) and 303.5 µs (beginning of phase 2), which is a difference of 35 µs.

What does it mean in terms of rock mechanics? All these changes among other things are close related to micro crack creation, sealing processes, swelling of OPA, stress redistribution and maybe pore water pressure changes. Up to now only limited experiences for a sound explanation / interpretation for such seismic parameter changes in OPA exist. Some laboratory tests exist. In the following chapters more details and some explanations will be given.

4 Layout of the phase 2 of the seismic transmission experiment

The phase 2 of the seismic transmission experiment in the EB niche started in July 2012. It focused on the characterization of alterations in the surrounding rock and the bentonite which were caused by the dismantling operation with the help of seismic parameters.

4.1 Location and layout with regard to the dismantling

After a successful geophysical characterization of the initial stage of parts of the EB niche a seismic array was installed for the phase 1 in spring 2002 as part of the seismic long-term monitoring and was used for nearly 600 days. It was described already in detail in chapter 2.1. For the phase 2 experiment most parts of this seismic array could be reused. Figure 4.1 shows the four boreholes with the theoretical ray coverage. In total 24 piezoelectric transducers were installed.

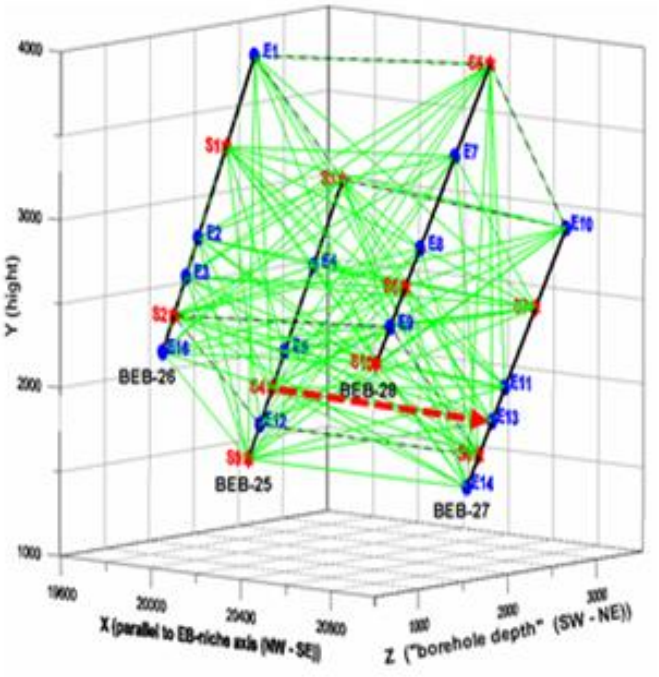

Fig. 4.1 Location and general layout of the seismic transmission experiment in the eastern wall of the EB niche with the maximum theoretical ray coverage.

The time period between phase 1 and phase 2 of the seismic monitoring was about 8.6 years. As a consequence of this interruption it could not be guaranteed that all transducers work properly and all cable connections are faultless. In September 2008, three years before the start of phase 2, a first test was conducted. Six out of ten emitters and 11 out of 14

receivers could be reactivated. Phase 2 of the monitoring started in July 2012. In order to overview the availability of usable seismic data a rough data analyses was performed with the data gained between July 2012 and March 2014. For each of the ten emitters the related seismic sections were analysed. Appropriate plots can be seen in Figure 6.8 and in the appendix. The following Table 4.1 summarizes an overview over the seismic data which finally could be used.

Tab. 4.1 Overview of availability of phase 2 data according to a rough data check. Data available from … on.

Emitter no.	first day 12.07.14	day 150	day 200	until day 598	Phase 1 data
E01	No	Yes	Yes	Yes	
E02	No	Yes	Yes	Yes	
E03	Yes	Yes	Yes	Yes	
E04	Yes	Yes	Yes	Yes	
E05	No	No	Yes	Yes	
E06	No	No	Yes	Yes	
E07	Yes	Yes	Yes	Yes	
E08	Yes	Yes	(Yes)	(Yes)	
E09	No	No	No	No	
E10	No	No	No	No	

The main reasons for data losses were defective piezoelectric transducers and cables and connectors which were affected by corrosion. At a later stage also cable cuts during the dismantling operation had to be taken into account. Before the resumption of the seismic monitoring and also at several times during the dismantling activities the seismic installation was repaired and maintained. According to the overview a selection of usable data was made for the further analyses.

The excavation front passed the seismic array during the dismantling operation. For better analyses of changes in seismic parameters and the advancing dismantling front some details are compiled in Figure 4.2 and in Table 4.2.

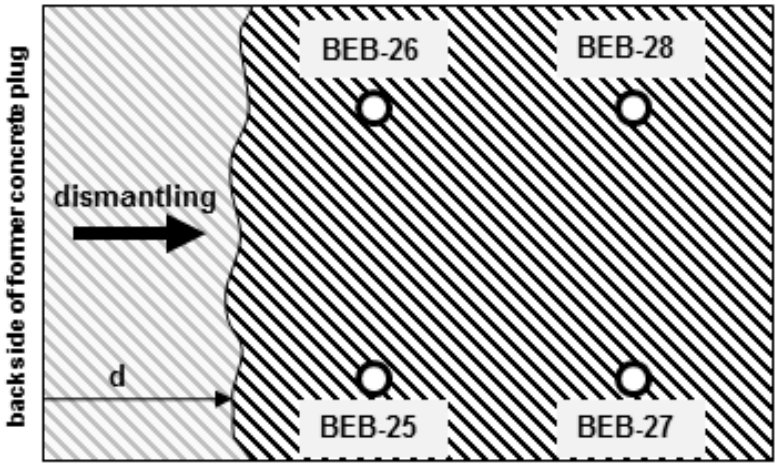

Fig. 4.2 Simplified sketch of the eastern wall of the EB niche with four borehole mouths, orientation of bedding planes and the advancing dismantling front.

The dismantling operation is described in detail by Palacios et al. (2013). It was performed during the 19th of October 2012 and the 1st of February 2013. With regard to the installed sensors it was performed very carefully. But in several cases a cable damage could not be avoided. In the following Table 4.2 some distances of the dismantling front in relation to the back side of the concrete plug and linked to the days of monitoring are compiled.

Tab. 4.2 Distance (d) of the excavation front from the back side of the concrete plug (see also Figure 4.2).

Day of seismic monitoring	distance from back of concrete plug (m)	distance to B-25 & B26 (m)	distance to B-27 & B28 (m)	activity
104	0	2.9	3.87	Start of dismantling
134	0	2.9	3.87	Concrete plug removed
141	0.75	2.15	3.12	Sampling section A1
158	1.87	1.03	2.00	Sampling section B1
184	2.98	-0.08	0.89	Sampling section E
194	4.10	-1.20	-0.23	Sampling section B2
103				End of dismantling

4.2 Instrumentation and technical parameters

Piezoelectric transducers were mounted on support frames and positioned in four boreholes and fixed mechanically with the support of springs. In total 24 transducers are used, Four transducers are located outside the boreholes as shown in Figure 2.5 in order to observe the development in the backfill material.

The transducers installed in the boreholes but also outside in the backfill area in general allow seismic waves travelling to all installed receivers along different orientations toward the bedding of the Opalinus Clay. All distances were calculated with the help of the borehole coordinates and considering the position of the transducers which are clamped to the borehole walls.

Regarding all installed transducers the automatic daily measurement between all emitter – receiver combinations results in 140 different ray paths which can be differentiated as follows:

- Ray paths inside the rock between boreholes: 88
- Ray paths inside the rock along borehole wall: 14
- Ray paths inside the backfill: 4
- Ray paths from backfill to rock between “boreholes”: 18
- Ray paths from backfill to rock along “boreholes”: 6
- Ray paths from rock to backfill between “boreholes”: 6
- Ray paths from rock to backfill along “boreholes”: 4

Which emitter – receiver combinations really was available was discussed in the previous chapter. For a first analysis the most relevant orientations of ray paths are the one running through the OPA parallel to the wall at different distances and directly through the bentonite. According to the experiences made in former experiments (VE and HE-E) the observation focuses on the first 50 centimetres of the rock, where the main changes in rock properties are expected.

The technical details of the used equipment are compiled in a short report (German) which was provided by GMuG. It can be found in the appendix. The most important parameters are:

- Piezoelectric transducers (built by GMuG), 10 emitters and 14 receivers, prefabricated on four rods, coupling via springs, de-coupling pneumatically
- Recording system (PC based): A/D converter with 16 bit @ 500 kHz (dt = 2 µs)
- Amplification: receivers: 40 dB (30 dB pre amp + 10 dB), high-pass filter: 1 kHz
- Emitter signal (one impulse generator, switches by a relay switch between all ten emitters): - 60 dB recorded at “receiver” 15
- Recording: daily measurement at 1:10 am
- For each emitter 2048 measurements are repeated and averaged (stacked)

- Length of recordings: 32.4 ms (16384 samples)
- Pre trigger: 25 %

The installation of all components was performed in spring 2002. Within the operational phase started in July 12, 2012 several tests were made additionally.

4.3 Acoustic emission monitoring

Our subcontractor GMuG offered to record during nights and over weekends potential acoustic emission (AE) signals with the same equipment. During that time no human activities in the rock laboratory are going on what enhances the chance to record acoustic emission signals originating from processes going on in the rock, e. g. creation of cracks due to stress redistribution. Only in case of effectual and successful data acquisition an additional processing should be performed. But the outcome was rather poor. One of the reasons could be the age of the EB niche. After more than 10 years after construction all the major stress redistribution processes are assumed to have come to an end. Comparable AE experiments were performed around and in the EB niche (see Fig. 2.1, Spies et al., 2002, Schuster et al., 2004a). Another reason for the poor outcome could be the layout of the seismic array which was mainly designed for the active part of the seismic experiment. Therefore the AE option was not used for additional analyses.

5 Seismic Parameters and uncertainties

The discrimination between seismic methods (in-situ or mining seismic) and ultrasonic methods (laboratory seismic) is assumed by some authors for signal frequencies of 10 kHz. The dominant frequency content of the signals we are dealing with in this report is in the range between 2 kHz and 30 kHz, at which 10 kHz can be seen as the lowermost edge of the ultrasonic range. Nevertheless, we use the term seismic, also to avoid confusion in the text. The main seismic parameters derived in phase 2 (started on July 12, 2012) from the recordings and used in this report are explained in this chapter. The processing, analyses and plotting of seismic records is performed with the seismic software tool ReflexW (Sandmeier, 2013).

All data were converted from a binary apparatus format to a PC-readable format. At the current status several amplitude variations of the individual emitter signals could not be

corrected. Maybe in a later stage all receiver data can be corrected to a normalized peak amplitude value by taking the different amplitudes of the source signal into account. This would guarantee that all amplitudes of the received signals are directly comparable. It is very important to mention, that the emitter start time is not affected by this missing processing step.

5.1 Derived seismic parameters

For all further calculations and processes the start time of the seismic signal emission is very important. It is derived from the recordings of the individual emitter signals. In Figure 5.1 a part of the emitter signal for emitter E01 as generated at day 300 is displayed and the main signal characteristics used for further processing are indicated. More details concerning the source signals are discussed in the next chapter. In this context only the start time (t0) is of interest.

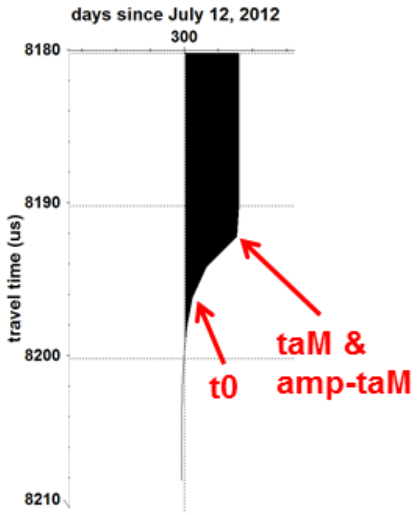

Fig. 5.1 Seismic trace witch was generated in the signal generator and used for the excitation of the piezoelectric signal transducers (emitters).

For a received signal at receiver R03 a part of a single seismic trace is shown in Figure 5.2 in order to explain the main first arrival P-wave onset characteristics used for the derivation of seismic parameters.

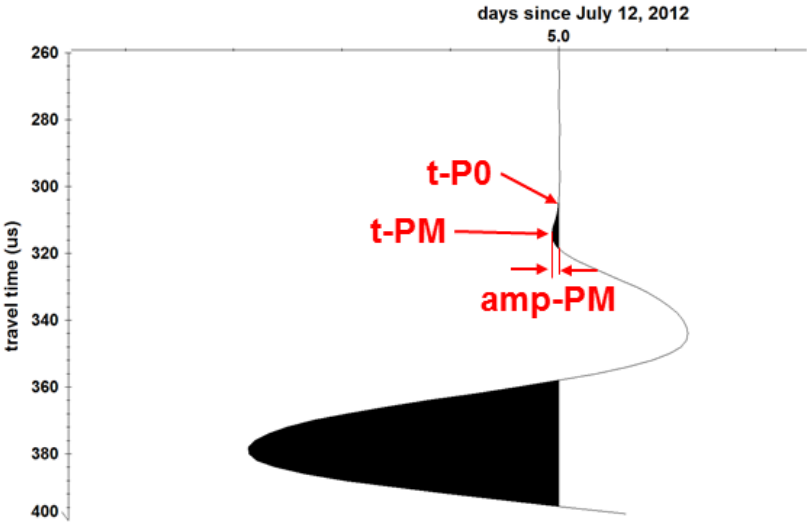

Fig. 5.2 Part of a seismic trace (E04-R03) with derived attributes (fifth trace from the section displayed in Fig. 6.2).

The following characteristic signal attributes are determined from the traces. The analyses, especially phase correlations and time picking of relevant phases, have to be made manually, because an automatic processing would not be precise enough. This is a time consuming part of the analyses.

- t-P0: travel time of first arrival P-wave onset (µs)
- t-PM: time of amplitude maximum of P-wave first arrival phase (µs)
- amp-PM: amplitude of maximum of P-wave first arrival phase (V)
- t0: source signal (start time, start of emitted source signal (µs), see Fig. 5.1)
- taM: source signal (time when max. amplitude of emitter signal is reached (µs), see Fig. 5.1)
- amp-taM: max. amplitude of source signal (V)

For further analyses the data are processed slightly in three steps:

- Subtraction of possible DC shifts
- Subtraction of pre trigger time (8196 µs)
- Moderate filter, meanfilter

The identification of relevant seismic phases and picking of appropriate seismic attributes (see Fig. 5.2) are the next steps. Figure 5.3 shows four first arrival phases which can be picked easily for further processing (red arrows). For a comprehensive interpretation of the

complete data set such identified first arrival phases should be recognizable until the end of the recording phase, even when the quality changes. This is not always the case. For the shown example the quality of these first arrival phases drops considerable between days 130 and 190 and from day 550 on, so that no reliable seismic attributes can be picked. In such situations sometimes it is helpful to pick a different phase which is part of the first arrival phase and can be followed through the complete seismic section until the end (day 598).

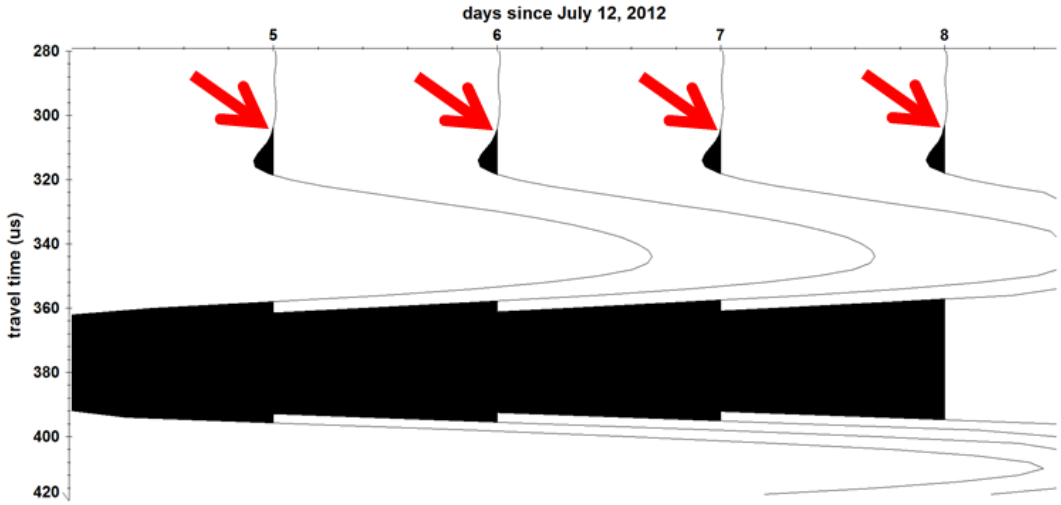

Fig. 5.3 Examples of first arrival picks for the emitter–receiver pair E04-R03, 38 cm from the interface. Picks are marked with red arrows.

In Figure 5.4 the same data set is displayed, but plotted differently. The scaling is unlike and the filling of negative and positive amplitude values is reversed. The advantage is that this picked phase can be followed through the entire section. Of course, both picked arrival times differ what would have an influence of the calculated absolute velocities. But using normalized velocities (see below) it would allow to describe the evolution of the scanned rock mass consistently.

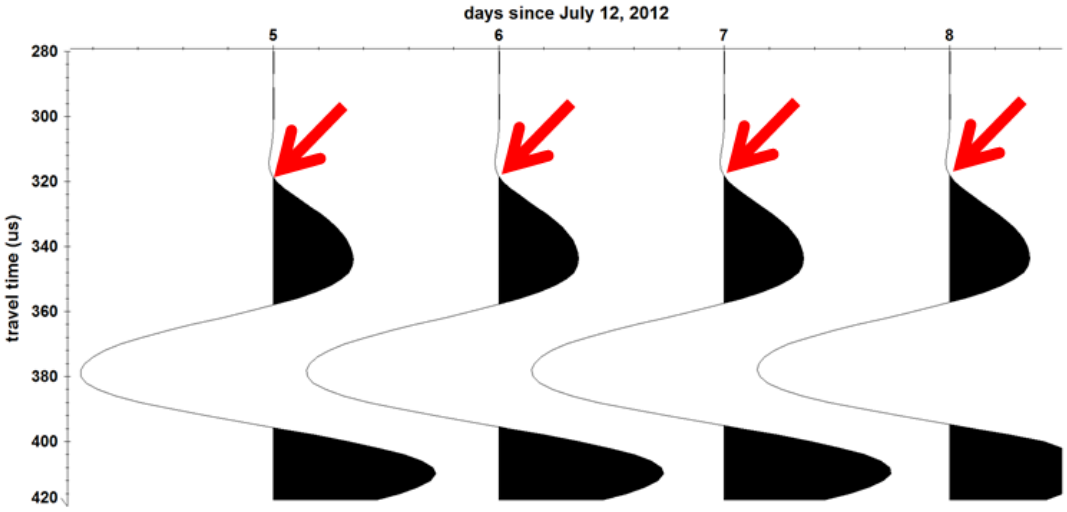

Fig. 5.4 Same data set as shown in Figure 5.3 but scaled and plotted differently.

This example shows that depending on the problem appropriate decisions concerning the phase correlation have to be made.

With the derived travel times (t) and the calculated distances (L) between piezoelectric emitters and receivers seismic P-wave velocities (v_p) are calculated (v_p = L / t) assuming straight ray propagation. All absolute v_p values are in the range of values which were obtained in the former seismic characterization of the EB niche and also from other own in-situ investigations outside the EDZ at comparable locations in the Mont Terri Rock Laboratory. Also the relative differences between the derived absolute velocities for different orientations towards the bedding are in line with the anisotropic structure of the OPA (v_p-normal < v_p-45° < v_p-parallel). The frequencies of the P-wave phases are in the range between 2 kHz and 30 kHz.

In order to optimize the comparison of different ray paths data the calculated velocities are also normalized to values derived for certain days in the phase 1 data set. This was done for emitter – receiver combinations where good correlative P-wave phases could be identified in both data sets, the phase 1 data and the phase 2 data. In these cases the values from phase 1 characterize the start situation (initial stage). Furthermore, due to minor uncertainties in the distance estimation with a v_p normalization an “over interpretation” of the absolute v_p-values is avoided.

5.2 Uncertainties – error estimation

Concerning the uncertainties we have to distinguish between technical failures, identification and correlation of seismic phases, picking of travel times as well as other signal attributes and geometrical parameters (coordinates/distances). The start time is important. It is controlled manually and found to be sufficiently good (see section 5.1 and 6.1). Travel time picking is more challenging, but due to the good quality of P-wave arrivals the first arrival picks (t-P0) can be determined with an uncertainty better than ± 0.5 µs for most of the traces. Only in cases where the attenuation is very strong the uncertainty goes up to values around ± 2 µs. In Figure 5.3 an example of first arrival phase picks is given, where the pick accuracy is rather better than ± 0.5 µs. When we consider an error in time of ± 2 µs it would result in a dv_p of ± 16 m/s for L = 0.9 m and a v_p of 2700 m/s. For the normalized v_p it would be ± 0.6 %.

Geometrical errors, for example imprecise borehole coordinates, are in general of great importance. They are often underestimated. For the above example (v_p = 2700 m/s, L = 0.9 m) an error of ± 1 cm would result in a dv_p of ± 30 m/s what is twice the error coming from a pick uncertainty of ± 2 µs. Because our installed seismic array is fixed we will neglect the possible errors in coordinates, because we are mainly interested in the evolution of seismic parameters as a time depending process, particularly when we dealing with normalized P-wave velocities. Nevertheless, we have to take into account the possibility that due to convergence and / or swelling / shrinking processes in the borehole the piezoelectric transducers can change their position slightly. Furthermore, the exact orientation of propagation paths towards bedding could only be assessed very roughly.

Amplitudes have to be regarded very carefully, because up to now the signal used for the emitters could not be corrected individually on a daily basis (see also section 5.1).

Finally, we have to mention that all processing and analyses work was done by one person, the author, and therefore the ineluctable errors should be similar (“constant error / shift”).

6 Data and first qualitative interpretation

The automatic daily measurement between all working emitter – receiver combinations results in 112 different ray paths. The regular measuring phase started on July 12th, 2012 with one measurement phase every night at about 1 o'clock am. During this measuring phase of approximately 20 minutes the 14 seismic receivers record successively seismic signals emitted by the 8 emitters. Each recording is repeated 2048 times in order to improve the signal to noise ratio. In total 112 different seismic traces are recorded every night. From these data, seismic parameters are derived for further interpretation. In this stage the focus is on the P-wave arrival phases. More data can be analyzed in a later stage.

6.1 Source signal data

The start time t0 describes the moment of emission of the seismic signal into the rock. It is derived from the signal sent from the signal generator to the emitter transducers. In Figure 6.1 (left) the emitter signal for emitter E01 as generated at day 5 is displayed in full. The source signal is characterized by a continuous and slow build-up of voltage over approximately 7000 µs and a sudden release at a defined time which generates the mechanical impulse in the piezoelectric transducer. This signal is recorded and stored as a special signal ('receiver' R15). The build-up of the signal amplitude starts at around 1200 µs and continuous gradually until 8192 µs, where the maximum amplitude is reached (circa 180 V). Within 4 µs the amplitude drops to circa 5 V (8196 µs). This is the time we are taking as the start time (t0) for emitting the seismic pulse. After another 2 µs the amplitude is nearly zero. As a consequence the seismic wave field is emitted and can be received at all 15 piezoelectric receivers. On the right side in Figure 6.1 the maximum amplitude (amp-taM) and the time which is used as start time (t0) are marked in the zoom-in display (30 µs) for day 1 and for several other days. Please note that the difference between taM and t0 is only 4 µs what corresponds to two sample steps.

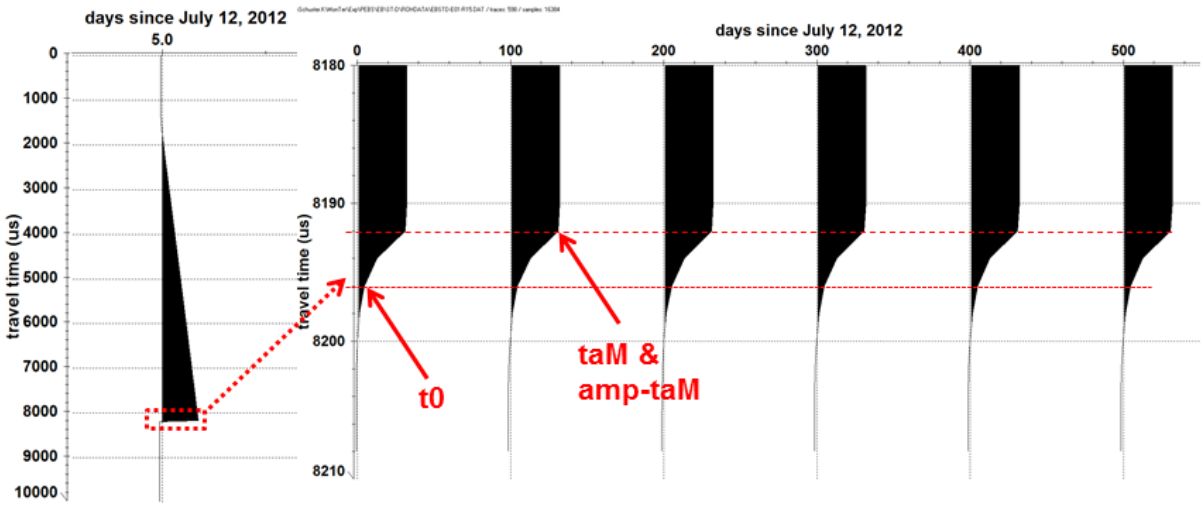

Fig. 6.1 Seismic traces which are generated in the signal generator and used for the excitation of the piezoelectric signal transducer E01 (emitter).

In order to emphasize that the start time for the emission of seismic pulses are well controlled and nearly constant over the time in Figure 6.2 a selection of the eight emitter signals are displayed. The data are scaled over the entire ensemble in order to allow the assessment of amplitude variations. It is clearly visible that for emitters E01, E02 and E07 amplitudes deviate from the maximum value at different times. For E01 it starts around day 140, for E02 from day 240 and for E07 from the beginning. Therefore a direct comparison of amplitudes of the received signals is not possible. Important for the velocity calculations is the fact that the decline of the ramp like signal behaves in the same way as discussed before. This is the case at all days. For the eight emitters only the amplitudes of the exciting signals vary with different intensities and gradients, but not the start time.

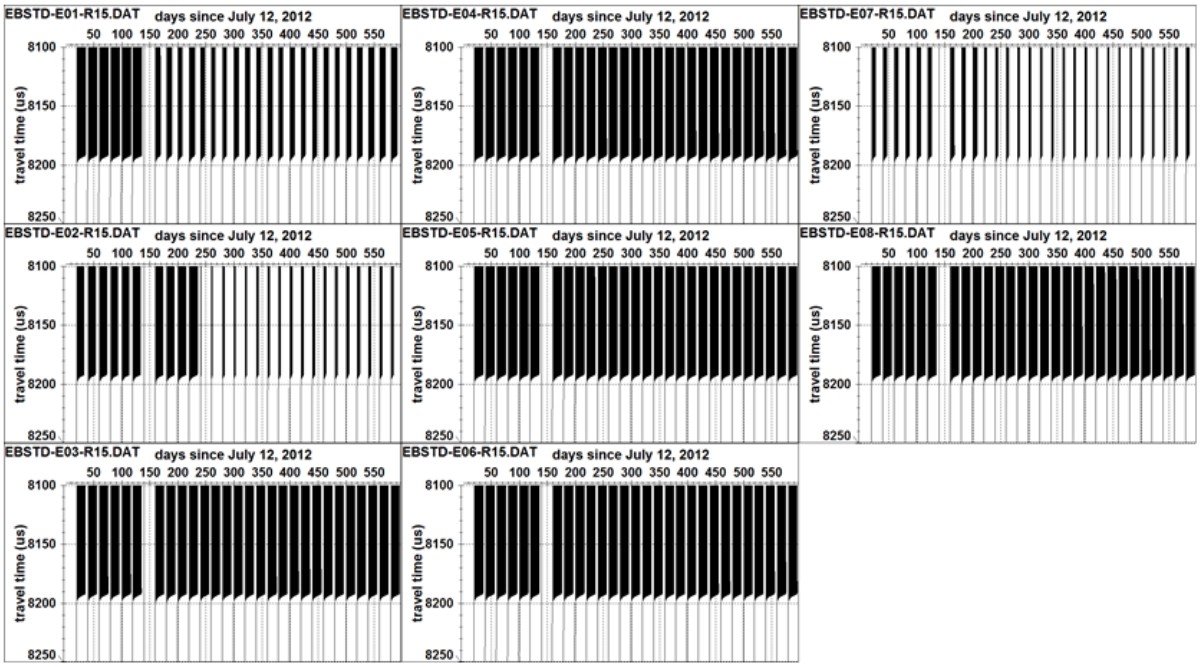

Fig. 6.2 Compilation of signals recorded for the eight emitters (E01–E08) which are generated in the signal generator and used for the excitation of the piezoelectric signal transducers (emitters). Every 20th signal is plotted (days 1 – 598).

6.2 Data from backfill

No usable emitter – receiver pairs are available because both emitters which were placed in the backfill (E09 and E10) could not be reactivated (see Table 4.1). Therefore no wave fields solely running through the bentonite can be analyzed.

6.3 Data from Opalinus Clay

In this section exemplarily for one emitter–receiver combination (E04-R03) different plots are presented which allows to assess the evolution of seismic parameters derived in the OPA in a qualitative way. Figure 6.3 shows the seismic section for ray paths running in the OPA approximately at 45° towards the bedding at a distance of 38 cm from the interface bentonite-OPA. The second part of the P-wave first arrival phase can be identified very clearly at around 320 µs (day 1). There are some data losses which were caused by a temporal disconnection of the sensor cables due to the dismantling activities. The data are trace normalised and therefore these phases can be traced until the end. A remarkable

variation in time and partly in amplitudes can be seen. The decrease of travel times until day 50 is difficult to explain. Most probably it is related to the reactivation of the measurements after 8.6 years. Although the boreholes were closed with a plastic plate it can't be excluded that some borehole wall instabilities lead to a poor contact between the piezoelectric transducers and the borehole wall during this very long period. Maybe for one or both transducers it took this time until the contact was 'readjusted'.

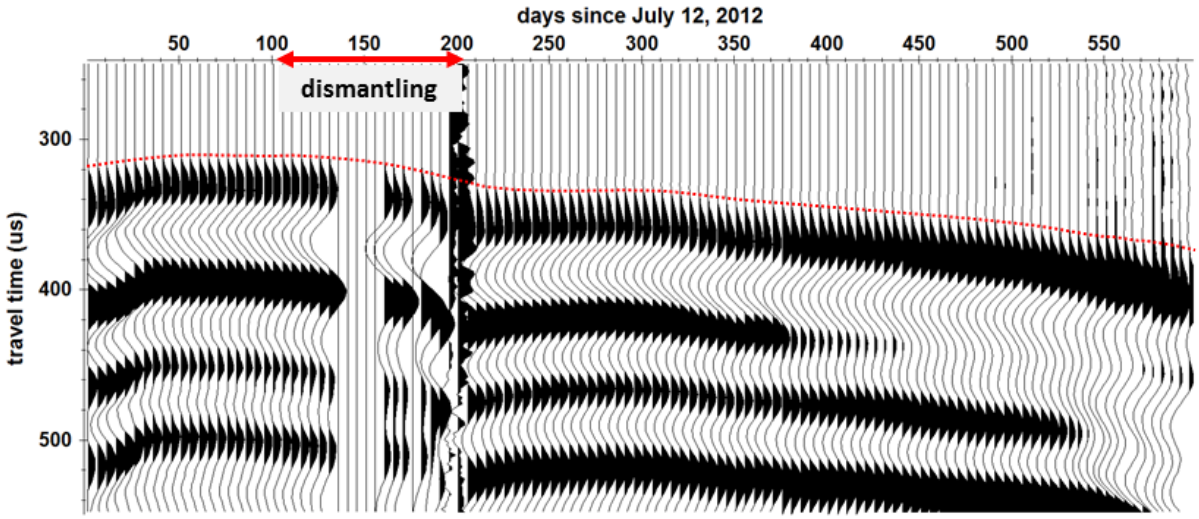

Fig. 6.3 Seismic section recorded in the OPA between emitter E04 and receiver R03, both located in the OPA at a distance of 38 cm from the interface bentonite-OPA, trace normalized, only every 5th trace is plotted.

Plotting the same data ensemble normalised, as in Figure 6.4, is a more realistic representation and allows for an integrated assessment. The pronounced variation of these phases (travel times and amplitudes) with time is a clear indication for changes of petrophysical properties of the OPA along the travel path. Around day 130 the travel times start to increase (v_p drops) and the strength of amplitudes drops. At this time the dismantling operations advanced towards the seismic array. Amplitudes become weaker and v_p decreases at the end of the dismanling. Around day 550 the phases seem to disappear in this representation. Travel times and amplitudes are very far from the starting situation. The P-wave phases change in the same time towards a lower frequency-content ("broader signal") and lower amplitudes (better visible in Figure 6.3, 6.5 and 6.6). The appropriate derived and normalised seismic P-wave velocity is plotted in Figure 7.5.

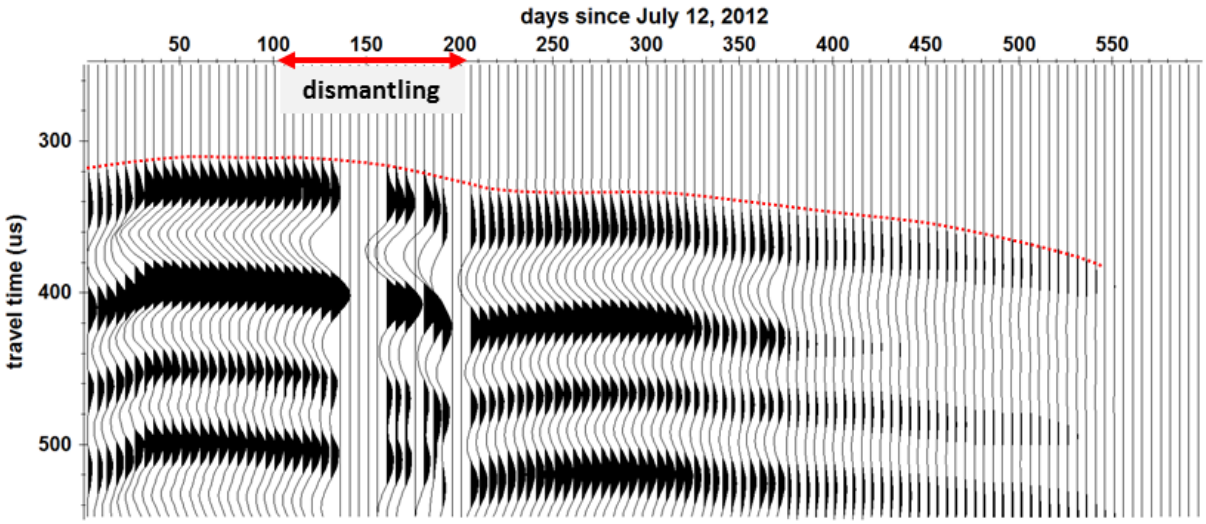

Fig. 6.4 The same data set as in Figure 6.3 (E04-R03) but ensemble normalized, only every 5th trace is plotted.

Figure 6.5 shows the same data set in a point mode plot with colour coded amplitudes and as an ensemble normalised section what allows a better assessment of the dynamic evolution of the scanned rock mass. For example we see during the dismantling activities a striking drop in time and approximately 170 days after the dismantling was finished (day 206) a weakening of amplitudes.

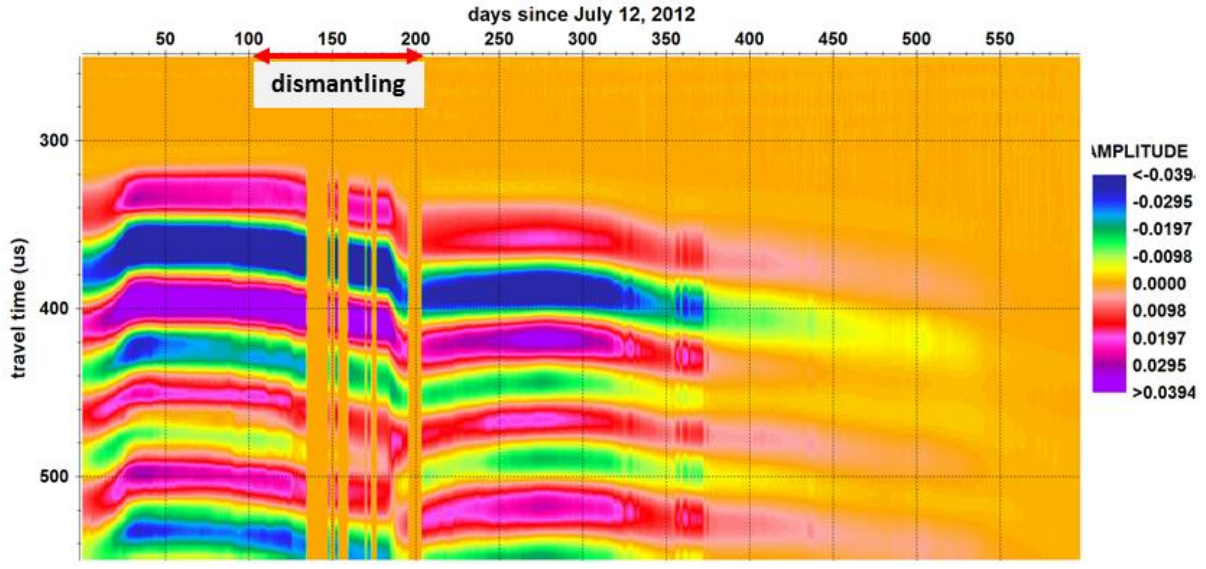

Fig. 6.5 Same data as in Fig. 6.4 (E04-R03) but with colour coded amplitudes. Ensemble normalized display.

In the following Figure 6.6 the frequency content of each seismic trace was calculated and all frequency trace spectra are displayed in a colour coded plot. Such plots show the variability of the shape of the seismic signals in a quantitative manner whereas a rather qualitative impression can be obtained already in the wiggle mode display in Figure 6.4. Until day 180 a broad range between 6 kHz and 18 kHz dominates the plot. Even after the end of the dismantling the frequency band moves slightly towards higher values. From day 340 on, 120 days after the dismantling, the higher frequency content disappears. The band around 3 kHz becomes a bit stronger from day 270 on.

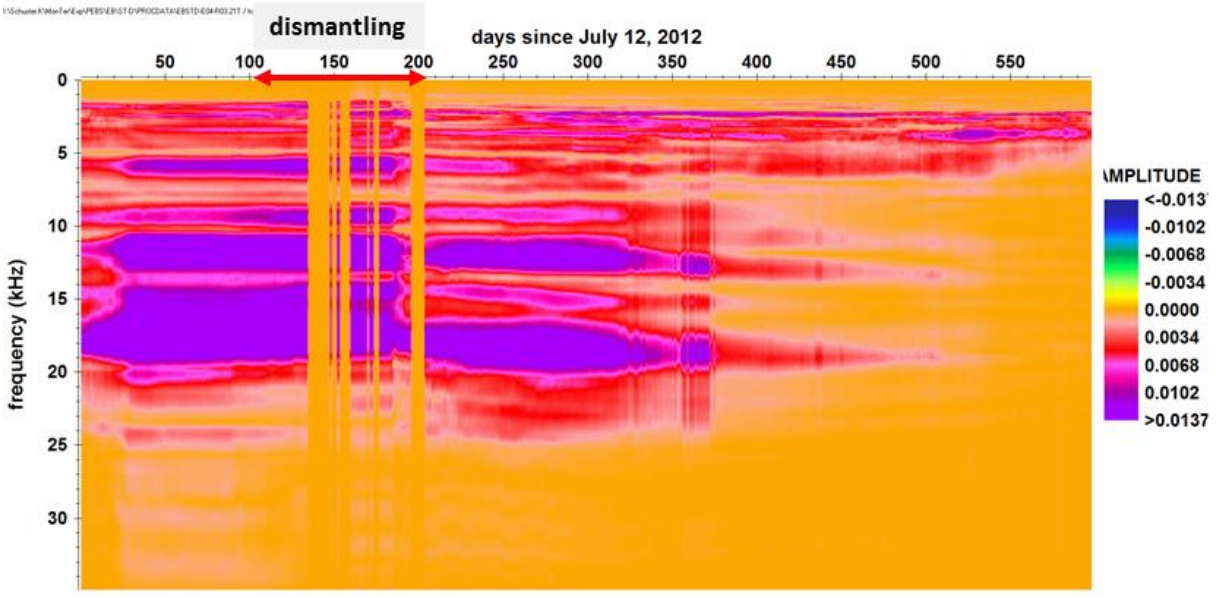

Fig. 6.6 Frequency content of the data set displayed in Fig. 6.3 (E04-R03). Ensemble normalized display with colour coded amplitudes.

For the same distance, 38 cm from the wall, a second emitter- receiver pair (E03-R13) shows a more gradually structured pattern, as pictured in Figure 6.7. The difference between the two ray paths orientations are the orientation towards the axis of the niche and therewith the orientation towards the dismantling front. The orientation towards the bedding is for both around 45° (cf. Figure 4.2). In the first case (E04-R03, BEB-25-BEB-26, distance = 0.92 m) travel paths run perpendicular to the niche axis upwards. The approaching dismantling front strikes this area more or less at once. Whereas in the second case (E04-R13, BEB-25-BEB-27, distance = 0.97 m) travel paths run in the direction of the advancing dismantling front. This could be an explanation for the rather gradual evolution of the frequency content from higher towards lower frequencies. It shows also the sensitivity of the method and the complexity of the rock mass behavior towards mechanical disturbances.

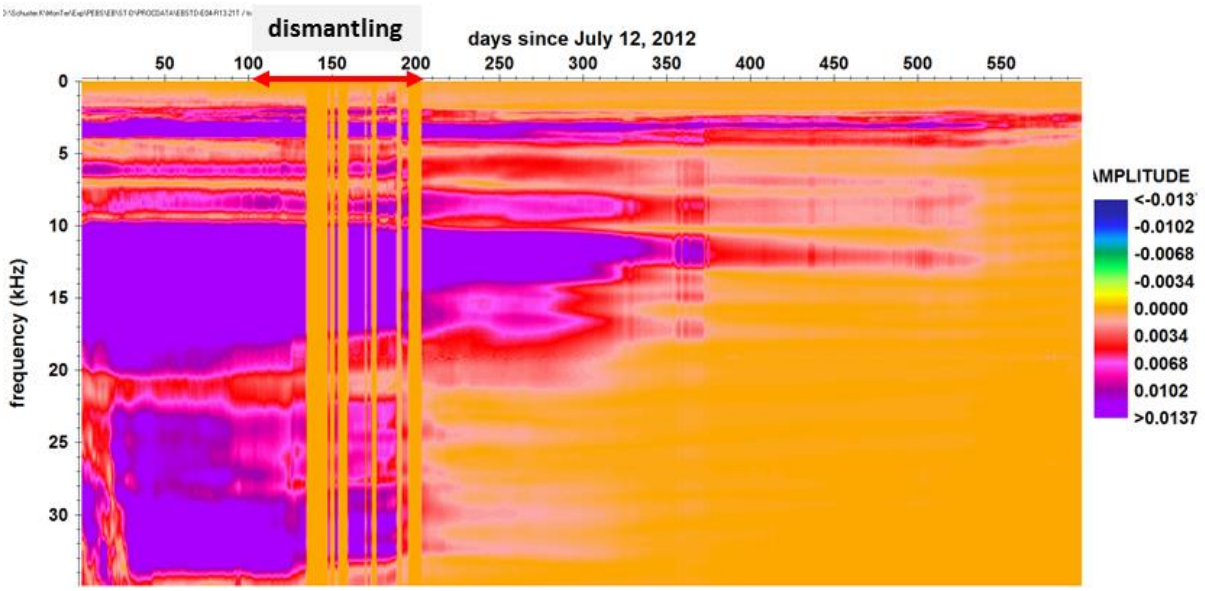

Fig. 6.7 Frequency content of the emitter – receiver pair E04 – E13, also 38 cm from the wall as E04-R03. Ensemble normalized display with colour coded amplitudes.

The total variability of seismic signals is shown exemplarily for one emitter (E04) and 14 related receivers in Figure 6.8 as trace normalised wiggle plots. The same compilation of data but displayed in an ensemble normalised version and with colour coded amplitudes is displayed in Figure 6.9. The appropriate receiver numbers can be found in each sub plot in the top line, for example: EBSTD-E04-R01.04T, for the emitter-receiver pair E04-R01. All eight seismic sections are compiled in Appendix I.

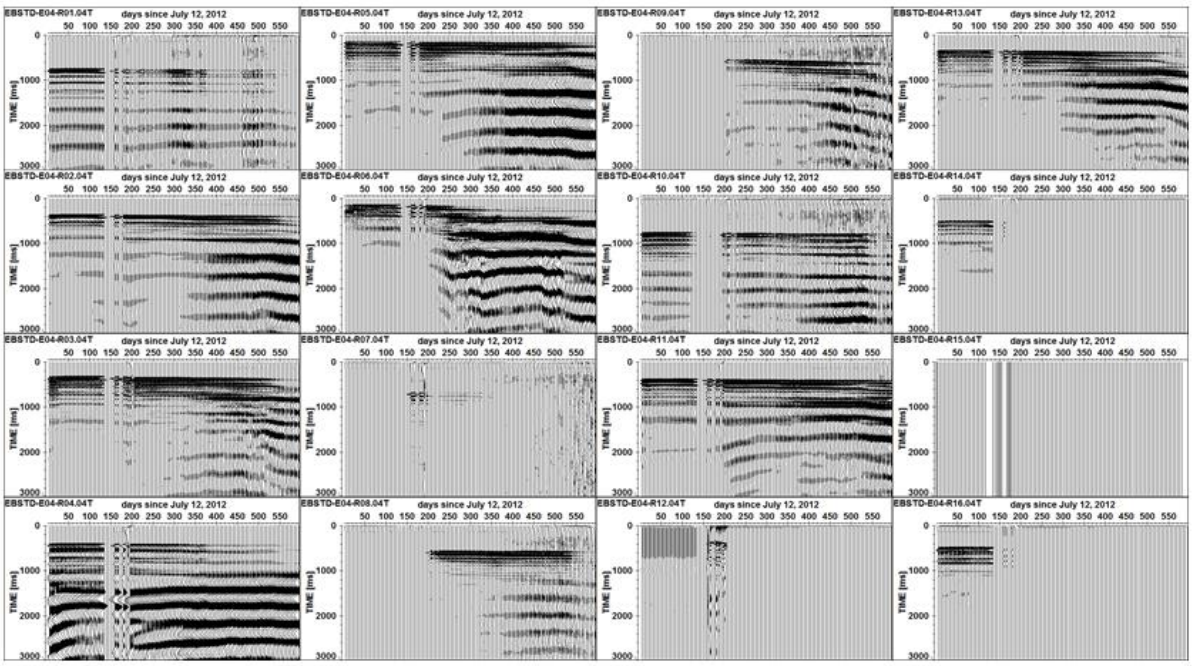

Fig. 6.8 Compilation of seismic sections belonging to emitter E04 and 14 receivers (R01- R16, in R15 the voltage signal for the emitter is recorded, not captured here). All sections are trace normalized and only every 5th trace is plotted.

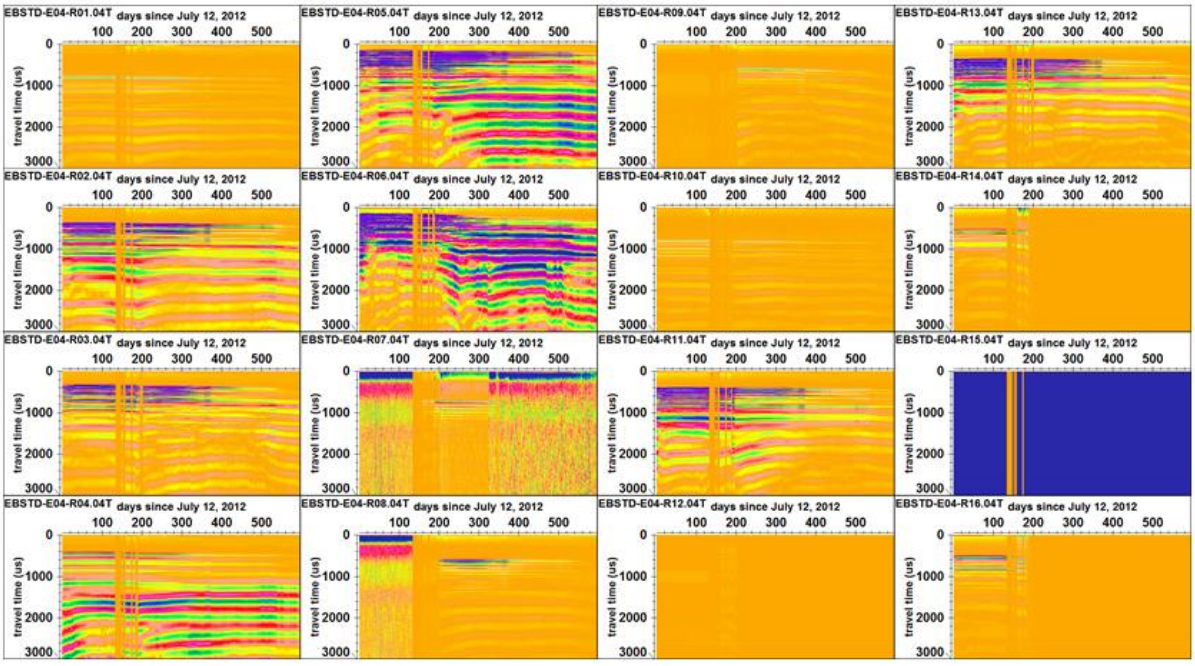

Fig. 6.9 Same data set (E04-RNN) as in Fig. 6.8 but the total display is ensemble normalized and amplitudes are colour coded.

For some emitter – receiver combinations the propagation paths cross the interface OPA-bentonite or reverse, for example E04 → R16 (OPA → bentonite). In such cases the interpretation becomes more complicated. A data set can be seen in Figure 6.10. The recording ends around day 185 after the excavation front passed the receiver completely and the receiver was removed.

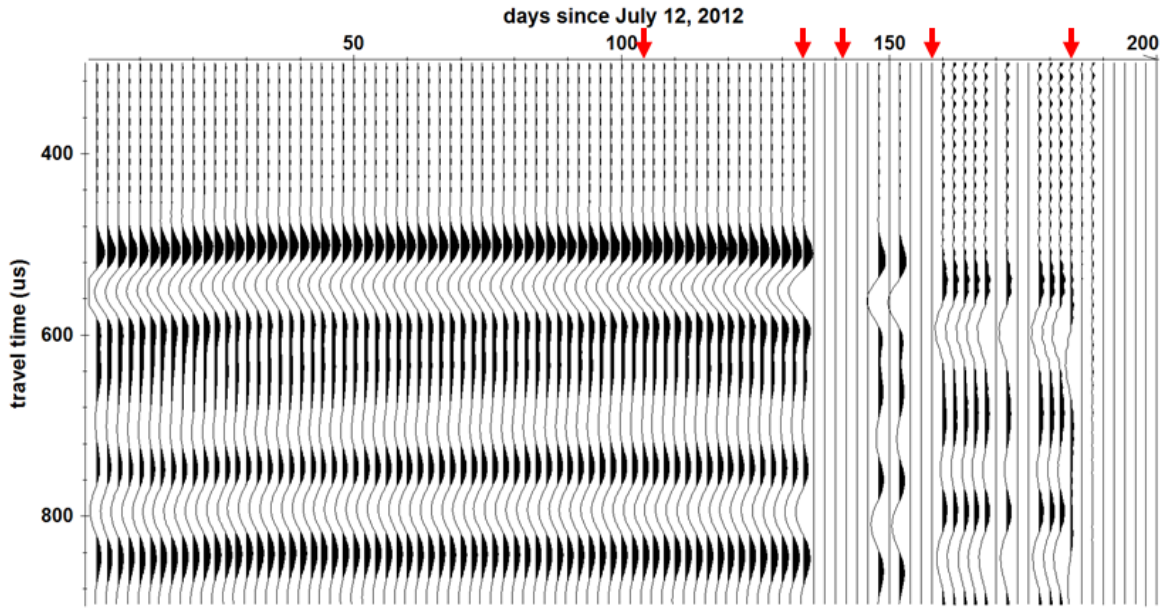

Fig. 6.10 Ensemble normalized trace plot for E04 (in OPA) – R16 (in bentonite). Only every 2nd trace is plotted.

The red arrows in Figure 6.10 indicate several stages of the diamantling operation. For details see also Figure 4.2 and Table 4.2.

- At day 104 the destruction of the concrete plug started.
- At day 134 the plug removal was finished and the bentonite removal started. Cables were disconnected for several days.
- At day 141 circa 2.15 m of compacted bentonite left between the excavation front and receiver R16.
- Around day 158 circa 1.03 m of compacted bentonite left between the excavation front and receiver R16.
- At day 184 the excavation front passed receiver R16. It was removed afterwards.

7 Results and preliminary interpretation

One of the key questions is how do the seismic parameters react to changes in the rock mass as a consequence of the advancing dismantling. For this reason three emitter – receiver pairs with the same orientation of the propagation paths (orientation to bedding) and with different distances from the interface bentonite-OPA were chosen. Please note that the distribution of emitters and receivers in the seismic array (see Figure 2.3) and the limited availability of usable seismic data did not allow to use more or arbitrary orientations and distances for a optimal comparison.

7.1 Dependency of seismic parameters from distance to the interface bentonite - OPA

Seismic trace plots for three different distances from the interface show a clear qualitative trend: the further the travel paths from the bentonite-OPA interface the less the P-wave phase variation is distinctive. In general this holds for travel times, frequencies and amplitudes of first arrival phases. The following emitter – receiver pairs were selected for closer analyses of the distance dependency (see also Figure 2.3):
E04-R13 – 38 cm from the interface, BEB-25 – BEB-27, distance: 879.1 mm
E07-R04 – 138 cm from the interface, BEB-27 – BEB-25, distance: 877.2 mm
E03-R10 – 208 cm from the interface, BEB-25 – BEB-27, distance: 880.8 mm

In Figure 7.1 the data are shown in an ensemble normalised wiggle plot. In Figure 7.2 the same data are presented in a colour coded point mode, whereas Figures 7.3 and 7.4 depict the frequency contents of the seismic sections. The figures show qualitatively how diverse the seismic wave field is affected by the EDZ / EdZ. A strong dependency from the distance of the interface bentonite-OPA is obvious. The area near the interface seems to be more affected what can be clearly seen by travel time increase, amplitudes becoming weaker and the shape of the first arrival phases change. This is in good accordance with features which are characterizing the degree and the extent of an EDZ.

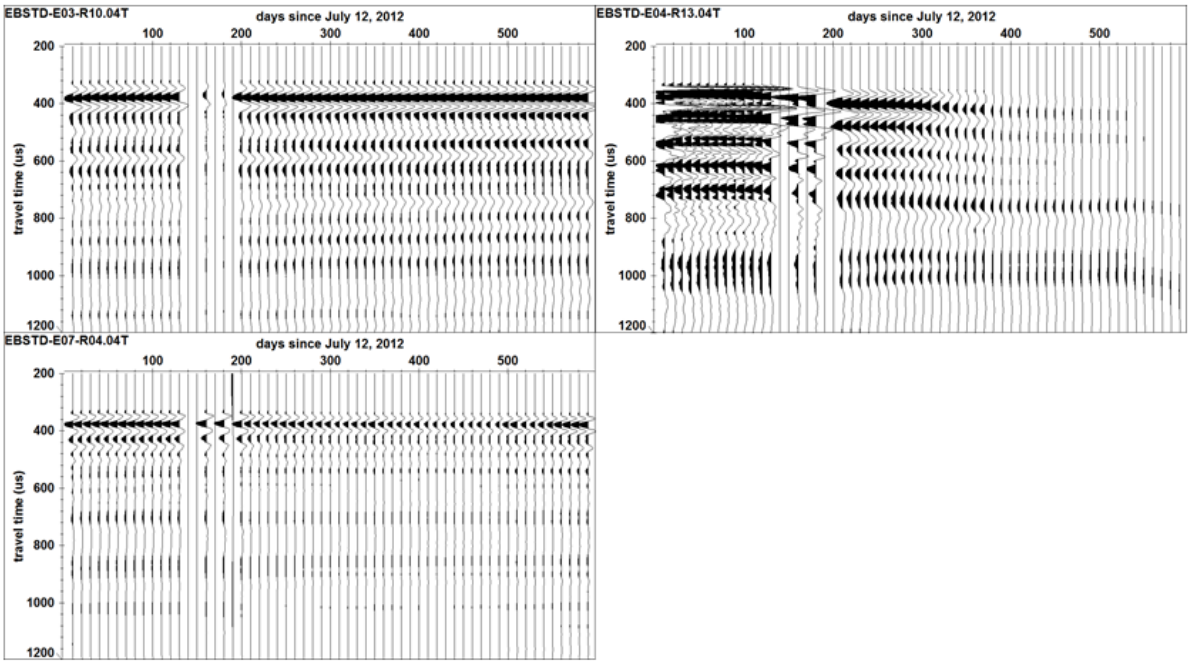

Fig. 7.1 Seismic section from three distances from the interface bentonite-OPA. E03-R10, 208 cm, E07-R04, 138 cm and E04-R13, 38 cm. Ensemble normalized, only every 10th trace plotted.

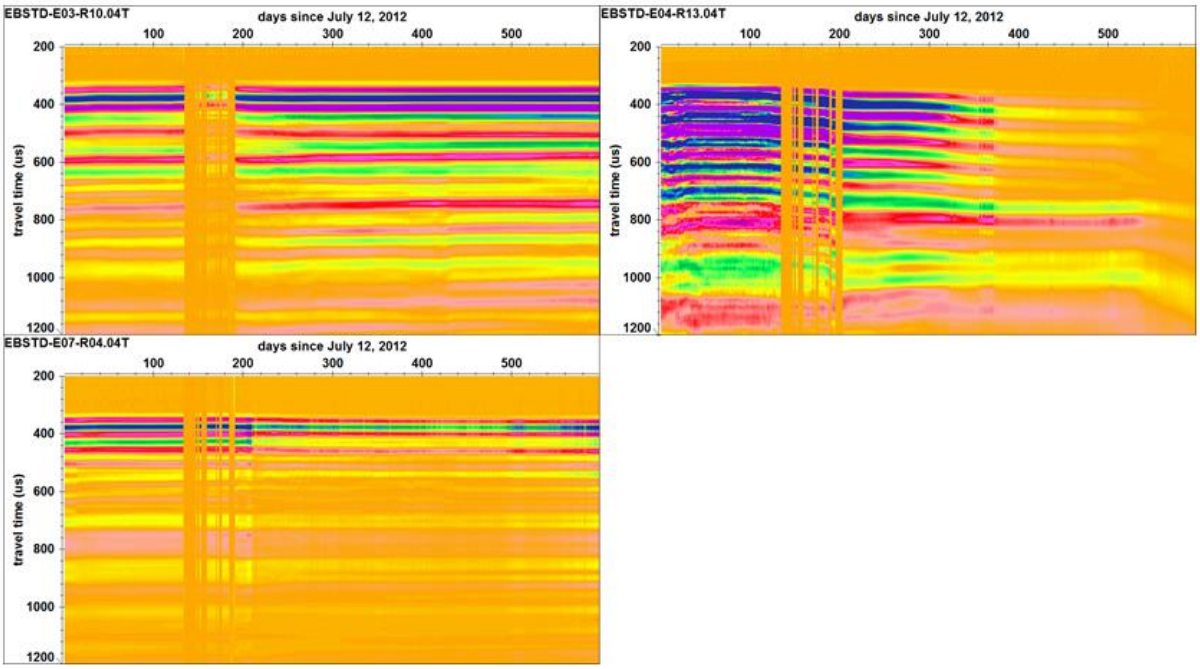

Fig. 7.2 Same data sets as in Fig. 7.1 but amplitudes are colour coded.

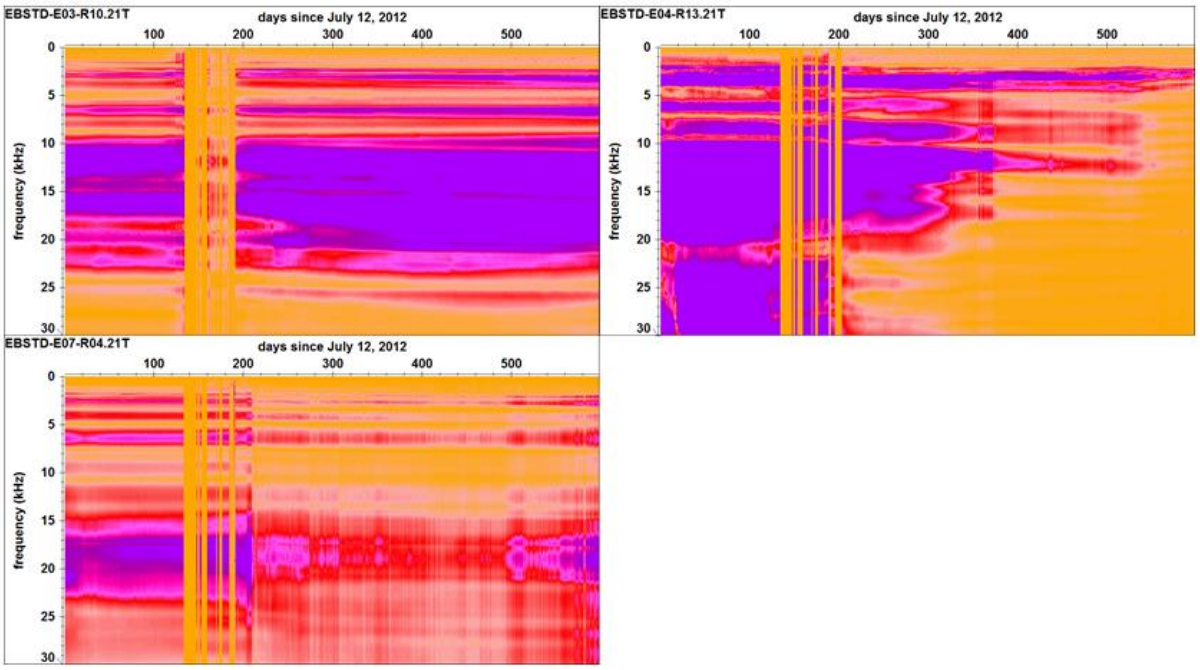

Fig. 7.3 Frequency content for the 3 seismic sections shown in Figure 7.1. Ensemble normalised and amplitudes are colour coded.

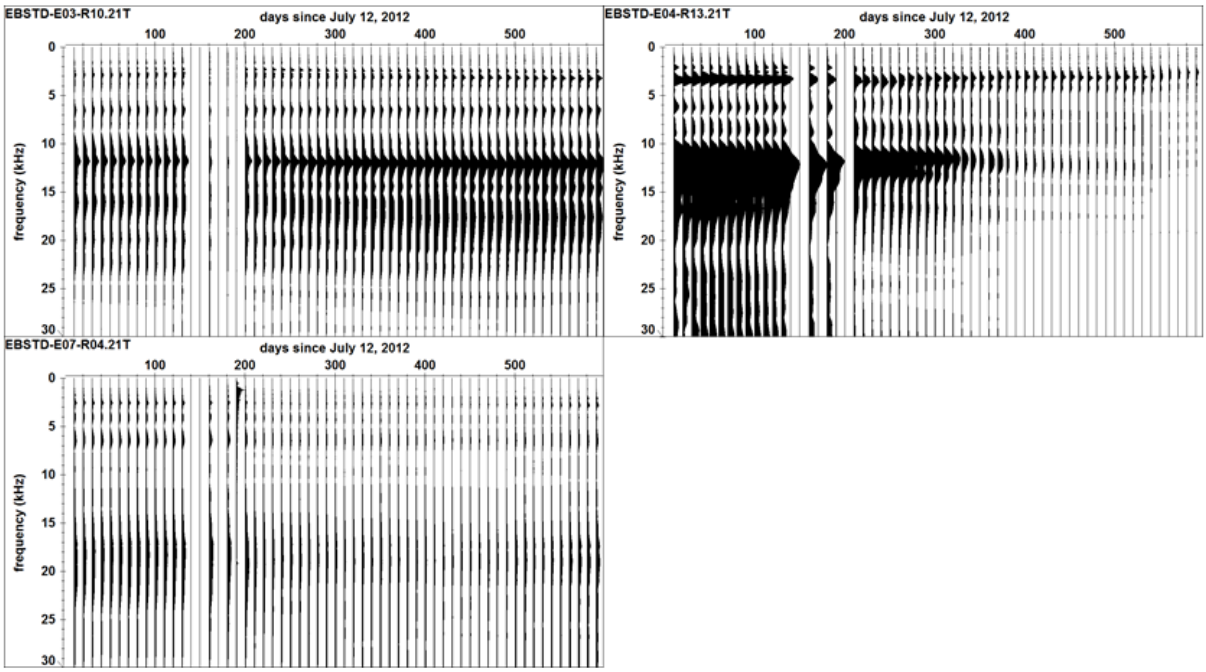

Fig. 7.4 Frequency content for the 3 seismic sections shown in Figure 7.1. Ensemble normalised wiggle plot.

For a more quantitative interpretation the seismic P-wave velocities of the first arrival phases were calculated as described in section 5.1. Because of the good data quality in many cases the negative part of the first arrival phase was chosen for travel time picking. In Figure 7.5 the derived v_p is plotted for E04-R03. Both transducers located at a distance of 38 cm from the interface in the OPA.

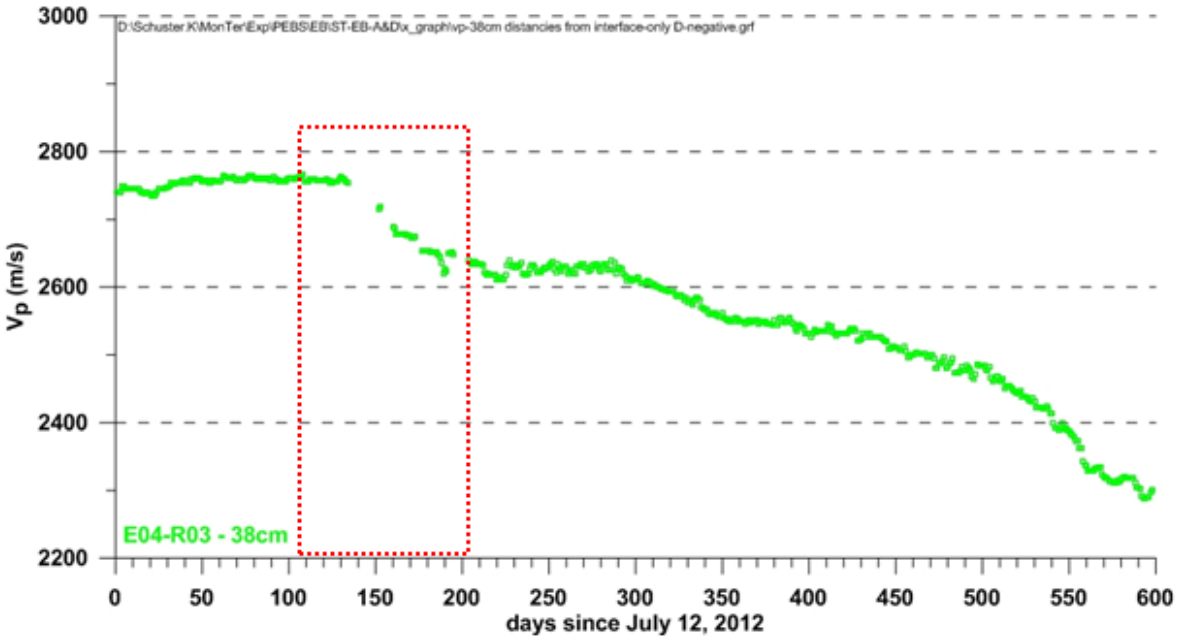

Fig. 7.5 Seismic P-wave velocity calculated from first arrival phase (negative part). The dotted rectangle indicates the start and the end of the dismantling.

The v_p reaches after 70 days a stable plateau around 2760 m/s. According to this v_p we assume that the EDZ / EdZ recovered or was on the way to recover. EDZ related features like micro cracks most probably were closed as a result of the hydration and the pressure of the swelling bentonite. An appropriate discussion was given in section 3 (cf. Figure 3.2). After the concrete plug was removed, around day 135 the v_p starts to drop with a very steep gradient. At this moment still 2.9 m of compacted and homogenized bentonite was left to the boreholes where both transducers are placed (cf. Figure 4.2). After 65 days a v_p of 2620 m/s is reached then it stays stable over 100 days before v_p decreases continuously to 2300 m/s, a velocity which indicates very clearly the existence of an EDZ.

In order to emphasize the reliability of the data results from a second emitter - receiver pair are plotted in Figure 7.6. The pair E04-R03 has the same distance (38 cm) to the wall but ray paths run upwards (vertical) whereas for E03-R13 ray paths run horizontal. For both the orientation towards bedding is 45°. Both trends are similar. Small differences could be

related to the way how the dismantling front approaches the transducers, suddenly for E04-R03 (boreholes BEB-B25-BEB-B26) and rather gradually for E04-R13 (boreholes BEB-B25-BEB-B27, cf. Fig. 4.2). Small scale variations of rock properties could also be responsible.

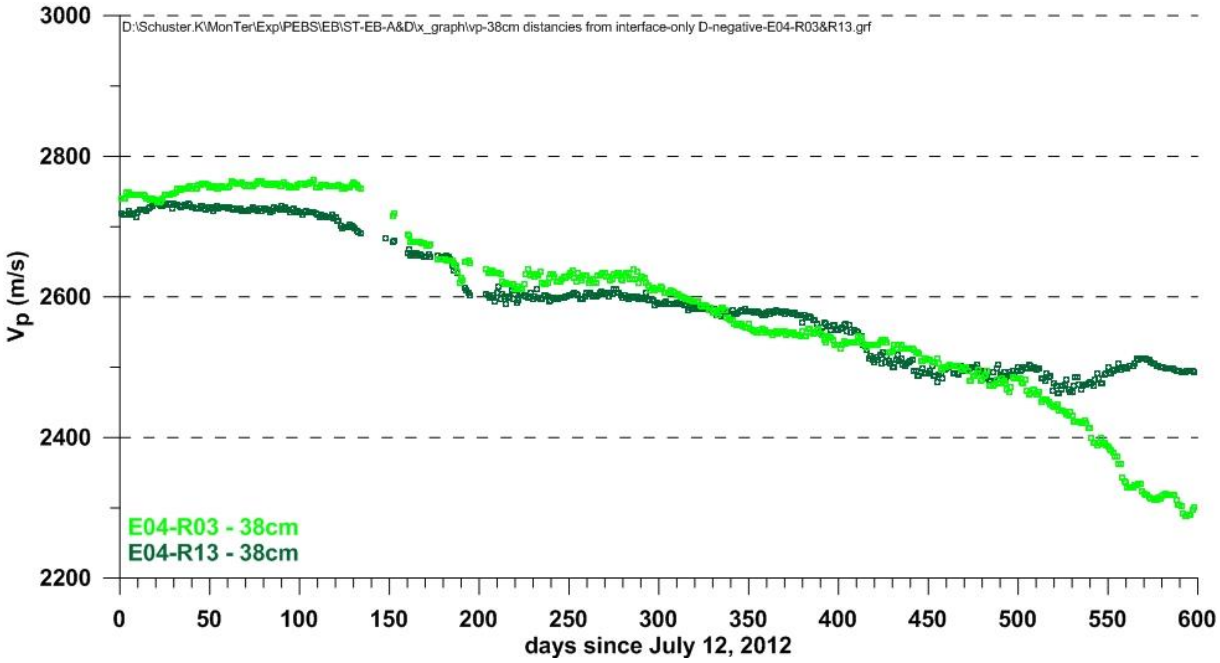

Fig. 7.6 Seismic P-wave velocity for two emitter - receiver pairs at the same distance from the interface but different orientations of related travel paths.

The evolution of v_p at three different distances from the wall can be seen in Figure 7.7. For the chosen emitter – receiver pairs the distances are:

E04 – R03: 38 cm
E07 – R04: 138 cm
E03 – R10: 208 cm

For all three pairs the ray paths run parallel to the wall and between the same boreholes (BEB-B25 – BEB-B27). The v_p for the 38 cm distance was discussed before. v_p for the 138 cm distance starts with the same value (2620 m/s) like the one for the 38 cm distance. Whereas v_p (38 cm) starts to decrease already during the dismantling operation the v_p (138 cm) stays constant until day 290, nearly 90 days after the dismantling was finished. Afterwards it drops with a weak slope. At a distance of 208 cm from the wall the v_p stays constant over the total observation time of 598 days. The rock mass at a distance of 208 cm from the wall seems to be unaffected from the dismantling activities and the opened niche.

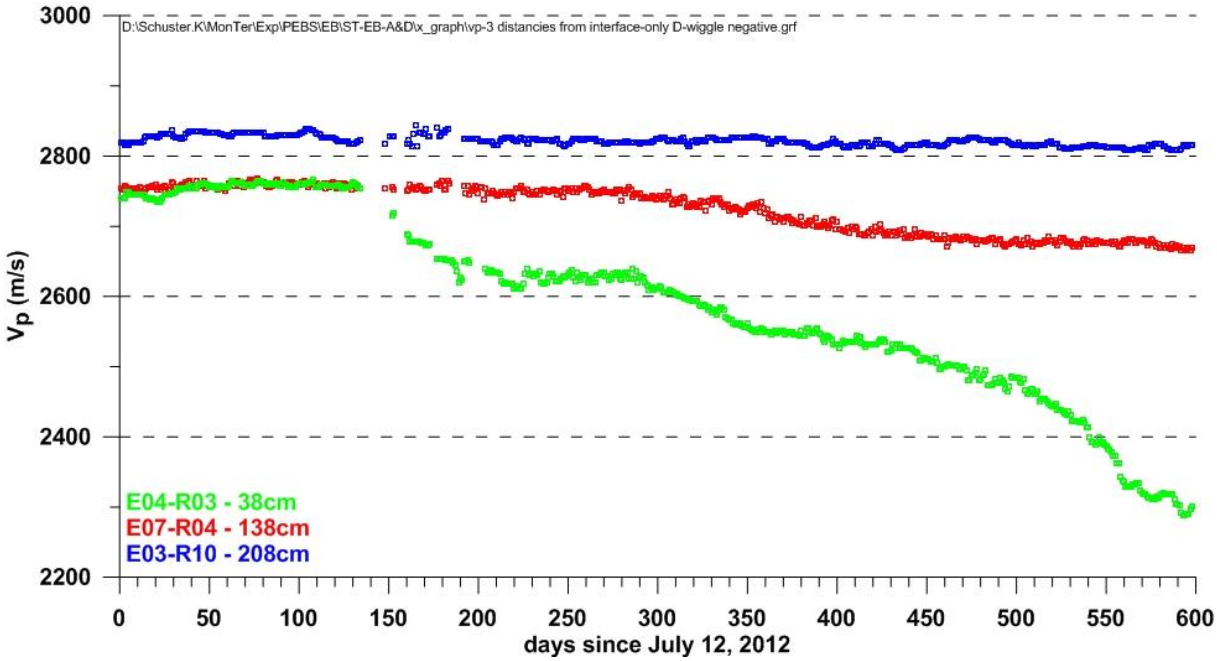

Fig. 7.7 Seismic P-wave velocity from emitter – receiver pairs at different distances from the interface. All three propagation paths run parallel to the wall.

Amplitudes of seismic traces were also derived for the characterization of the evolution of the OPA. In the following three Figures 7.8 – 7.10 the mean of the sum for each seismic trace is plotted. This parameter is closely linked to the attenuation of seismic wave energy in the rock.

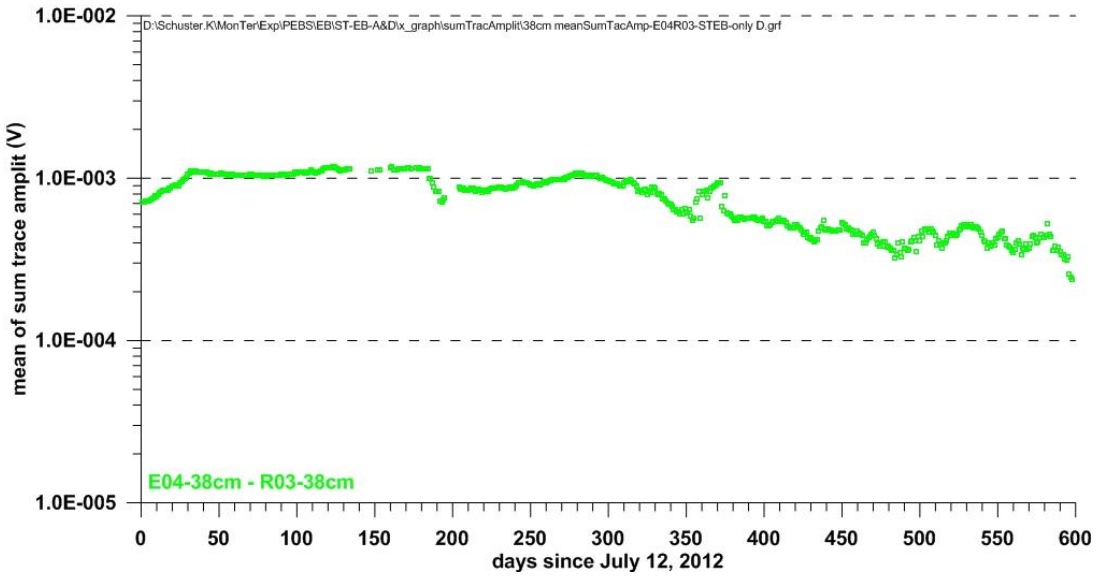

Fig. 7.8 Seismic amplitudes calculated as mean of each sum of trace amplitudes for E04-R03 at 38 cm distance from the wall.

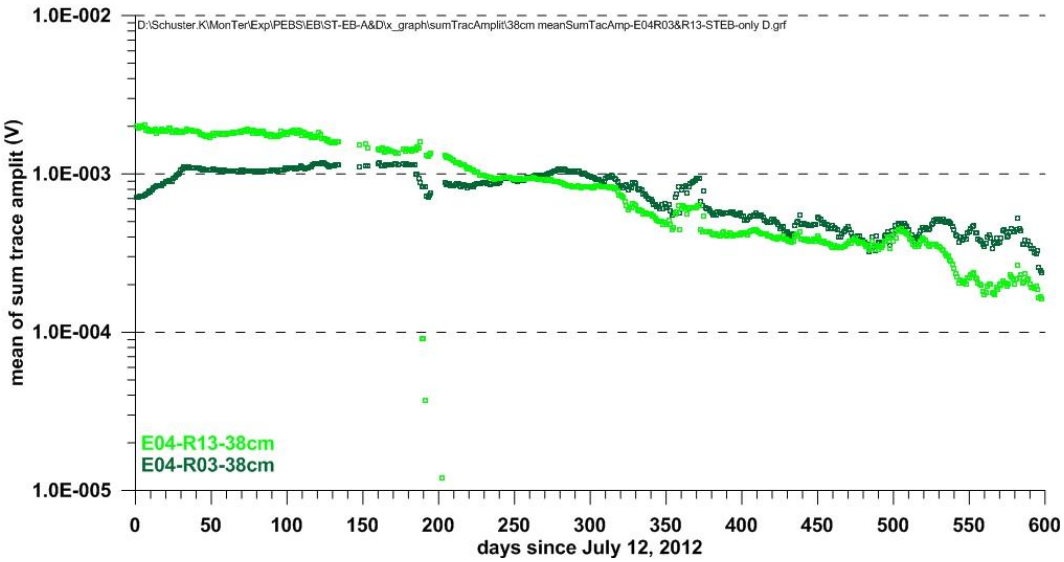

Fig. 7.9 As Figure 7.8 but E04-R13 data (also 38 cm from the wall) added.

Finally the amplitude evolution from three distances from the interface are compiled in Figure 7.10. Amplitudes for the 38 cm distance show a similar trend like the v_p (cf. Figure 7.7). The drop of the amplitudes from the 138 cm distance is astonishing and does not have an equivalent in the v_p graph. The 208 cm amplitude graph shows a continuous increase, except the disturbance during the dismantling. At the moment we have no explanation for the trends in the amplitudes. Maybe differences in the emitter signal as discussed in section 6.1 could be one of the reasons.

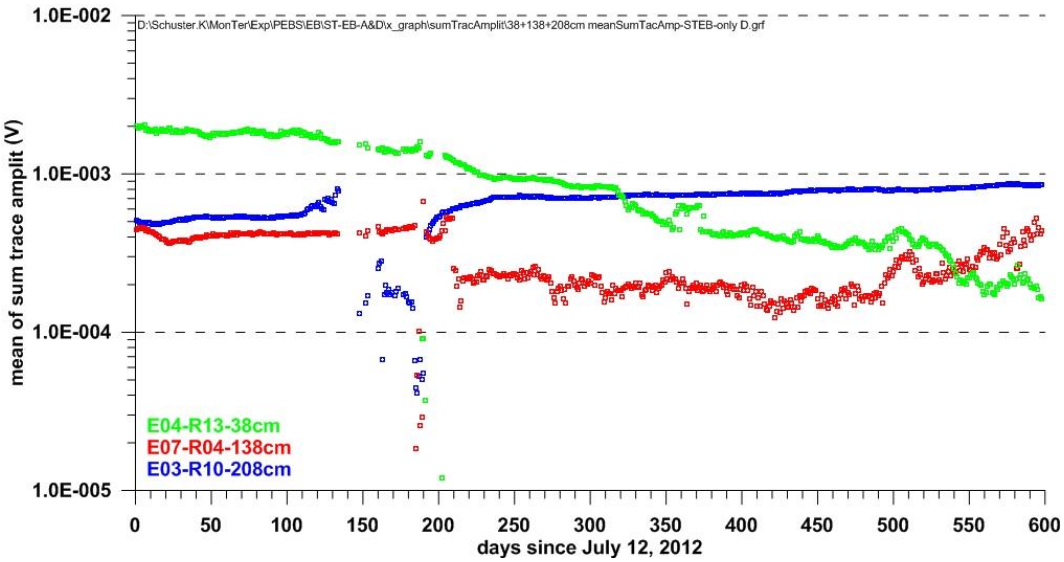

Fig. 7.10 Seismic amplitudes from different distances of the propagation paths of the seismic wave field from the interface bentonite-OPA.

The v_p data for the emitter – receiver pair E04-R13 is exemplarily compared with the nearby recorded total pressure data in Figure 7.11. The sensor is located at the interface bentonite – OPA at a distance of 2.9 m from the back side of the concrete plug. For the v_p determination the better correlative second part of the P-wave phase was chosen (cf. top in Figure 7.11 only every 2nd trace is plotted, trace normalized plot).

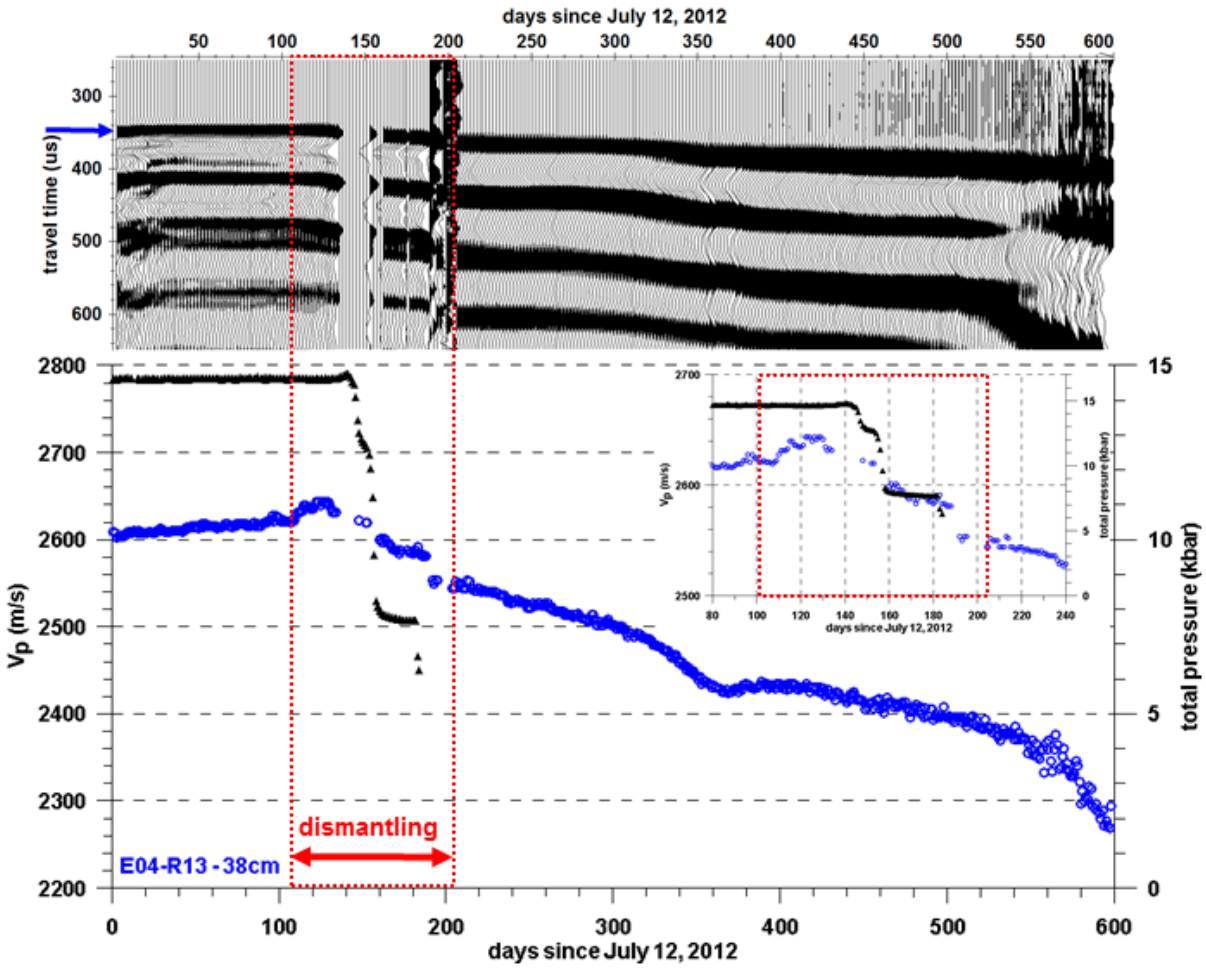

Fig. 7.11 Comparison of evolution of total pressure (black triangles) and seismic P-wave velocities (derived from second part of P-wave phase, blue circles, E04-R13). On top the seismic section is plotted. The relevant phase starts at 340 µs.

Remarkable is that immediately after the dismantling started a significant change in the seismic signal and consequently in v_p is visible although the thickness of the bentonite until the first transducer (borehole BEB-B25, cf. Fig. 4.2) is 2.9 m.

7.2 Comparison of phase 1 and phase 2 data

The experiment gives the unique opportunity to compare seismic parameters recorded under identical situations over a time of 12 years (April 2002 – March 2014), with an interruption of 8.6 years.

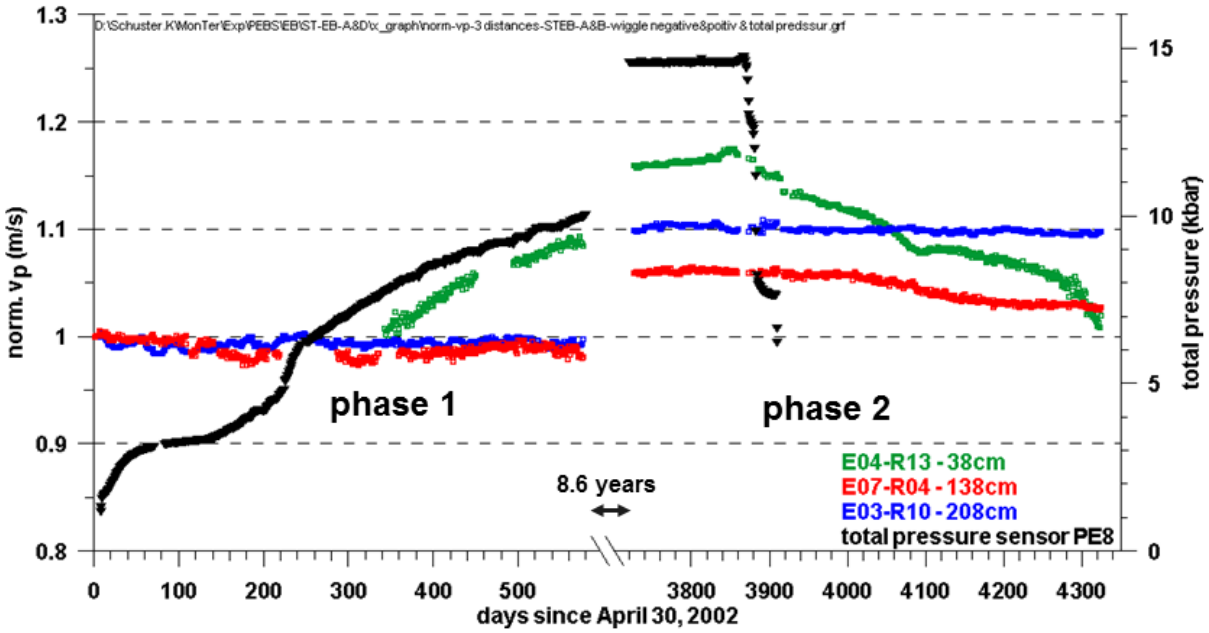

Fig. 7.12 Normalised seismic P-wave velocities for three distances from the interface. Data were normalized with the mean value from phase 1 (days 1-3, for E04-R13: days 342 – 344).

In Figure 7.12 the normalized v_p is plotted for three distances from the wall. For the normalization the first available phase picks from each phase 1 data set was taken (day 1-3). For the E04-R13 data set the first correlative data were available around day 342, therefore days 342 – 344 had to be taken in this case. Additionally the total pressure data as discussed before are added. In phase 1 v_p at 138 cm and 208 cm depths stays nearly constant what implies that no major changes in the rock were going on after the closure of the niche and the hydration of the bentonite. It seems that there was no EDZ developed. For the 38 cm distance it is completely different. The normalized v_p is increasing till the end of the monitoring in phase 1. The existing EDZ seems to be on the way to recover. When values around day 1 could be used for the normalization the increase would be by far more pronounced.

Remarkable are the jumps between phase 1 and phase 2 data, even with the limitation discussed for the 38 cm depth data. In detail the jumps are:

Norm. v_p at 38 cm: only 8 % because days 342 - 344 had to be taken for the normalization
Norm. v_p at 138 cm: 8 %
Norm. v_p at 138 cm: 10 %

The total pressure data jump, where the sensor is located at the bentonite – OPA interface is about 40 %. The fact that the v_p jump at 208 cm distance is higher than at 138 cm could be related to small scale variation of rock parameters as discussed in section 2.2 (cf. also Figure 2.7).

8 Overall results and conclusions

Within an engineered barrier experiment the evolution of the potential host rock Opalinus Clay (OPA) and the backfill material FEBEX bentonite (Almeria, Spain) was characterized with the help of seismic parameters. Especially EDZ / EdZ features were of interest. It is an unique opportunity to observe changes in seismic parameters over 12 years.

After 8.6 years a seismic array consisting of 24 piezoelectric transducers could be reactivated. It was used between April 2002 and November 2003 over 576 days for a seismic monitoring on a daily basis (phase 1). The seismic array covers a volume of 1m x 1m x 2m in the OPA and a part of the backfill. During this first phase the EDZ created by the excavation of the EB niche was on the way to recover (sealing of EDZ) according to the seismic parameter changes.

The resumption of the long-term monitoring started in July 2012 five month before the complete dismantling of the EBS (phase2) and is ongoing. Potentially 112 different propagation paths of the seismic wave filed can be used. Seismic parameters like P-wave velocity, amplitudes and the frequency content of seismic traces were derived. As a result of the dismantling the gradual recreation of an EDZ / EdZ was observed with the help of these seismic parameters. The evolution is different at different depth levels with different intensities.

Seismic P-wave velocities jumped by about 10 % between the end of phase 1 and the restart after 8.6 years (phase 2) whereas the total pressure values, measured nearby, jumped by about 40 %.

Several derived seismic parameters are in good accordance with results gained in the initial phase of the EB Experiment and from other experiments performed by BGR.

Although not all correlations and dependencies between varying seismic parameters and related rock property changes are completely understood until now it is shown however that seismic monitoring is a useful tool for the characterization of continuously ongoing changes of rock properties.

9 Acknowledgements

The research leading to these results has received funding from the European Atomic Energy Community's Seventh Framework Programme (FP7/2007-2011) under grant agreement n° 249681.

The BGR contribution is co-funded by the German Ministry of Economy and Technology (BMWi), FKZ 02 E 10689.

We thank Thierry Theurillat (swisstopo) for his technical support of several spontaneous on-site work.

10 References

Aitemin (2001): Engineered Barrier Emplacement Experiment in Opalinus Clay “EB” Experiment. TEST PLAN. Madrid, 76 pp.

Aitemin (2007): Engineered Barrier Emplacement Experiment in Opalinus Clay “EB” Experiment. Sensors data report Nº 19 and Mont Terri TN2007-11. Period 22/11/2001 to 30/06/2007, 38 pp.

Aitemin (2012): Engineered Barrier Emplacement Experiment in Opalinus Clay “EB” Experiment. Sensors data report Nº 29. Period 22/11/2001 to 30/06/2012 (3874days), 35 pp.

Furche, M. & Schuster, K. (2014): Engineered Barrier Emplacement Experiment in Opalinus Clay “EB” Experiment. Geoelectrical monitoring of dismantling operation. PEBS Deliverable D2.1-9.

Mayor, J. C., et al, (2007): Engineered barrier emplacement experiment in Opalinus Clay for the disposal of radioactive waste in underground repositories. In: Bossart, P. and Nussbaum, C. (Eds.): Mont Terri Project – Heater Experiment, Engineered Barriers Emplacement and Ventilation Tests (p. 115-179). – Rep. Swiss Geol. Surv. I.

Palacios, B., Rey, M., Garcia-Siñerez, J. L., Villar, M. V., Mayor, C & Velasco, M. (2013): Engineered Barrier Emplacement Experiment in Opalinus Clay “EB” Experiment. As-built of dismantling operation. PEBS Deliverable D2.1-4

Sandmeier, K.-J. (2013): Reflex-Win, Version 7, Sandmeier scientific software, http://www.sandmeier-geo.de/

Schuster, K., Alheid, H.-J. & Böddener, D. (2001): Seismic investigation of the Excavation damaged zone in Opalinus Clay, Engng. Geol. 61: 189-197.

Schuster, K. (2002): Seismic in situ Methods for the Characterisation of Excavation Damaged Zones – Final Report, Projektträger des BMBF und BMWi für Wassertechnologie und Entsorgung, Contract-No. 02E9098, 155 p.

Schuster, K. (2004): Engineered Barrier Emplacement Experiment in Opalinus Clay; Seismic Characterisation of the EDZ – Seismic Long Term Observation in the EB Niche, Final EC Report, FIKW-CT-2000-00017, 138p.

Schuster, K., Alheid, H.-J., Kruschwitz, S., Siebrands, S., Yaramanci, U., Trick, T., Manthei, G. (2004a), Observation of an Engineered Barrier Experiment in the Opalinus Clay of the Mont Terri Rock Laboratory (CH) with Geophysical and Hydraulic Methods, 2 posters and abstract, Euradwaste'04, Radioactive waste management - Community policy and research initiatives, Sixth European Commission Conference on the Management and Disposal of Radiactive Waste, 29. March - 1. April 2004, Luxembourg.

Schuster, K. (2007): High resolution seismic investigations within the VE-Experiment, Mont Terri Technical Report TR 07-06, swisstopo, Wabern, Switzerland.

Schuster, K. (2012): Detection of borehole disturbed zones and small scale rock heterogeneities with geophysical methods, Proceedings of the EC-TIMODAZ-THERESA International Conference, Impact of thermo-hydro-mechanical chemical (THMC) processes on the safety of underground radioactive waste repositories, Luxembourg, 29 Sep. - 1 Oct. 2009, p. 135-145

Schuster, K. (2014): Engineered Barrier Emplacement Experiment in Opalinus Clay “EB” Experiment. HE-E Seismik. PEBS Deliverable D2.1-10.

Schuster, K., Furche. M., Schulte, F., Tietz, T., Sanchez Herrero, S., Velasco, M., García-Sineriz, J.-L., Gaus, I., Trick, T., Mayor, C. (2014): Engineered Barrier Emplacement Experiment in Opalinus Clay “EB” Experiment. EBS Pilotboreholes – sampling, geophysical and geotechnical measurements. PEBS Deliverable D2.1-1.

Spies, T., Heidrich, D., Kruschwitz, S. (2002): Geophysical Characterisation of the Excavation Disturbed Zone (ED-C): Acoustic emission measurements during the excavation of the EN niche – a mine-by experiment, Mont Terri Technical Note TN 2002-08 (internal report), swisstopo, Wabern, Switzerland.

11 Appendix I – seismic sections of all 112 emitter - receiver combinations

In this appendix all 112 seismic data sets which were recorded within the first 598 days of monitoring are presented as a whole. This data set contains the combination of all emitters (E01 – E08) with all related receivers (R01 – R16). At 'receiver' 15 the emitter voltage itself is recorded. It results in a total number of 66'976 single seismic traces. Not all of them were shown or discussed in the report. This compilation allows additionally a rough overview over the data quality, even main features can be compared individually, like travel time and amplitude evolutions. In Figure 11.1 the locations of all piezoelectric transducers (emitters and receivers) are shown once more.

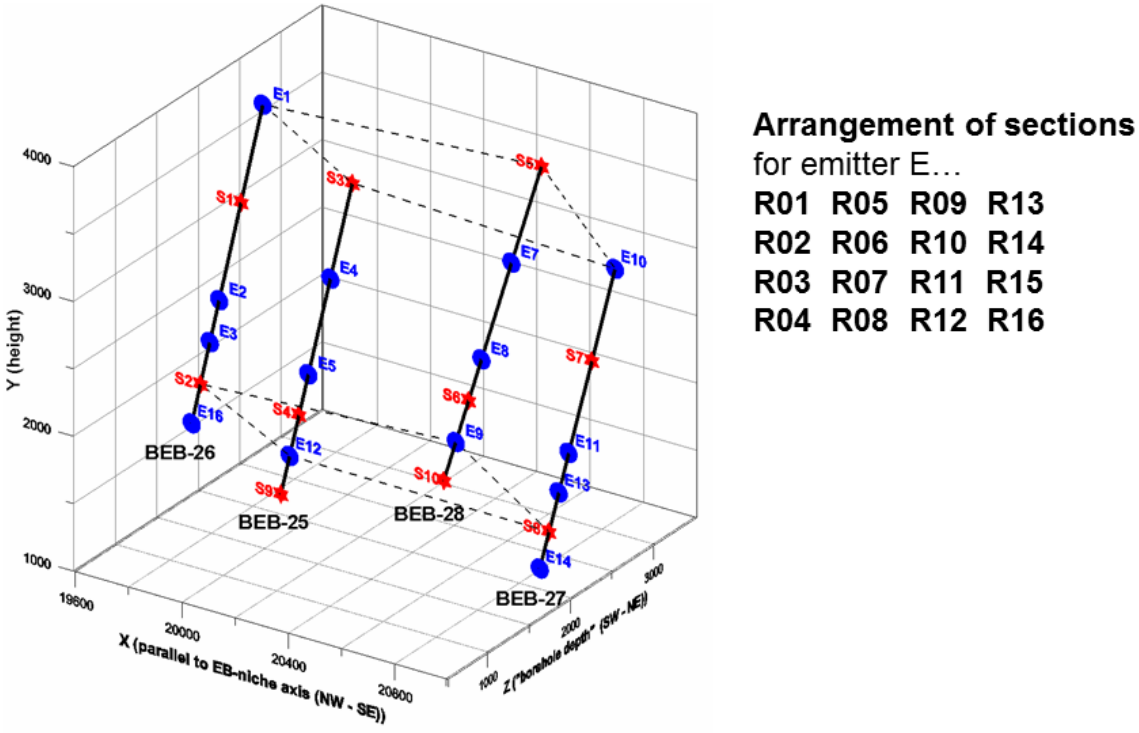

Fig. 11.1 Overview of the locations of ten emitters S01 (E01) – S10 (E10) and 14 receivers (E01 (R01) – E16 (R16)) in four boreholes.

All seismic sections are presented in the following order. They are sorted according to receiver numbers. On each page for one emitter all 14 belonging receiver combinations are displayed in a trace normalized mode (Figure 11.2 – 11.9). This plot mode allows to assess the data quality of each seismic trace individually. Subsequently the same data sets are plotted in an ensemble normalized mode, which gives access to comparison of selected traces and even of sections among themselves (Figures 11.10 – 11.17). For all ensemble

normalized plots a compromise had to be made concerning the magnification. Nevertheless it cannot be excluded that in certain situations one section is overemphasized whereas another one is hardly visible. This represents the whole dynamic range.

For a better overview a sketch of the plot order four each sub section is given in Figure 11.1 (upper right side). The appropriate receiver numbers can be found in each sub plot in the top line, for example: EBSTD-E04-R01.04T, for the emitter-receiver pair E04-R01.

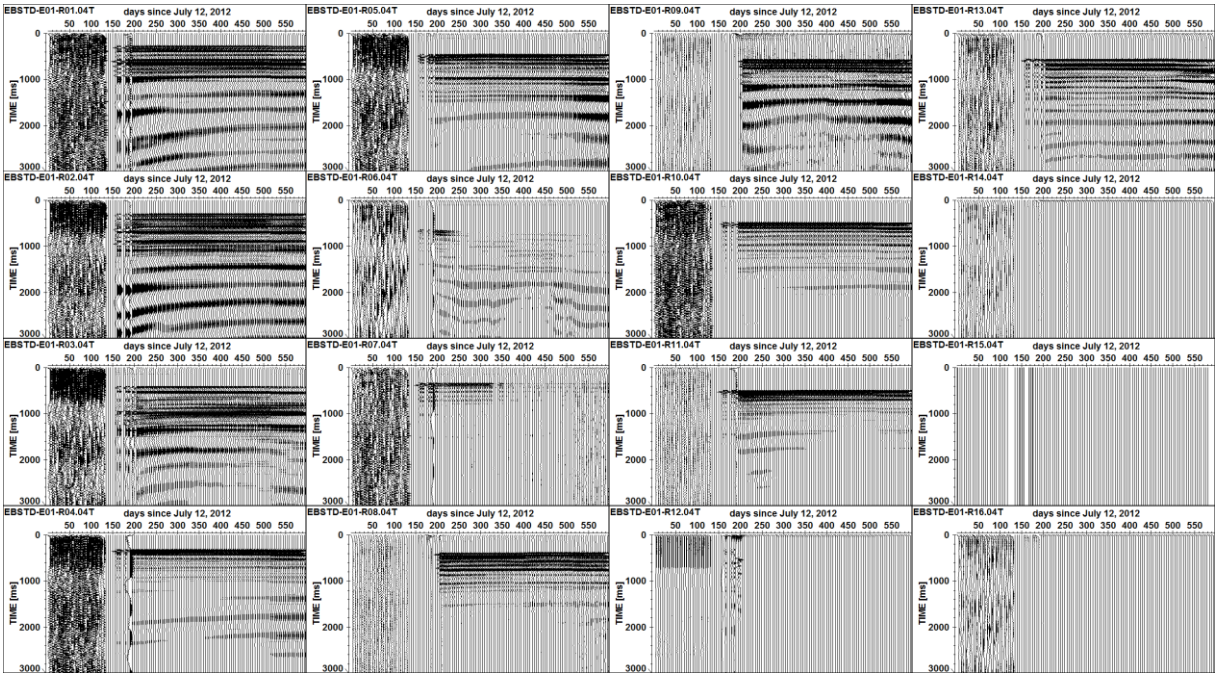

Fig. 11.2 Trace normalized seismic sections for emitter E01 with all receivers R01–R16. Only every 5th trace is plotted.

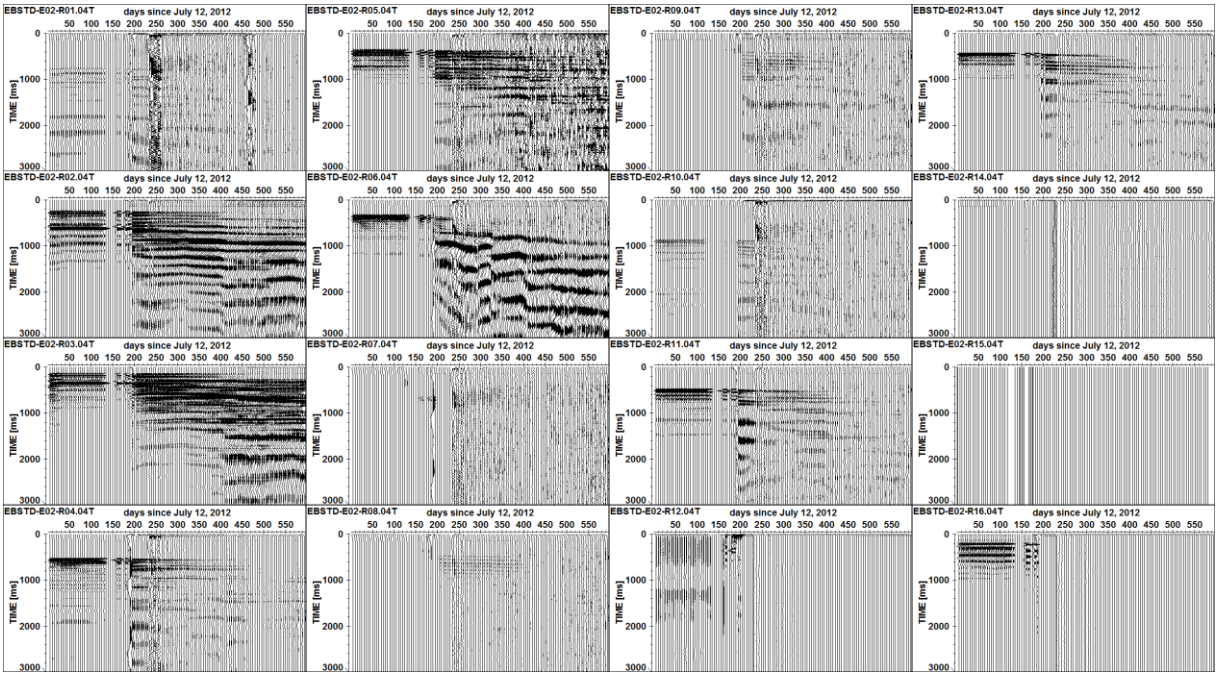

Fig. 11.3 Trace normalized seismic sections for emitter E02 with all receivers R01–R16. Only every 5th trace is plotted.

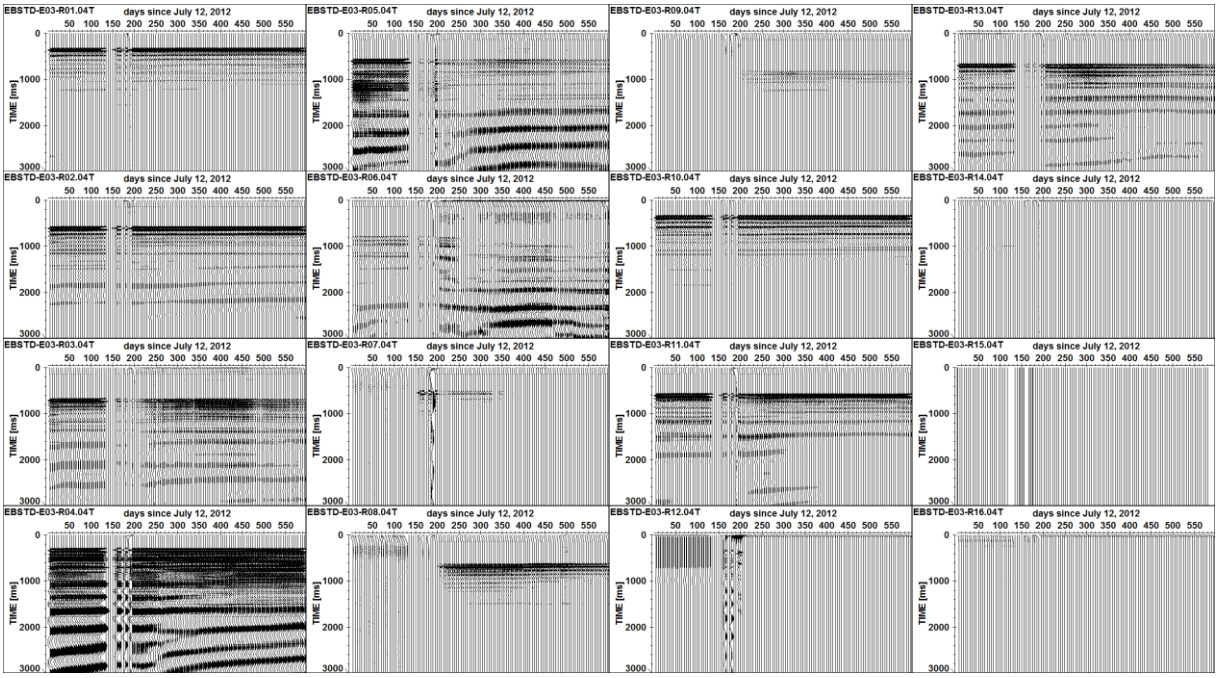

Fig. 11.4 Trace normalized seismic sections for emitter E03 with all receivers R01–R16. Only every 5th trace is plotted.

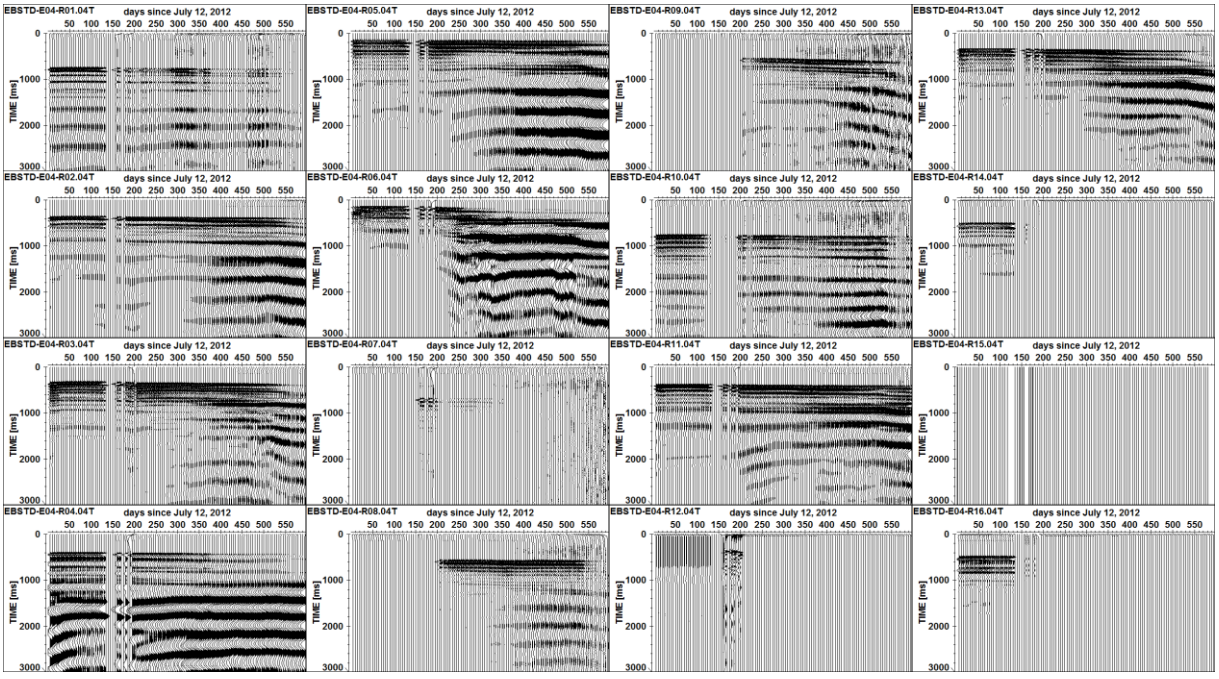

Fig. 11.5 Trace normalized seismic sections for emitter E04 with all receivers R01–R16. Only every 5th trace is plotted.

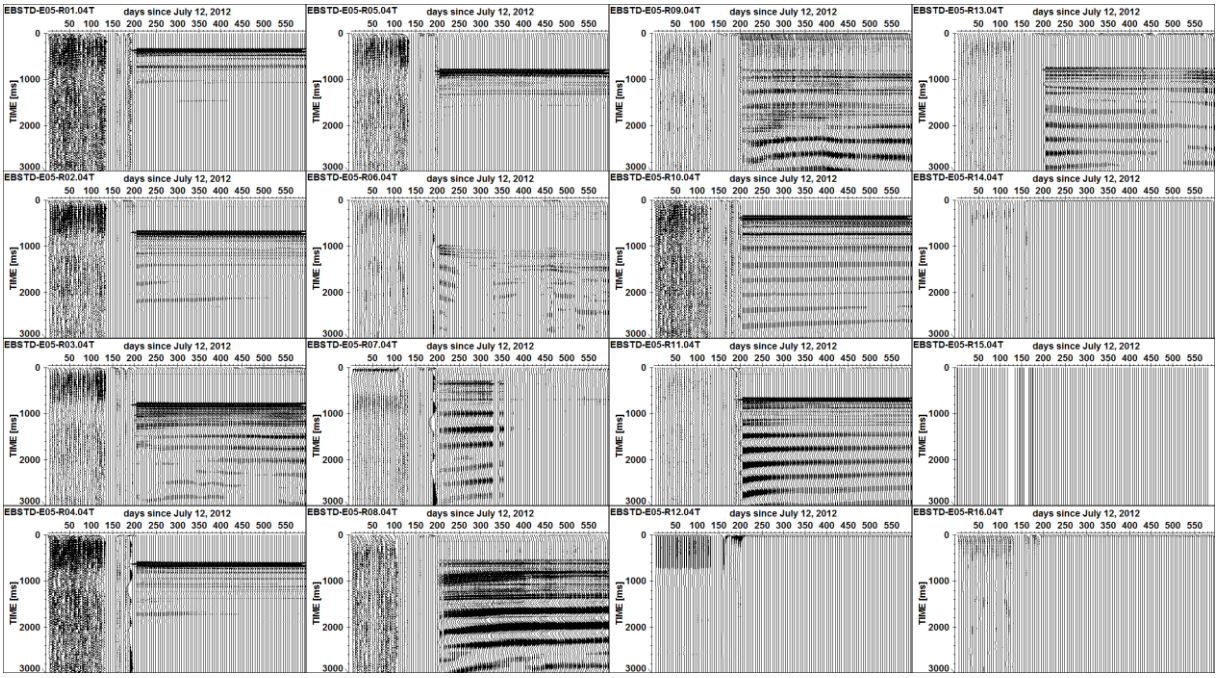

Fig. 11.6 Trace normalized seismic sections for emitter E05 with all receivers R01–R16. Only every 5th trace is plotted.

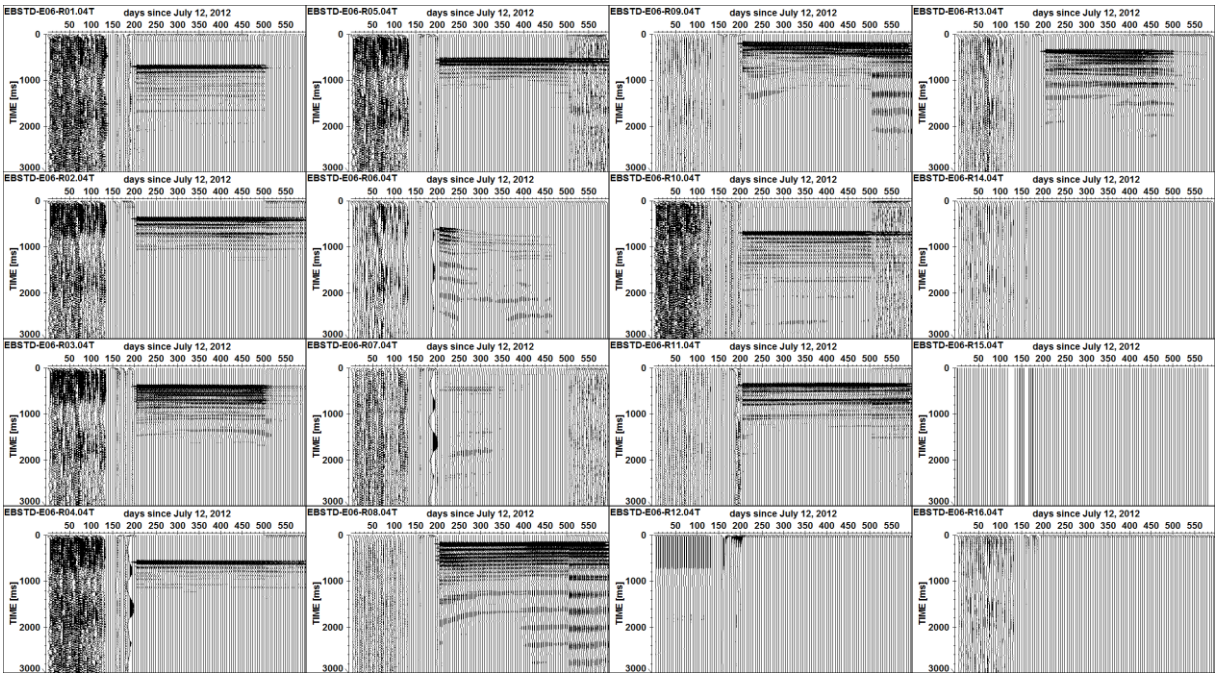

Fig. 11.7 Trace normalized seismic sections for emitter E06 with all receivers R01–R16. Only every 5th trace is plotted.

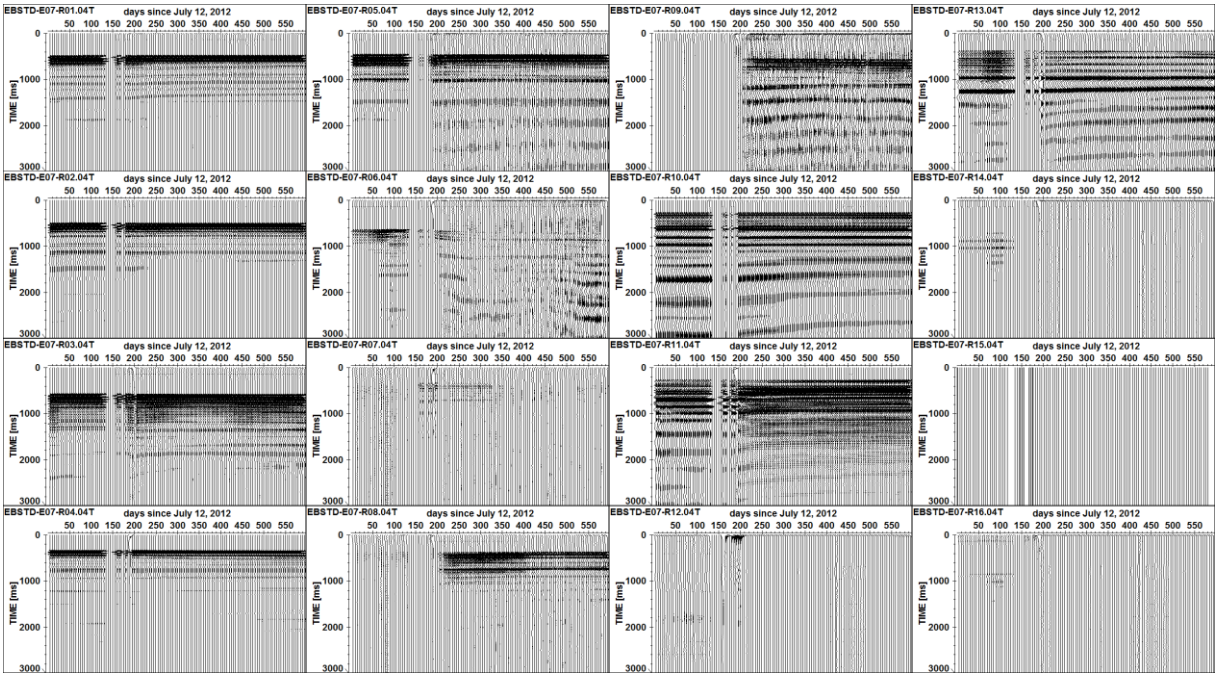

Fig. 11.8 Trace normalized seismic sections for emitter E07 with all receivers R01–R16. Only every 5th trace is plotted.

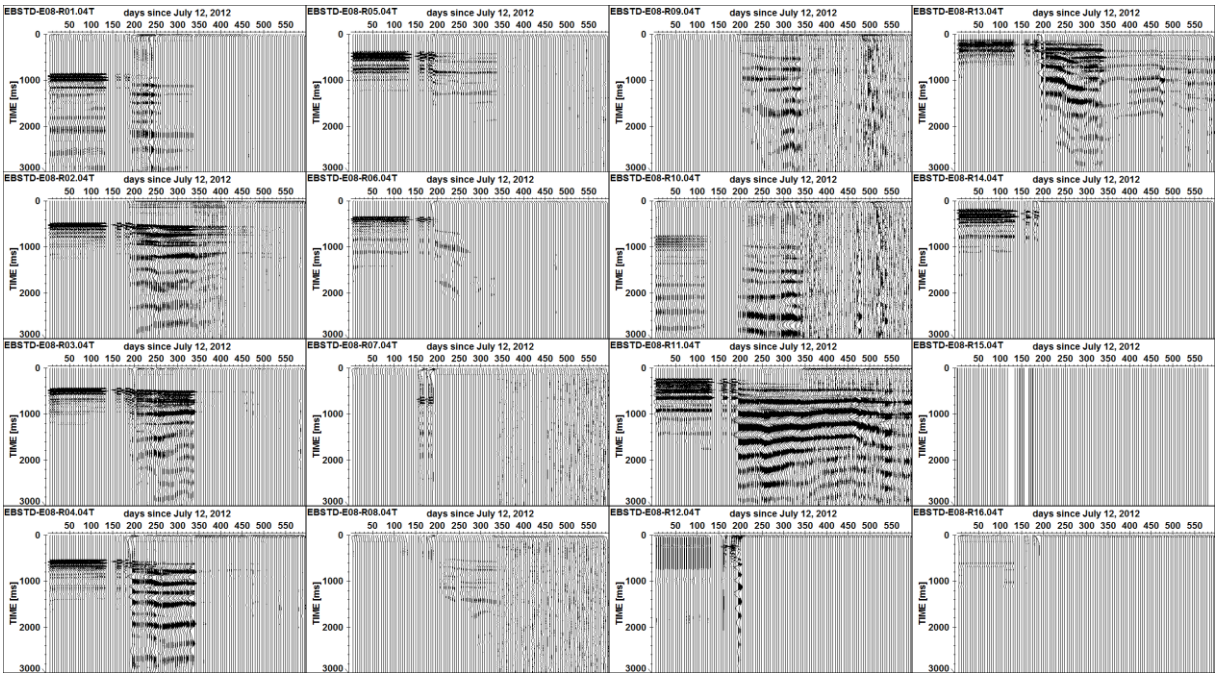

Fig. 11.9 Trace normalized seismic sections for emitter E08 with all receivers R01–R16. Only every 5th trace is plotted.

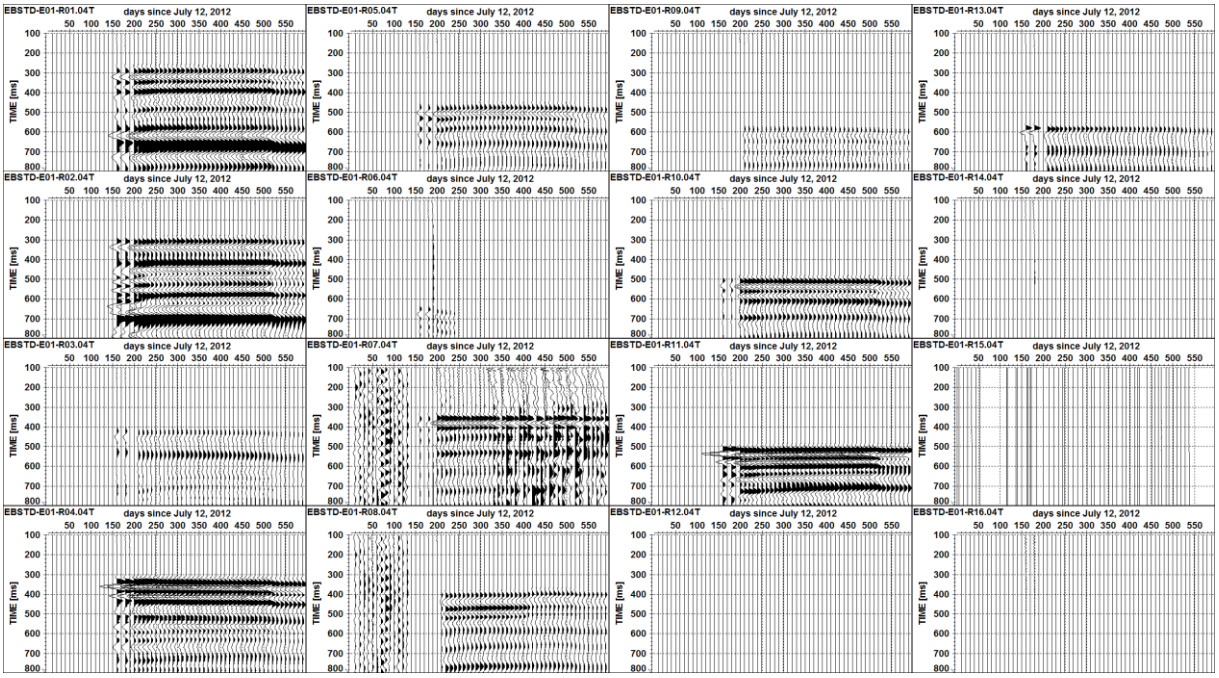

Fig. 11.10 Ensemble normalized seismic sections for emitter E01 with all receivers R01–R16. Only every 10th trace is plotted.

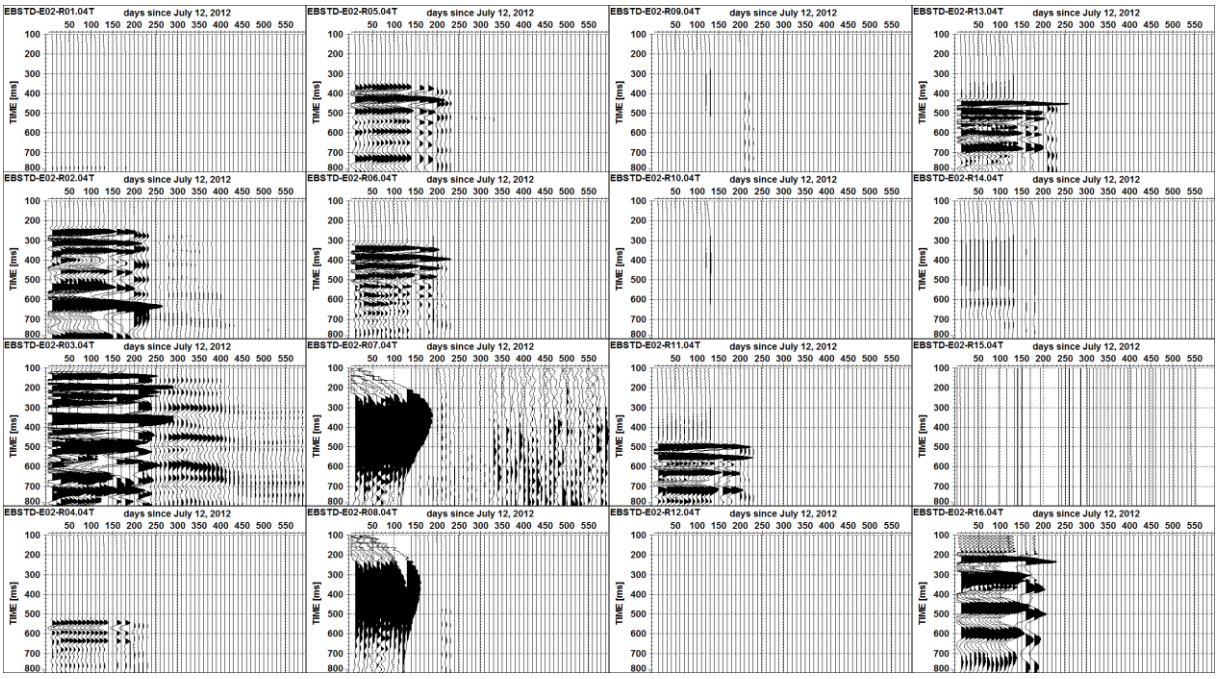

Fig. 11.11 Ensemble normalized seismic sections for emitter E02 with all receivers R01–R16. Only every 10th trace is plotted.

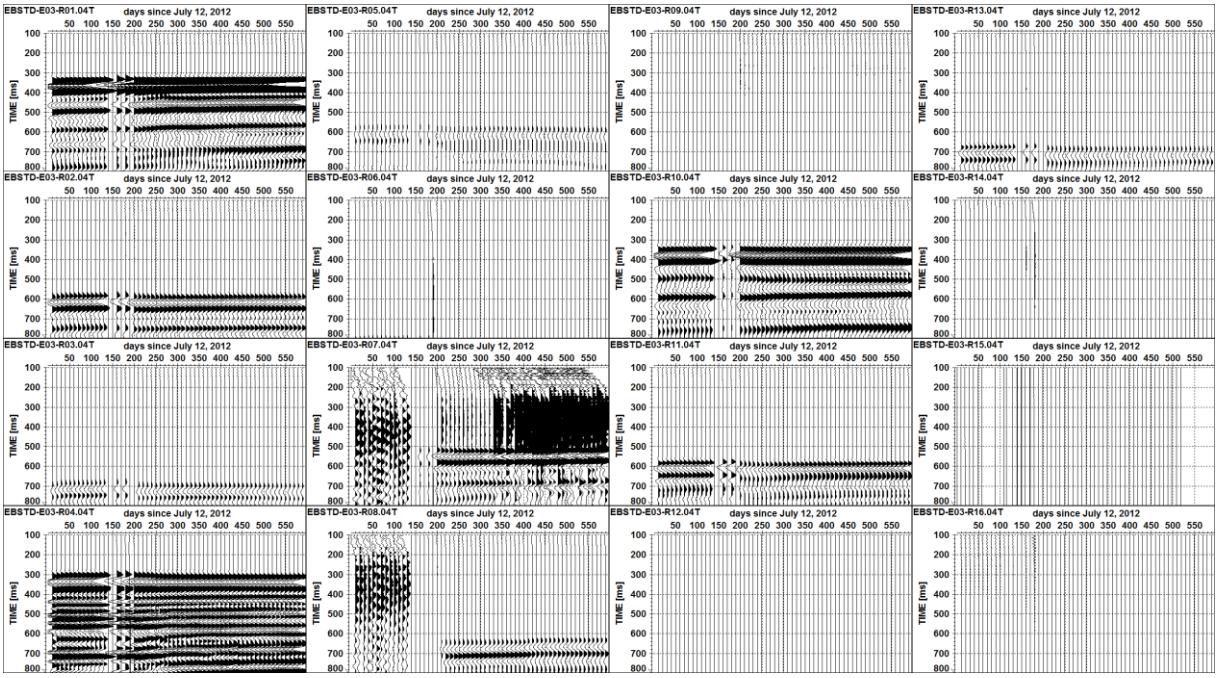

Fig. 11.12 Ensemble normalized seismic sections for emitter E03 with all receivers R01–R16. Only every 10th trace is plotted.

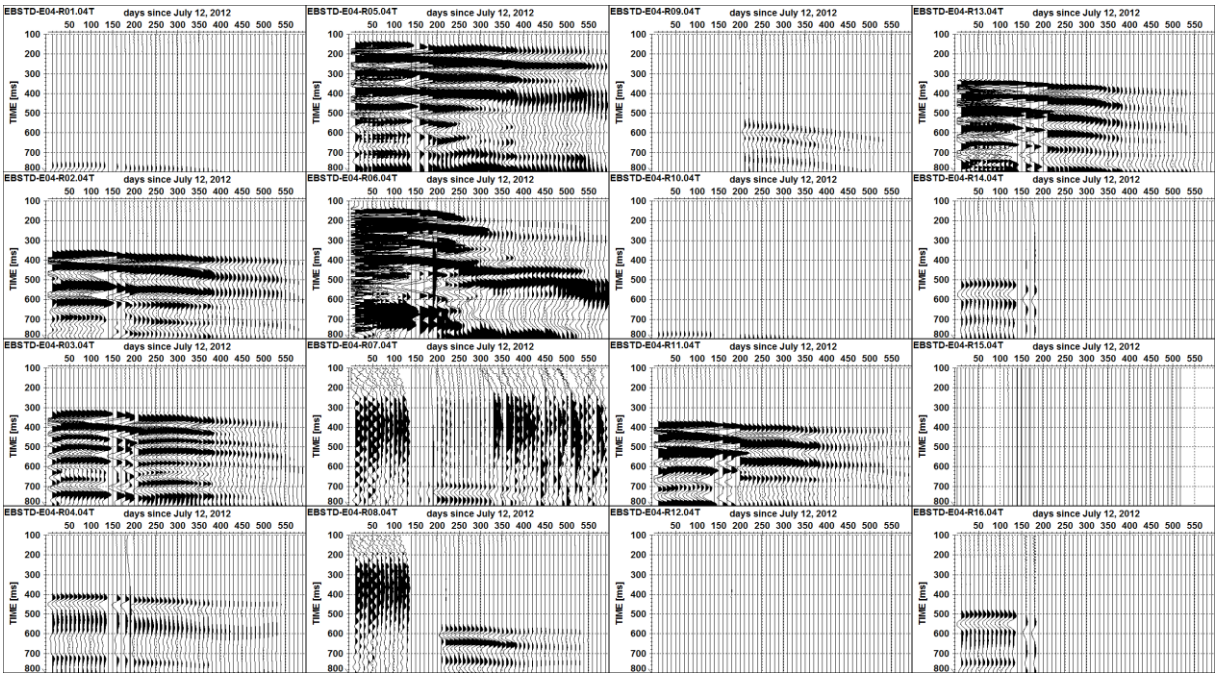

Fig. 11.13 Ensemble normalized seismic sections for emitter E04 with all receivers R01–R16. Only every 10th trace is plotted.

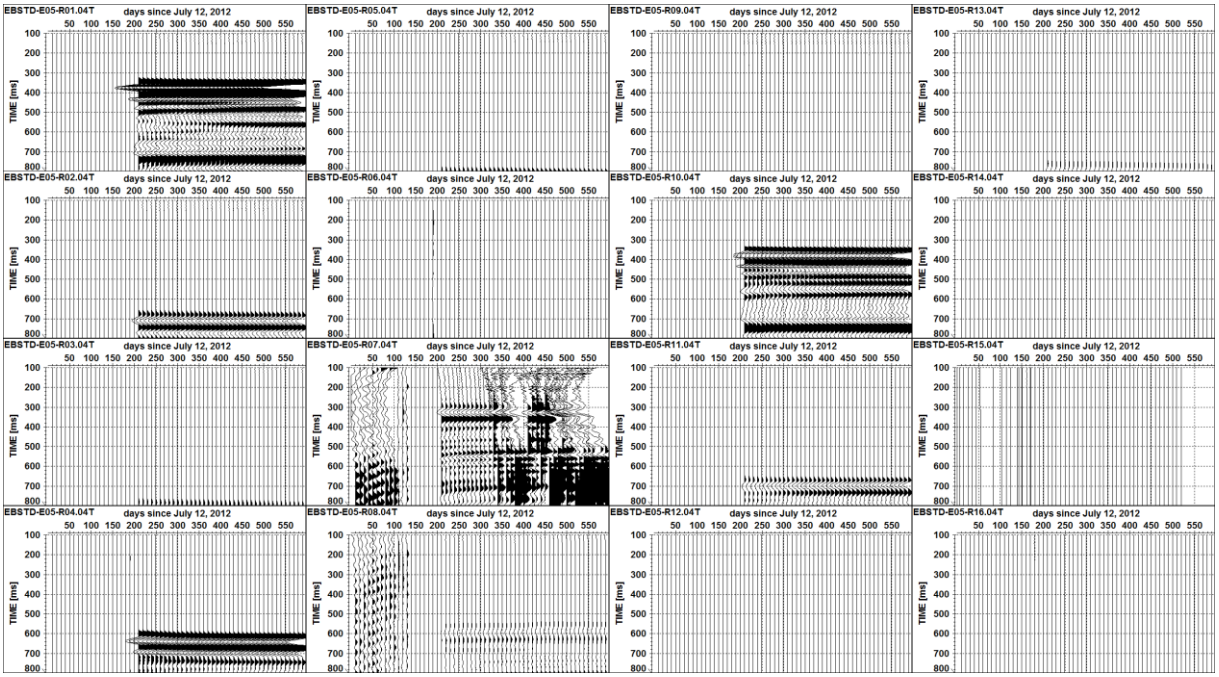

Fig. 11.14 Ensemble normalized seismic sections for emitter E05 with all receivers R01–R16. Only every 10th trace is plotted.

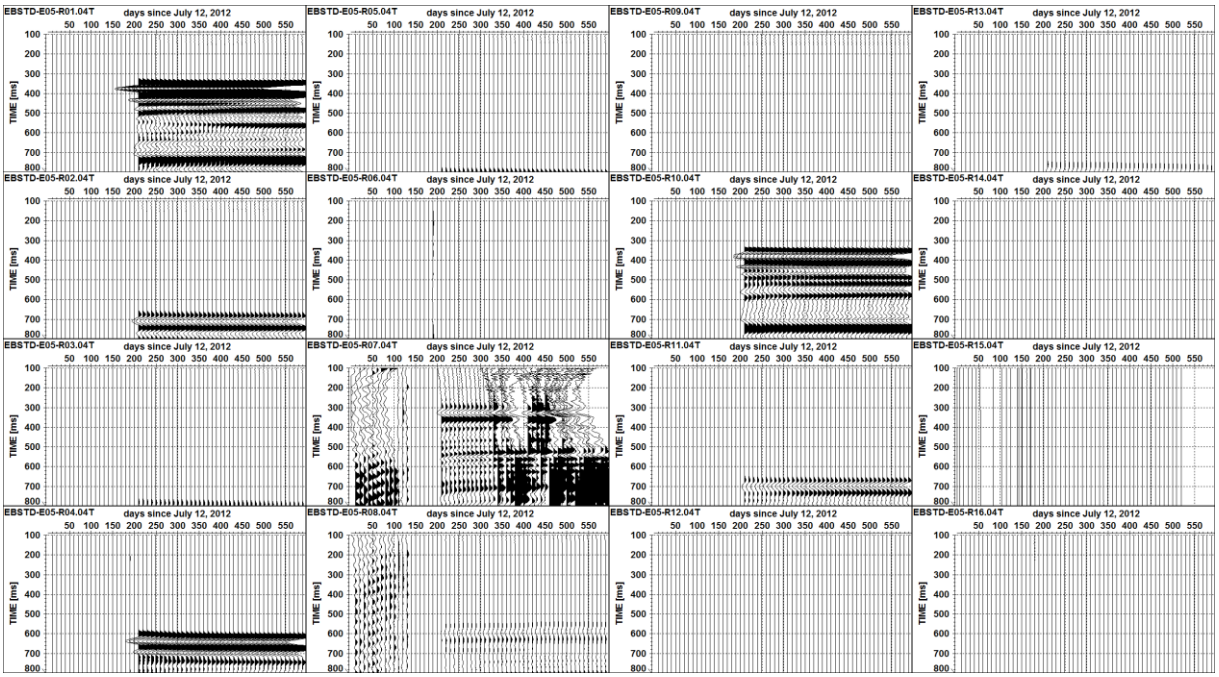

Fig. 11.15 Ensemble normalized seismic sections for emitter E06 with all receivers R01–R16. Only every 10th trace is plotted.

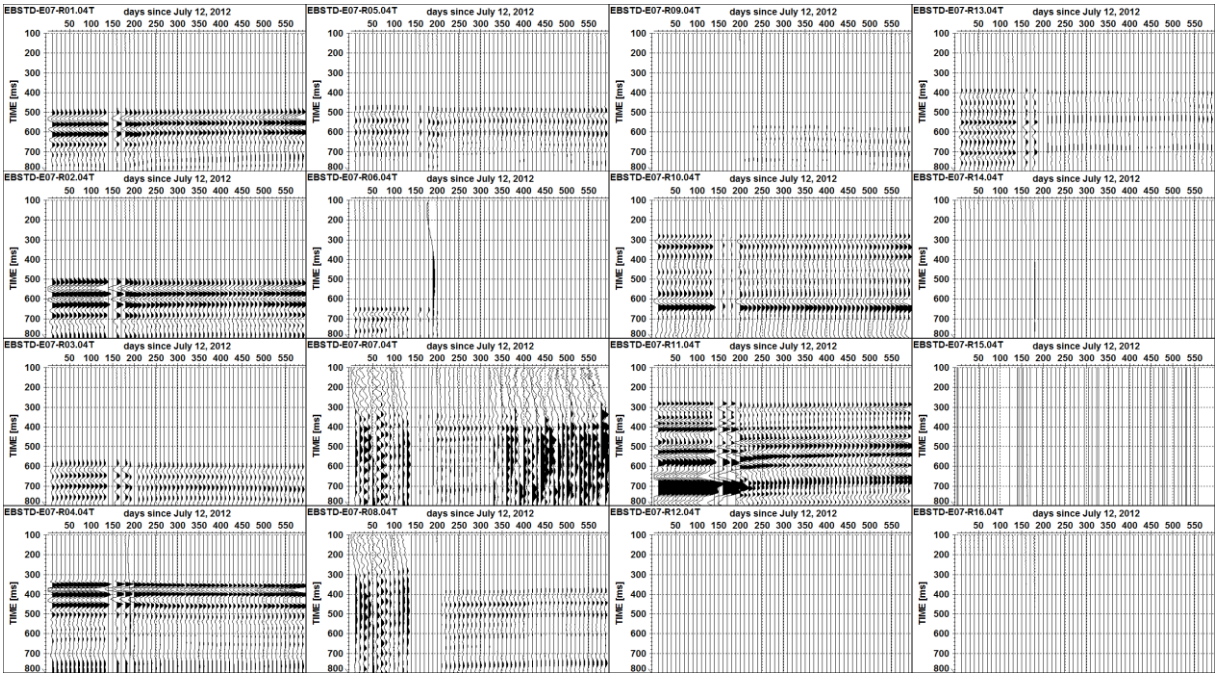

Fig. 11.16 Ensemble normalized seismic sections for emitter E07 with all receivers R01–R16. Only every 10th trace is plotted.

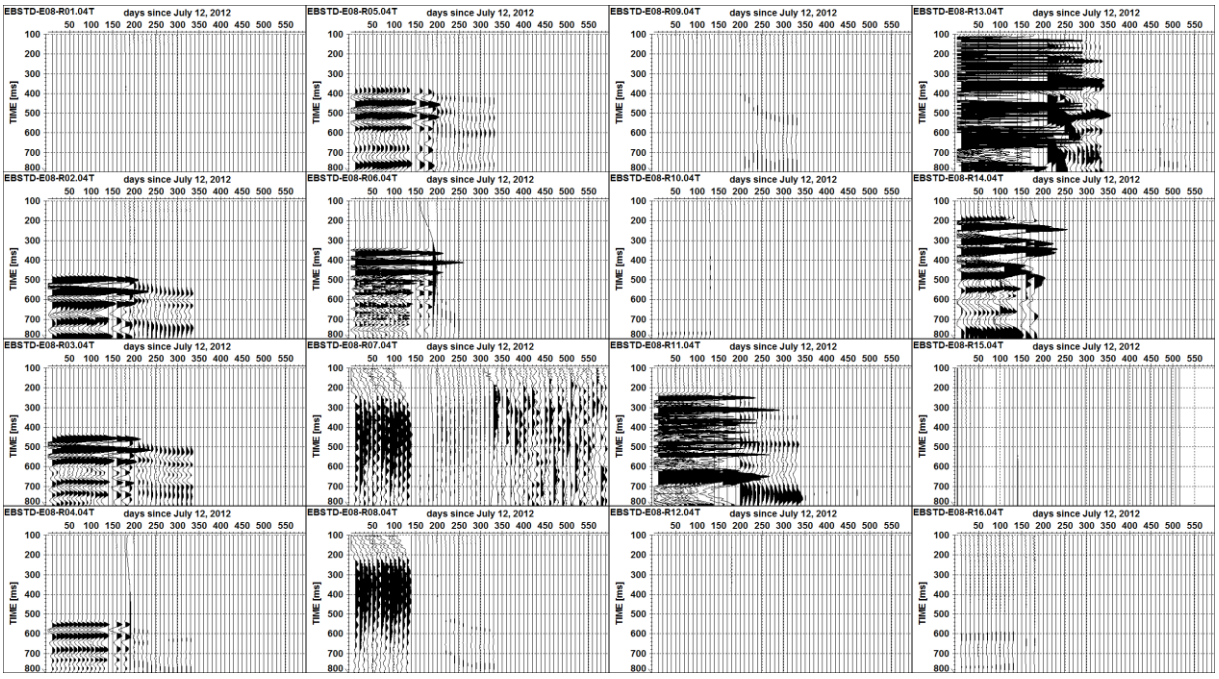

Fig. 11.17 Ensemble normalized seismic sections for emitter E08 with all receivers R01–R16. Only every 10th trace is plotted.

12 Appendix II – Data Report in German

EB Seismik, Mt. Terri, 2012-2013 - Stichpunktartige Protokollierung der Messungen von Thomas Fischer (GMuG)

EB Seismik, Mt.Terri, 2012 - 2013

Stichpunktartige Protokollierung der Messung

Author: Thomas Fischer

6. November 2013

GMuG Gesellschaft für Materialprüfung und Geophysik mbH * D-61231 Bad Nauheim

EB Seismic 2012

Einleitung

Die EB Seismik wurde 2001/2002 installiert und die Messkampagne dauerte bis Ende 2003. In vier parallelen Bohrungen sind 24 piezoelektrische Transducer über eine Länge von ca. 2.1 m verteilt. Die Ansatzpunkte der Bohrungen liegen an den Ecken eines Quadrats mit einer Seitenlänge von ca. 1 m. Die Orientierung der Bohrungen ist senkrecht zur Tunnelachse, 45° steigend.
Im Rahmen der EB Seismik wurden hauptsächlich Durchschallungs-Messungen durchgeführt, und zwar im Zeitraum vom 30. April 2002 bis 26. November 2003. Mikroakustik wurde ebenfalls registriert. Thema des Experiments war das Verhalten des Umgebungsgesteins nach dem Einbau eines Testbehälters in den Tunnel. Nach über 10 Jahren Standzeit soll der Testkörper noch im Jahr 2012 wieder abgebaut werden. Die Abbauphase und die daraus resultierenden Veränderungen im Umgebungsgestein sollen ebenfalls durch seismische Messungen in den nächsten Monaten begleitet werden.
Der Anschluss der 2001 eingebauten Transducer an eine neue Registrier- und Steueranlage erfolgte am 11. Juli 2012. Die Wiederinbetriebnahme der Messeinrichtung, sowie Messungen vor und später nach dem Abbau des Testkörpers sind Gegenstand dieser Dokumentatiton.

0.1 Beschreibung

Anordnung und Bezeichnung der Sensoren

In verschiedenen Dokumenten werden unterschiedliche Bezeichnungen für Bohrungen und Transducer verwendet. Es folgt eine kurze Gegenüberstellung der bisher bekannten Varianten. Informativ sind die Berichte von G. Manthei 2001 + 2003 (siehe Referenzen).
Die piezoelektrischen Transducer sind in vier Bohrlöchern angeordnet. Es gibt insgesamt 14 Empfänger, deren Nummerierung von 01 bis 16 reicht. 'Empfänger 06' und 'Empfänger 12' scheinen denselben Sensor zu bezeichnen, einen 'Empfänger 15' gibt es nicht. Auf Kanal 15 wird stattdessen das Sendesignal aufgezeichnet. In jedem Bohrloch befindet sich ein Strang mit 6 Sensoren, die einheitlich in einer (relativen) Tiefe von 0.2 m, 0 m, -0.3 m, -0.6 m, -1.3 m und -2.0 m angebracht sind. Die Zählrichtung von negativen zu positiven Werten entspricht der Richtung vom Bohrlochtiefsten zum Bohrlochmund. Je zwei Sensor-Stränge sind gleich aufgebaut: BEB-25 und BEB-28 mit je 3 Sendern und 3 Empfängern, sowie BEB-26 und BEB-27 mit je 2 Sendern und 4 Empfängern. Die Bezeichnung der Bohrlöcher ist je nach Quelle etwas unterschiedlich:
Konvention I: BEB-25 bis BEB-28 (Abschlussbericht Manthei 2003 + Skizze)
Konvention II: Nach Sensorbezeichnungen STB- oder SRB- , Bohrloch-Nummern 25 bis 28 (Sensorkabel + Ordner mit Messungen)
Konvention III: BEB-27 bis BEB-30 (Installationsbericht Manthei 2001)
Bei Konvention I und II scheinen die Bohrloch-Nummern, unter Berücksichtigung der eingebauten Sensoren, gleich zu sein. Der Unterschied zwischen I und III scheint in einer um 2 verschobenen Bohrlochnummerierung zu liegen, jedoch sind in III die äußeren Transducer S09, S10, E12, E16 in den Bohrlochsträngen nicht eingezeichnet.

Messanlage 2012

Anschlüsse für bis zu 16 Empfänger und 24 Sender
A/D-Wandler: 16 Bit @500kHz (dt=2us), mit integriertem Anti-Aliasing Filter

Quelle: Impulsgenerator mit Relais-Umschaltung
Verstärkungsfaktoren:
Empfänger: 40 dB (Zweistufig, 30 dB im Vorverstärker + 10 dB Nachverstärkung)
Hochpass: 1kHz
Tiefpass: -
Sendesignal: -60 dB Aufzeichnung via unkompensierten Teiler
Sensor-Belegung Juli 2012
Sender: 5 funktionsfähig [2,3,4,7,8] von ursprünglich 10
Empfänger: 11 funktionsfähig [1-6,10,11,13,14,16] von ursprünglich 14
Die Transducer sind entsprechend ihrer ursprünglichen Nummerierung (soweit bekannt) angeschlossen, unabhängig von ihrer Funktionsfähigkeit. Auf Empfänger Kanal 15 wird das Sendesignal aufgezeichnet, da diese Nummer bisher nicht verwendet wurde.

Automatischer Betrieb

Durchschallungsmessung:
Einmal täglich erfolgt eine Durchschallungsmessung mit allen Sendern. Bei dieser Messung sind die folgenden Parameter eigestellt:
Startzeitpunkt: 01:10 Uhr, nachts
Sendesignal, Peak to Peak Spannung: nominal 200 V
Aufnahmedauer je Kanal: 32.4 ms bzw. 16384 Samples
Pretrigger: 25% (Nullpunkt-Sample = 4096)
Je Sender: 2048 fache Wiederholung / Stapelung
Bei dem gegenwärtigen Setup dauert die gesamte Durchschallungsmessung mit 8 Sendern ca. 20 Minuten, das entspricht ca. 70ms für die Einzelmessung.
Mikroakustische Messung:
Diese Messung ist nicht Teil des Auftrags, wird aber zur Zeit aktiv durchgeführt. Die eingestellten Triggerlevel werden noch angepasst, wenn die akustische Umgebung besser bekannt ist. Später wird insbesondere der Beginn der Bauarbeiten zu berücksichtigen sein.
Zeitplan: Aktuell 24 Stunden aktiv
A/D-Wandler: +/-10V Bereich
Triggerlevel: 30mV

Unterschiede zwischen Messanlage 2001 und 2012

Sendesignal: In der Version von 2001 wurde bei Durchschallungsmessungen mit 8 verschiedenen Signalformen gearbeitet. Zur Erzeugung der Signalform ist ein Verstärker und eine D/A-Wandlerkarte notwendig. Sieben der verwendeten Signale bestehen aus quasi monofrequenten Sinusschwingungen jeweils mit verschiedenen Grundfrequenzen f_0, das achte Signal hat einen rampenförmigen Verlauf mit einem Sprung vom positiver zu negativer Spannung am zeitlichen Nullpunkt der Messung. Die sinusförmigen Signale bestehen aus 5 Perioden einer Grundfrequenz f_0, die mit einer Cos^4-Funktion mit $f=f_0/10$ amplitudenmoduliert werden. Durch Amplitudenmodulation wird ein stetiger Signalverlauf am Beginn und am Ende des Sendesignals erreicht.
Die Version von 2012 enthält einen Impulsgenerator, der eine sägezahnförmige Ausgangsspannung mit einstellbarer Maxiamlamplitude ausgibt. Der Spannungsverlauf beginnt bei 0 V und steigt linear in ca. 7 ms auf den Maximalwert an. Dann erfolgt der Sprung zurück auf 0 V. Dieses Signal ist gut vergleichbar mit dem Rampen-Signal der Version von 2001.

([Weitere Unterschide ? Amplitude ?, Anzahl Samples ?])

0.2 Durchführung der Arbeiten

Wiederanschluss der Sensoren

Im September 2008 wurden erste Testmessungen vorgenommen um zu sehen, ob die eingebauten Sensoren noch funktionieren. 6 Sender und 11 Empfänger waren zu diesem Zeitpunkt funktionsfähig.

Im Juli 2012 wurde eine neue Registrieranlage am Messort aufgebaut und die bereits installierten Sensoren angeschlossen. Dazu wurden zusätzlich 10 m lange BNC-Kabel benötigt. Kritisch war der Anschlß an den eingebauten Sensorzuleitungen. Es wurde versucht, nicht funktionsfähige Sonden durch neue BNC-Stecker und gekürzte Kabel wieder in Funktion zu bringen. Kabelkorrosion ist eine Ursache für einen möglichen Sensordefekt. Um einen Eindruck von der Schädigumg der Sensoren zu erhalten, wurden elektrische Kenndaten der Sensor-Kabel-Impezanz gemessen.

Kabelkorrosion:
Einige Sensor-Kabel weisen eine starke Korrosion des Außenleiters auf. Beim Versuch solch ein Kabel vorsichtig abzuisolieren zerfällt das Kupfergeflecht des Aussenleiters zu schwarzen Staub und Kabelstückchen kleiner 5 mm. Der Innenleiter scheint weniger betroffen zu sein und war bei allen Sensor-Kabeln ausreichend stabil zum Krimpen. Nach Abschluss der Bauphase könnte nochmals versucht werden weitere Sensoren wiederanzuschließen, da die Kabel dann näher am Sensor zugänglich sind.

Elektrische Messung an den Sensorkabeln:
Bei den Installationsarbeiten wurden elektrische Kenndaten der Sensoren mit einem RLC-Meter gemessen (Messfrequenz = 1 kHz). Im wesentlichen sind das die Kapazität Cp und der Parallelwiderstand Rp der komplexen Impedanz aus Kabel, Sensor und diversen Verlustwiderständen z.B. durch Alterung, mechanische Beschädigung, Eindeingen von Elektrolyten, Kurzschluss, etc.. Die in der folgenden Tabelle gezeigten Messwerte sind nicht korrigiert und beinhalten noch die Basis-Kapazität des verwendeten Messkabels von 190 pF.
BNC-Kabel haben eine recht konstante Kapazität von ca. 100 pF pro Meter, das Sensorelement üblicherweise eine Kapazität von einigen hundert pF (Empfänger) bis einige nF (Sender). Kapazitätsmesswerte von 200-300 pF lassen einen kontaktlosen BNC-Stecker vermuten. Parallelwiderstände kleiner 100 kΩ deuten auf eine verringerte Empfindlichkeit hin. Praktisch scheint das für die Durchschallungsmessung nicht so relevant zu sein, da z.B. die Empfänger E05 und E10 oder die Sender S07 und S08 mit Rp < 10kΩ zumindest funktionieren. Andererseits zeigt z.B. Empfänger 16 eine sehr geringe Signalamplitude, die elektrischen Kennwerte scheinen durchaus gut zu sein. Sender S07 zeigt im Vergleich mit den übrigen Sendern eine deutlich reduzierte Spannung von etwa -50%. Dies ist bedingt durch seine sehr niedrige Impedanz, für die der Impulsgenerator nicht genug Strom liefern kann. Die absoluten Signalamplituden an den einzelnen Sonden sind durch die Schädigung nicht mehr direkt vergleichbar.

Die genannten Daten sind in der folgenden Tabelle zusammengefasst:

	Tiefe[m]	Bohrung	2008	2012	Cp [pF]	Rp [kΩ]	
Empfänger							
E01	-2.0	BEB-26			3700	19	
E02	-0.6	BEB-26			300	100	
E03	-0.3	BEB-26			3100	122	
E04	-1.3	BEB-25			3900	71	
E05	-0.6	BEB-25			4500	7	
E06 = E12	0.0	BEB-25			4000	13	
E07	-1.3	BEB-28	**(-)**	**(-)**	280	7000	schwankend
E08	-0.6	BEB-28	**(-)**	**(-)**	280	950	
E09	0.0	BEB-28	**(-)**	**(-)**	1100	1.2	
E10	-2.0	BEB-27			4700	8.2	
E11	-0.6	BEB-27			3100	20	
E13	-0.3	BEB-27			3600	14.6	
E14	0.2	BEB-27			2680	15	
E16	0.2	BEB-26			2400	290	
Sender							
S01	-1.3	BEB-26		**(-)**	200	3000	nicht möglich
S02	0.0	BEB-26			250	300	5500 pF, 400 kΩ
S03	-2.0	BEB-25			5500		
S04	-0.3	BEB-25			5600	28	
S05	-2.0	BEB-28	**(-)**	**(-)**	770		800 pF
S06	-0.3	BEB-28	**(-)**	**(-)**	220	50	800 pF, 48 MΩ
S07	-1.3	BEB-27			20000	2.6	
S08	0.0	BEB-27			5700	6.3	
S09	0.2	BEB-25	**(-)**	**(-)**		0.0013	schwankend
S10	0.2	BEB-28	**(-)**	**(-)**	890		

Die erste Durchschallungsmessung erfolgte am 12. Juli 2012. Die Messung ist in **Abbildung 1 und 2** gezeigt. Weitere Messungen vom 01. und 22. August 2012 sind in den **Abbildungen 3 bis 6** zu sehen. Die Zeitreihen sind in zwei Auflösungen dargestellt: Einmal 20 ms, mit dem gesamten Sendesignal und einmal 1.4 ms mit dem Fokus auf den Ersteinsätze. Es sind die Messungen mit den funktionsfähigen Sendern 2,3,4,7,8 (in Spalten) gezeigt. Auf Empfängerseite (in Zeilen) sind die Kanäle 7,8,9,12 defekt, und auf Kanal 15 is das Sendesignal in rot dargestellt.

Bemerkungen zu den Signalen

1) Hochfrequentes Signal bei Messung mit Sender 8 auf Empfänger 12: Dies ist verwunderlich, da an Kanal 12 kein Empfänger angeschlossen ist. Das besondere an diesem vermutlich elektrischen Störsignal ist, dass es eine Laufzeit zu haben scheint.

Signale mit ungewöhnlich hohen Frequenzwn traten anfangs **Abbildung 2** bei den Kombinationen 'Sender 4 auf Empfänger 06' und 'Sender 8 auf Empfänger 13' auf, wobei das Signal auf Kanal 12 (Sender 8) kaum zu sehen war. Später **Abbildung 6** zeigten sich Signalformen mit einem 'zackigen' Verlauf auch bei Messungen mit Sender 4 auf die Empfänger 5, 6 und 13, sowie mit Sender 8 auf die Empfänger 6,11,12 und 13.

0.3 Anhang

Datenfiles Durchschallungsmessung

Dateiformate:
Die Dateinamen bestehen aus einem Prefix 'Durchschallung_EB_', einer sechsstelligen laufenden Nummer und einer Extension ('.asc', '.dur' oder '.dzu'). Ein möglicher Dateiname wäre z.B. 'Durchschallung_EB_123456.asc'.
Die Dateien haben je nach Extension den folgenden Inhalt:

- .asc Spannungswerte der Empfänger als ASCII-Tabelle mit: Zeile = Samplenummer bzw. Zeit und Spalte = Empfänger; mit vorangestellter Kommentarzeile '# Emitter N'. Bei mehr als einem Sender: Zeile = Samplenummer + N_Sender*(N_Samples+1)
- .dur Spannungswerte der Empfänger als binäre 'int16' Zahl
- .dzu Einstellparameter der Messung, Aufbau ähnlich einer Ini-Datei

Die .asc-Datei enthält keine zusätzlichen Informationen und könnte aus den .dur- und .dzu-Dateien erstellt werden. Das Textformat ist jedoch einfacher zu handhaben als eine binäre Datei und einige Fragestellungen oder Unklarheiten können gegebenenfalls mit einem Editor überprüft werden.

Dateiliste:
Die aufgezeichneten Datenfiles sind recht kontinuierlich vorhanden, einzig während des Dis-Mantelings sind Daten-Lücken im Zeitraum 23. November 2012 bis 1. Februar 2013 aufgetreten. Durch die Bauarbeiten kam es einmal zu einem kompletten Ausfall der Messanlage, sowie relativ häufig zu durchtrennten Sensor-Kabeln, so dass immerwieder unregelmässig Sensoren ausgefallen sind. Der Verlauf kann anhand der Dateiliste nachvollzogen werden.

Tabelle 1: Liste der Datenfiles, Durchschallungsmessung

File-Nummer	Datum Uhrzeit	
Durchschallung_EB_000001	2012-07-12 01:45	1. Messung mit 16 Sendern, dannach 8 Sender
Durchschallung_EB_000002	2012-07-13 01:27	
Durchschallung_EB_000003	2012-07-14 01:27	
Durchschallung_EB_000004	2012-07-15 01:27	
Durchschallung_EB_000005	2012-07-16 01:27	
Durchschallung_EB_000006	2012-07-17 01:27	
Durchschallung_EB_000007	2012-07-18 01:27	
Durchschallung_EB_000008	2012-07-19 01:27	
Durchschallung_EB_000009	2012-07-20 01:27	
Durchschallung_EB_000010	2012-07-21 01:27	
Durchschallung_EB_000011	2012-07-22 01:27	
Durchschallung_EB_000012	2012-07-23 01:27	
Durchschallung_EB_000013	2012-07-24 01:27	
Durchschallung_EB_000014	2012-07-25 01:27	
Durchschallung_EB_000015	2012-07-26 01:27	
Durchschallung_EB_000016	2012-07-27 01:27	
Durchschallung_EB_000017	2012-07-28 01:27	
Durchschallung_EB_000018	2012-07-29 01:27	
Durchschallung_EB_000019	2012-07-30 01:27	
Durchschallung_EB_000020	2012-07-31 01:27	
Durchschallung_EB_000021	2012-08-01 01:27	

Tabelle 1: (continued)

File-Nummer	Datum Uhrzeit	
Durchschallung_EB_000022	2012-08-02 01:27	
Durchschallung_EB_000023	2012-08-03 01:27	
Durchschallung_EB_000024	2012-08-04 01:27	
Durchschallung_EB_000025	2012-08-05 01:27	
Durchschallung_EB_000026	2012-08-06 01:27	
Durchschallung_EB_000027	2012-08-07 01:27	
Durchschallung_EB_000028	2012-08-08 01:27	
Durchschallung_EB_000029	2012-08-09 01:27	
Durchschallung_EB_000030	2012-08-10 01:27	
Durchschallung_EB_000031	2012-08-11 01:27	
Durchschallung_EB_000032	2012-08-12 01:27	
Durchschallung_EB_000033	2012-08-13 01:27	
Durchschallung_EB_000034	2012-08-14 01:27	
Durchschallung_EB_000035	2012-08-15 01:27	
Durchschallung_EB_000036	2012-08-16 01:27	
Durchschallung_EB_000037	2012-08-17 01:27	
Durchschallung_EB_000038	2012-08-18 01:27	
Durchschallung_EB_000039	2012-08-19 01:27	
Durchschallung_EB_000040	2012-08-20 01:27	
Durchschallung_EB_000041	2012-08-21 01:27	
Durchschallung_EB_000042	2012-08-22 01:27	
Durchschallung_EB_000043	2012-08-23 01:27	
Durchschallung_EB_000044	2012-08-24 01:27	
Durchschallung_EB_000045	2012-08-25 01:27	
Durchschallung_EB_000046	2012-08-26 01:27	
Durchschallung_EB_000047	2012-08-27 01:27	
Durchschallung_EB_000048	2012-08-28 01:27	
Durchschallung_EB_000049	2012-08-29 01:27	
Durchschallung_EB_000050	2012-08-30 11:27	
Durchschallung_EB_000051	2012-08-31 01:27	
Durchschallung_EB_000052	2012-09-01 01:27	
Durchschallung_EB_000053	2012-09-02 01:27	
Durchschallung_EB_000054	2012-09-03 01:27	
Durchschallung_EB_000055	2012-09-04 01:27	
Durchschallung_EB_000056	2012-09-05 01:27	
Durchschallung_EB_000057	2012-09-06 01:27	
Durchschallung_EB_000058	2012-09-07 01:27	
Durchschallung_EB_000059	2012-09-08 01:27	
Durchschallung_EB_000060	2012-09-09 01:27	
Durchschallung_EB_000061	2012-09-10 01:27	
Durchschallung_EB_000062	2012-09-11 01:27	
Durchschallung_EB_000063	2012-09-12 01:27	
Durchschallung_EB_000064	2012-09-13 01:27	
Durchschallung_EB_000065	2012-09-14 01:27	
Durchschallung_EB_000066	2012-09-15 01:27	

Tabelle 1: (continued)

File-Nummer	Datum Uhrzeit	
Durchschallung_EB_000067	2012-09-16 01:27	
Durchschallung_EB_000068	2012-09-17 01:27	
Durchschallung_EB_000069	2012-09-18 01:27	
Durchschallung_EB_000070	2012-09-19 01:27	
Durchschallung_EB_000071	2012-09-20 01:27	
Durchschallung_EB_000072	2012-09-21 01:27	
Durchschallung_EB_000073	2012-09-22 01:27	
Durchschallung_EB_000074	2012-09-23 01:27	
Durchschallung_EB_000075	2012-09-24 01:27	
Durchschallung_EB_000076	2012-09-25 01:27	
Durchschallung_EB_000077	2012-09-26 01:27	
Durchschallung_EB_000078	2012-09-27 01:27	
Durchschallung_EB_000079	2012-09-28 01:27	
Durchschallung_EB_000080	2012-09-29 01:27	
Durchschallung_EB_000081	2012-09-30 01:27	
Durchschallung_EB_000082	2012-10-01 01:27	
Durchschallung_EB_000083	2012-10-02 01:27	
Durchschallung_EB_000084	2012-10-03 01:27	
Durchschallung_EB_000085	2012-10-04 01:27	
Durchschallung_EB_000086	2012-10-05 01:27	
Durchschallung_EB_000087	2012-10-06 01:27	
Durchschallung_EB_000088	2012-10-07 01:27	
Durchschallung_EB_000089	2012-10-08 01:27	
Durchschallung_EB_000090	2012-10-09 01:27	
Durchschallung_EB_000091	2012-10-10 01:27	
Durchschallung_EB_000092	2012-10-11 01:27	
Durchschallung_EB_000093	2012-10-12 01:27	
Durchschallung_EB_000094	2012-10-13 01:27	
Durchschallung_EB_000095	2012-10-14 01:27	
Durchschallung_EB_000096	2012-10-15 01:27	
Durchschallung_EB_000097	2012-10-16 01:27	
Durchschallung_EB_000098	2012-10-17 01:27	
Durchschallung_EB_000099	2012-10-18 01:27	
Durchschallung_EB_000100	2012-10-19 01:27	
Durchschallung_EB_000101	2012-10-20 01:27	
Durchschallung_EB_000102	2012-10-21 01:27	
Durchschallung_EB_000103	2012-10-22 01:27	
Durchschallung_EB_000104	2012-10-23 01:27	
Durchschallung_EB_000105	2012-10-24 01:27	
Durchschallung_EB_000106	2012-10-25 01:27	
Durchschallung_EB_000107	2012-10-26 01:27	
Durchschallung_EB_000108	2012-10-27 01:27	
Durchschallung_EB_000109	2012-10-28 01:27	
Durchschallung_EB_000110	2012-10-29 01:27	
Durchschallung_EB_000111	2012-10-30 01:27	

Tabelle 1: (continued)

File-Nummer	Datum Uhrzeit	
Durchschallung_EB_000112	2012-10-31 01:27	
Durchschallung_EB_000113	2012-11-01 01:27	
Durchschallung_EB_000114	2012-11-02 01:27	
Durchschallung_EB_000115	2012-11-03 01:27	
Durchschallung_EB_000116	2012-11-04 01:27	
Durchschallung_EB_000117	2012-11-05 01:27	
Durchschallung_EB_000118	2012-11-06 01:27	
Durchschallung_EB_000119	2012-11-07 01:27	
Durchschallung_EB_000120	2012-11-08 01:27	
Durchschallung_EB_000121	2012-11-09 01:27	
Durchschallung_EB_000122	2012-11-10 01:27	
Durchschallung_EB_000123	2012-11-11 01:27	
Durchschallung_EB_000124	2012-11-12 01:27	
Durchschallung_EB_000125	2012-11-13 01:27	
Durchschallung_EB_000126	2012-11-14 01:27	
Durchschallung_EB_000127	2012-11-15 01:27	
Durchschallung_EB_000128	2012-11-16 01:27	
Durchschallung_EB_000129	2012-11-17 01:27	
Durchschallung_EB_000130	2012-11-18 01:27	
Durchschallung_EB_000131	2012-11-19 01:27	
Durchschallung_EB_000132	2012-11-20 01:27	
Durchschallung_EB_000133	2012-11-21 01:27	
Durchschallung_EB_000134	2012-11-22 01:27	*
	2012-11-23	* 0) System not running
	...	* 0) System not running
	2012-12-05	* 0) System not running
Durchschallung_EB_000135	2012-12-06 01:27	* 4) error / bad data
Durchschallung_EB_000150	2012-12-06 15:27	*
	2012-12-07	* 0) System not running
	2012-12-08	* 0) System not running
	2012-12-09	* 0) System not running
Durchschallung_EB_000151	2012-12-10 11:27	*
Durchschallung_EB_000152	2012-12-11 01:27	*
Durchschallung_EB_000153	2012-12-12 01:27	* 1) Sensor cables cutted
Durchschallung_EB_000154	2012-12-13 01:27	* 1) Sensor cables cutted
Durchschallung_EB_000155	2012-12-14 01:27	* 1) Sensor cables cutted
Durchschallung_EB_000156	2012-12-15 01:27	* 1) Sensor cables cutted
Durchschallung_EB_000157	2012-12-16 01:27	* 1) Sensor cables cutted
Durchschallung_EB_000158	2012-12-17 01:27	* 1) Sensor cables cutted
Durchschallung_EB_000159	2012-12-18 01:27	* 1) Sensor cables cutted
Durchschallung_EB_000170	2012-12-18 14:27	* 2) Test measurement
Durchschallung_EB_000171	2012-12-18 16:27	*
Durchschallung_EB_000172	2012-12-19 01:27	*
Durchschallung_EB_000173	2012-12-19 10:57	* 2) Test measurement
Durchschallung_EB_000174	2012-12-20 00:27	*

Tabelle 1: (continued)

File-Nummer	Datum Uhrzeit	
Durchschallung_EB_000175	2012-12-21 01:27	*
Durchschallung_EB_000176	2012-12-22 01:27	*
Durchschallung_EB_000177	2012-12-23 01:27	*
Durchschallung_EB_000178	2012-12-24 01:27	*
Durchschallung_EB_000179	2012-12-25 01:27	*
Durchschallung_EB_000180	2012-12-26 01:27	*
Durchschallung_EB_000181	2012-12-27 01:27	*
Durchschallung_EB_000182	2012-12-29 01:27	*
Durchschallung_EB_000183	2012-12-30 01:27	*
Durchschallung_EB_000184	2012-12-31 01:27	*
	2013-01-01	* 0) System not running
	2013-01-02	* 0) System not running
	2013-01-03	* 0) System not running
Durchschallung_EB_000185	2013-01-04 10:27	*
Durchschallung_EB_000186	2013-01-05 01:27	*
Durchschallung_EB_000187	2013-01-06 01:27	*
Durchschallung_EB_000188	2013-01-07 01:27	*
Durchschallung_EB_000189	2013-01-08 01:27	*
Durchschallung_EB_000190	2013-01-09 01:27	*
Durchschallung_EB_000191	2013-01-10 01:27	*
Durchschallung_EB_000192	2013-01-11 01:27	*
Durchschallung_EB_000193	2013-01-12 01:27	*
Durchschallung_EB_000194	2013-01-13 01:27	*
Durchschallung_EB_000195	2013-01-14 01:27	*
Durchschallung_EB_000196	2013-01-15 01:27	*
Durchschallung_EB_000197	2013-01-16 01:27	*
Durchschallung_EB_000198	2013-01-17 01:27	*
Durchschallung_EB_000199	2013-01-18 01:27	*
Durchschallung_EB_000200	2013-01-19 01:27	*
Durchschallung_EB_000201	2013-01-20 01:27	*
Durchschallung_EB_000202	2013-01-21 01:27	*
Durchschallung_EB_000203	2013-01-22 01:27	*
Durchschallung_EB_000204	2013-01-23 01:27	*
Durchschallung_EB_000205	2013-01-24 01:27	*
Durchschallung_EB_000206	2013-01-25 01:27	*
Durchschallung_EB_000207	2013-01-26 01:27	*
Durchschallung_EB_000208	2013-01-27 01:27	*
Durchschallung_EB_000209	2013-01-28 01:27	*
Durchschallung_EB_000210	2013-01-29 01:27	*
Durchschallung_EB_000211	2013-01-30 01:27	*
Durchschallung_EB_000212	2013-01-31 01:27	* 4) error / bad data
Durchschallung_EB_000213	2013-01-31 10:47	* 2) Test measurement
Durchschallung_EB_000214	2013-01-31 13:27	* 2) Test measurement
Durchschallung_EB_000215	2013-01-31 14:07	*
Durchschallung_EB_000216	2013-02-01 01:27	* 4) error / bad data

Tabelle 1: (continued)

File-Nummer	Datum Uhrzeit	
Durchschallung_EB_000217	2013-02-01 12:18	*
Durchschallung_EB_000218	2013-02-02 02:18	*
Durchschallung_EB_000219	2013-02-03 02:18	
Durchschallung_EB_000220	2013-02-04 02:18	
Durchschallung_EB_000221	2013-02-05 02:18	
Durchschallung_EB_000222	2013-02-06 02:18	
Durchschallung_EB_000223	2013-02-07 02:18	
Durchschallung_EB_000224	2013-02-08 02:18	
Durchschallung_EB_000225	2013-02-09 02:18	
Durchschallung_EB_000226	2013-02-10 02:18	
Durchschallung_EB_000227	2013-02-11 02:18	
Durchschallung_EB_000228	2013-02-12 02:18	
Durchschallung_EB_000229	2013-02-13 02:18	
Durchschallung_EB_000230	2013-02-14 02:18	
Durchschallung_EB_000231	2013-02-15 12:18	
Durchschallung_EB_000232	2013-02-16 02:18	
Durchschallung_EB_000233	2013-02-17 02:18	
Durchschallung_EB_000234	2013-02-18 02:18	
Durchschallung_EB_000235	2013-02-19 02:18	
Durchschallung_EB_000236	2013-02-20 02:18	
Durchschallung_EB_000237	2013-02-21 02:18	
Durchschallung_EB_000238	2013-02-22 02:18	
Durchschallung_EB_000239	2013-02-23 02:18	
Durchschallung_EB_000240	2013-02-24 02:18	
Durchschallung_EB_000241	2013-02-25 02:18	
Durchschallung_EB_000242	2013-02-26 02:18	
Durchschallung_EB_000243	2013-02-27 02:18	
Durchschallung_EB_000244	2013-02-28 02:18	
Durchschallung_EB_000245	2013-03-01 02:18	
Durchschallung_EB_000246	2013-03-02 02:18	
Durchschallung_EB_000247	2013-03-03 02:18	
Durchschallung_EB_000248	2013-03-04 02:18	
Durchschallung_EB_000249	2013-03-05 02:18	
Durchschallung_EB_000250	2013-03-06 02:18	
Durchschallung_EB_000251	2013-03-07 02:18	
Durchschallung_EB_000252	2013-03-08 02:18	
Durchschallung_EB_000253	2013-03-09 02:18	
Durchschallung_EB_000254	2013-03-10 02:18	
Durchschallung_EB_000255	2013-03-11 02:18	
Durchschallung_EB_000256	2013-03-12 02:18	
Durchschallung_EB_000257	2013-03-13 02:18	
Durchschallung_EB_000258	2013-03-14 02:18	
Durchschallung_EB_000259	2013-03-15 02:18	
Durchschallung_EB_000260	2013-03-16 02:18	
Durchschallung_EB_000261	2013-03-17 02:18	

Tabelle 1: (continued)

File-Nummer	Datum Uhrzeit	
Durchschallung_EB_000262	2013-03-18 02:18	
Durchschallung_EB_000263	2013-03-19 02:18	
Durchschallung_EB_000264	2013-03-20 02:18	
Durchschallung_EB_000265	2013-03-21 02:18	
Durchschallung_EB_000266	2013-03-22 02:18	
Durchschallung_EB_000267	2013-03-23 02:18	
Durchschallung_EB_000268	2013-03-24 02:18	
Durchschallung_EB_000269	2013-03-25 02:18	
Durchschallung_EB_000270	2013-03-26 02:18	
Durchschallung_EB_000271	2013-03-27 02:18	
Durchschallung_EB_000272	2013-03-28 02:18	
Durchschallung_EB_000273	2013-03-29 02:18	
Durchschallung_EB_000274	2013-03-30 02:18	
Durchschallung_EB_000275	2013-03-31 03:18	
Durchschallung_EB_000276	2013-04-01 02:18	
Durchschallung_EB_000277	2013-04-02 02:18	
Durchschallung_EB_000278	2013-04-03 02:18	
Durchschallung_EB_000279	2013-04-04 02:18	
Durchschallung_EB_000280	2013-04-05 02:18	
Durchschallung_EB_000281	2013-04-06 02:18	
Durchschallung_EB_000282	2013-04-07 02:18	
Durchschallung_EB_000283	2013-04-08 02:18	
Durchschallung_EB_000284	2013-04-09 02:18	
Durchschallung_EB_000285	2013-04-10 02:18	
Durchschallung_EB_000286	2013-04-11 02:18	
Durchschallung_EB_000287	2013-04-12 02:18	
Durchschallung_EB_000288	2013-04-13 02:18	
Durchschallung_EB_000289	2013-04-14 02:18	
Durchschallung_EB_000290	2013-04-15 02:18	
Durchschallung_EB_000291	2013-04-16 02:18	
Durchschallung_EB_000292	2013-04-17 02:18	
Durchschallung_EB_000293	2013-04-18 02:18	
Durchschallung_EB_000294	2013-04-19 02:18	
Durchschallung_EB_000295	2013-04-20 02:18	
Durchschallung_EB_000296	2013-04-21 02:18	
Durchschallung_EB_000297	2013-04-22 02:18	
Durchschallung_EB_000298	2013-04-23 02:18	
Durchschallung_EB_000299	2013-04-24 02:18	
Durchschallung_EB_000300	2013-04-25 02:18	
Durchschallung_EB_000301	2013-04-26 02:18	
Durchschallung_EB_000302	2013-04-27 02:18	
Durchschallung_EB_000303	2013-04-28 02:18	
Durchschallung_EB_000304	2013-04-29 02:18	
Durchschallung_EB_000305	2013-04-30 02:18	
Durchschallung_EB_000306	2013-05-01 02:18	

Tabelle 1: (continued)

File-Nummer	Datum Uhrzeit	
Durchschallung_EB_000307	2013-05-02 02:18	
Durchschallung_EB_000308	2013-05-03 02:18	
Durchschallung_EB_000309	2013-05-04 02:18	
Durchschallung_EB_000310	2013-05-05 02:18	
Durchschallung_EB_000311	2013-05-06 02:18	
Durchschallung_EB_000312	2013-05-07 02:18	
Durchschallung_EB_000313	2013-05-08 02:18	
Durchschallung_EB_000314	2013-05-09 02:18	
Durchschallung_EB_000315	2013-05-10 02:18	
Durchschallung_EB_000316	2013-05-11 02:18	
Durchschallung_EB_000317	2013-05-12 02:18	
Durchschallung_EB_000318	2013-05-13 02:18	
Durchschallung_EB_000319	2013-05-14 02:18	
Durchschallung_EB_000320	2013-05-15 02:18	
Durchschallung_EB_000321	2013-05-16 02:18	
Durchschallung_EB_000322	2013-05-17 02:18	
Durchschallung_EB_000323	2013-05-18 02:18	
Durchschallung_EB_000324	2013-05-19 02:18	
Durchschallung_EB_000325	2013-05-20 02:18	
Durchschallung_EB_000326	2013-05-21 02:18	
Durchschallung_EB_000327	2013-05-22 02:18	
Durchschallung_EB_000328	2013-05-23 02:18	
Durchschallung_EB_000329	2013-05-24 02:18	
Durchschallung_EB_000330	2013-05-25 02:18	
Durchschallung_EB_000331	2013-05-26 02:18	
Durchschallung_EB_000332	2013-05-27 02:18	
Durchschallung_EB_000333	2013-05-28 02:18	
Durchschallung_EB_000334	2013-05-29 02:18	
Durchschallung_EB_000335	2013-05-30 02:18	
Durchschallung_EB_000336	2013-05-31 02:18	
Durchschallung_EB_000337	2013-06-01 02:18	
Durchschallung_EB_000338	2013-06-02 02:18	
Durchschallung_EB_000339	2013-06-03 02:18	
Durchschallung_EB_000340	2013-06-04 02:18	
Durchschallung_EB_000341	2013-06-05 02:18	
Durchschallung_EB_000342	2013-06-06 02:18	
Durchschallung_EB_000343	2013-06-07 02:18	
Durchschallung_EB_000344	2013-06-08 02:18	
Durchschallung_EB_000345	2013-06-09 02:18	
Durchschallung_EB_000346	2013-06-10 02:18	
Durchschallung_EB_000347	2013-06-11 02:18	
Durchschallung_EB_000348	2013-06-12 02:18	
Durchschallung_EB_000349	2013-06-13 02:18	
Durchschallung_EB_000350	2013-06-14 02:18	
Durchschallung_EB_000351	2013-06-15 02:18	

Tabelle 1: (continued)

File-Nummer	Datum Uhrzeit	
Durchschallung_EB_000352	2013-06-16 02:18	
Durchschallung_EB_000353	2013-06-17 02:18	
Durchschallung_EB_000354	2013-06-18 02:18	
Durchschallung_EB_000355	2013-06-19 02:18	
Durchschallung_EB_000356	2013-06-20 02:18	
Durchschallung_EB_000357	2013-06-21 02:18	
Durchschallung_EB_000358	2013-06-22 02:18	
Durchschallung_EB_000359	2013-06-23 02:18	
Durchschallung_EB_000360	2013-06-24 02:18	
Durchschallung_EB_000361	2013-06-25 02:18	
Durchschallung_EB_000362	2013-06-26 02:18	
Durchschallung_EB_000363	2013-06-27 02:18	
Durchschallung_EB_000364	2013-06-28 02:18	
Durchschallung_EB_000365	2013-06-29 02:18	
Durchschallung_EB_000366	2013-06-30 02:18	
Durchschallung_EB_000367	2013-07-01 02:18	
Durchschallung_EB_000368	2013-07-02 02:18	
Durchschallung_EB_000369	2013-07-03 02:18	
Durchschallung_EB_000370	2013-07-04 02:18	
Durchschallung_EB_000371	2013-07-05 02:18	
Durchschallung_EB_000372	2013-07-06 02:18	
Durchschallung_EB_000373	2013-07-07 02:18	
Durchschallung_EB_000374	2013-07-08 02:18	
Durchschallung_EB_000375	2013-07-09 02:18	
Durchschallung_EB_000376	2013-07-10 02:18	
Durchschallung_EB_000377	2013-07-11 02:18	
Durchschallung_EB_000378	2013-07-12 02:18	
Durchschallung_EB_000379	2013-07-13 02:18	
Durchschallung_EB_000380	2013-07-14 02:18	
Durchschallung_EB_000381	2013-07-15 02:18	
Durchschallung_EB_000382	2013-07-16 02:18	
Durchschallung_EB_000383	2013-07-17 02:18	
Durchschallung_EB_000384	2013-07-18 02:18	
Durchschallung_EB_000385	2013-07-19 02:18	
Durchschallung_EB_000386	2013-07-20 02:18	
Durchschallung_EB_000387	2013-07-21 02:18	
Durchschallung_EB_000388	2013-07-22 02:18	
Durchschallung_EB_000389	2013-07-23 02:18	
Durchschallung_EB_000390	2013-07-24 02:18	
Durchschallung_EB_000391	2013-07-25 02:18	
Durchschallung_EB_000392	2013-07-26 02:18	
Durchschallung_EB_000393	2013-07-27 02:18	
Durchschallung_EB_000394	2013-07-28 02:18	
Durchschallung_EB_000395	2013-07-29 02:18	
Durchschallung_EB_000396	2013-07-30 02:18	

Tabelle 1: (continued)

File-Nummer	Datum Uhrzeit	
Durchschallung_EB_000397	2013-07-31 02:18	
Durchschallung_EB_000398	2013-08-01 02:18	
Durchschallung_EB_000399	2013-08-02 02:18	
Durchschallung_EB_000400	2013-08-03 02:18	
Durchschallung_EB_000401	2013-08-04 02:18	
Durchschallung_EB_000402	2013-08-05 02:18	
Durchschallung_EB_000403	2013-08-06 02:18	
Durchschallung_EB_000404	2013-08-07 02:18	
Durchschallung_EB_000405	2013-08-08 02:18	
Durchschallung_EB_000406	2013-08-09 02:18	
Durchschallung_EB_000407	2013-08-10 02:18	
Durchschallung_EB_000408	2013-08-11 02:18	
Durchschallung_EB_000409	2013-08-12 02:18	
Durchschallung_EB_000410	2013-08-13 02:18	
Durchschallung_EB_000411	2013-08-14 02:18	
Durchschallung_EB_000412	2013-08-15 02:18	
Durchschallung_EB_000413	2013-08-16 02:18	
Durchschallung_EB_000414	2013-08-17 02:18	
Durchschallung_EB_000415	2013-08-18 02:18	
Durchschallung_EB_000416	2013-08-19 02:18	
Durchschallung_EB_000417	2013-08-20 02:18	
Durchschallung_EB_000418	2013-08-21 02:18	
Durchschallung_EB_000419	2013-08-22 02:18	
Durchschallung_EB_000420	2013-08-23 02:18	
Durchschallung_EB_000421	2013-08-24 02:18	
Durchschallung_EB_000422	2013-08-25 02:18	
Durchschallung_EB_000423	2013-08-26 02:18	
Durchschallung_EB_000424	2013-08-27 02:18	
Durchschallung_EB_000425	2013-08-28 02:18	
Durchschallung_EB_000426	2013-08-29 02:18	
Durchschallung_EB_000427	2013-08-30 02:18	
Durchschallung_EB_000428	2013-08-31 02:18	
Durchschallung_EB_000429	2013-09-01 02:18	
Durchschallung_EB_000430	2013-09-02 02:18	
Durchschallung_EB_000431	2013-09-03 02:18	
Durchschallung_EB_000432	2013-09-04 02:18	
Durchschallung_EB_000433	2013-09-05 02:18	
Durchschallung_EB_000434	2013-09-06 02:18	
Durchschallung_EB_000435	2013-09-07 02:18	
Durchschallung_EB_000436	2013-09-08 02:18	
Durchschallung_EB_000437	2013-09-09 02:18	
Durchschallung_EB_000438	2013-09-10 02:18	
Durchschallung_EB_000439	2013-09-11 02:18	
Durchschallung_EB_000440	2013-09-12 02:18	
Durchschallung_EB_000441	2013-09-13 02:18	

Tabelle 1: (continued)

File-Nummer	Datum Uhrzeit	
Durchschallung_EB_000442	2013-09-14 02:18	
Durchschallung_EB_000443	2013-09-15 02:18	
Durchschallung_EB_000444	2013-09-16 02:18	
Durchschallung_EB_000445	2013-09-17 02:18	
Durchschallung_EB_000446	2013-09-18 02:18	
Durchschallung_EB_000447	2013-09-19 02:18	
Durchschallung_EB_000448	2013-09-20 02:18	
Durchschallung_EB_000449	2013-09-21 02:18	
Durchschallung_EB_000450	2013-09-22 02:18	
Durchschallung_EB_000451	2013-09-23 02:18	
Durchschallung_EB_000452	2013-09-24 02:18	
Durchschallung_EB_000453	2013-09-25 02:18	
Durchschallung_EB_000454	2013-09-26 02:18	
Durchschallung_EB_000455	2013-09-27 02:18	
Durchschallung_EB_000456	2013-09-28 02:18	
Durchschallung_EB_000457	2013-09-29 02:18	
Durchschallung_EB_000458	2013-09-30 02:18	
Durchschallung_EB_000459	2013-10-01 02:18	
Durchschallung_EB_000460	2013-10-02 02:18	
Durchschallung_EB_000461	2013-10-03 02:18	
Durchschallung_EB_000462	2013-10-04 02:18	
Durchschallung_EB_000463	2013-10-05 02:18	
Durchschallung_EB_000464	2013-10-06 02:18	
Durchschallung_EB_000465	2013-10-07 02:18	
Durchschallung_EB_000466	2013-10-08 02:18	
Durchschallung_EB_000467	2013-10-09 02:18	
Durchschallung_EB_000468	2013-10-10 02:18	
Durchschallung_EB_000469	2013-10-11 02:18	
Durchschallung_EB_000470	2013-10-12 02:18	
Durchschallung_EB_000471	2013-10-13 02:18	
Durchschallung_EB_000472	2013-10-14 02:18	
Durchschallung_EB_000473	2013-10-15 02:18	
Durchschallung_EB_000474	2013-10-16 02:18	
Durchschallung_EB_000475	2013-10-17 02:18	
Durchschallung_EB_000476	2013-10-18 02:18	
Durchschallung_EB_000477	2013-10-19 02:18	
Durchschallung_EB_000478	2013-10-20 02:18	
Durchschallung_EB_000479	2013-10-21 02:18	
Durchschallung_EB_000480	2013-10-22 02:18	
Durchschallung_EB_000481	2013-10-23 02:18	
Durchschallung_EB_000482	2013-10-24 02:18	
Durchschallung_EB_000483	2013-10-25 02:18	
Durchschallung_EB_000484	2013-10-26 02:18	
Durchschallung_EB_000485	2013-10-27 02:18	
Durchschallung_EB_000486	2013-10-28 02:18	

Tabelle 1: (continued)

File-Nummer	Datum Uhrzeit	
Durchschallung_EB_000487	2013-10-29 02:18	
Durchschallung_EB_000488	2013-10-30 02:18	
Durchschallung_EB_000489	2013-10-31 02:18	
Durchschallung_EB_000490	2013-11-01 02:18	
Durchschallung_EB_000491	2013-11-02 02:18	
Durchschallung_EB_000492	2013-11-03 02:18	
Durchschallung_EB_000493	2013-11-04 02:18	
Durchschallung_EB_000494	2013-11-05 02:18	

* : dismanteling Phase, Fehler durch Bauarbeiten
0 : System not running
1 : Sensor cables cutted
2 : Test measurement
3 :
4 : error / bad data

0.4 Definitionen + Referenzen

Nomenklatur
Alternative Bezeichnungen für Empfänger : Receiver
Alternative Bezeichnungen für Sender : Transmitter, Emitter
Bezeichnungen sowohl für Sender als auch Empfänger : Sensor, Sonde, Transducer

Zeitlicher Nullpunkt bei Durchschallungsmessungen
Bei der HE-E Seismic wurden dazu Überlegungen angestellt, die übertragbar sein sollten, da beide Messanlagen weitgehend gleich aufgebaut sind. Betrachtet wird der mittels eines Teilers aufgezeichnete Spannungsverlauf am jeweiligen Sender.
Definition: 'Zeitlicher Nullpunkt = Sample nach dem Maximum'
Dieses Nullpunkt-Sample hat eine Amplitude von 99% der Maximalamplitude. Das folgende Sample hat eine Amplitude von ca. 50%, was eindeutig besser wiederzufinden ist, und das danach folgende Sample hat eine Amplitude von ca. 10% (Bild xxx).
Begründung: Die Aufzeichnung erfolgt mit einem unkompensiertem Spannungsteiler, d. h. die Kapazität des Verbindungskabels zum A/D-Wandler und die Widerstände des Teilers bilden einen Tiefpassfilter. Damit wird der der Teilungsfaktor leicht frequenzabhänggig, und die Flankensteilheit (die maximal mögliche zeitliche Änderung des Signalverlaufs) wird reduziert. Nimmt die so aufgezeichnete Spannung am Sender auch nur leicht ab, hat der Abfall schon längst begonnen.
Unabhängig davon gibt es eine Eigenschatft der A/D-Wandlerkarte: Die Anzahl Samples im Pretrigger-Bereich ist immer durch vier teilbar (der Speicher wird so ausgelesen, dass der Triggerzeitpunkt auf einem vierer Raster liegt [4, 8, 12, ...]).
In Zahlen bedeuet das für die bisher aufgenommenen seismischen Messungen:
5% Pretrigger, 8192 Samples : Zero-Sample = 412 (HE-E)
20% Pretrigger, 16384 Samples : Zero-Sample = 3280 (HE-E Stadard)
25% Pretrigger, 16384 Samples : Zero-Sample = 4096 (EB, HE-E)

Bei der EB Seismic ist der Spannungs-Verlauf um einen Sample-Index verschoben!
Das Sample mit 99% der Maximalamplitude liegt hat den Index '4097', anstatt '4096'.

Die Ursache dafür ist bisher unbekannt. Die bei HE-E- und EB-Seismic eingesetzten Spannungsteiler unterscheiden sich in der Dimensionierung (EB: 1:1000, 8 MΩ | HE-E: 1:100, 500 kΩ). Der Teiler bei EB hat eine höhere Impedanz , was bei gleicher Kabellänge bzw. Kapazität eine größere Zeitkonstante zur Folge hat.

(Bild xxx)

Referenzen

(Manthei 2001)
Titel: 'Durchführung von Durchschallungs- und mikroakustischen Messungen zur Überwachung eines Langzeitversuchs im Felslabor Mont Terri (Schweiz) - Installation der Sonden und Durchführung von Testmessungen'
Author: G. Manthei
Bericht-Nummer 101373.1 (Oktober 2001)
(Manthei 2003)
Titel: 'Durchführung von Durchschallungs- und mikroakustischen Messungen zur Überwachung eines Langzeitversuchs im Felslabor Mont Terri (Schweiz) - Abschlussbericht'
Author: G. Manthei
Bericht-Nummer 101373.2 (Juni 2003)

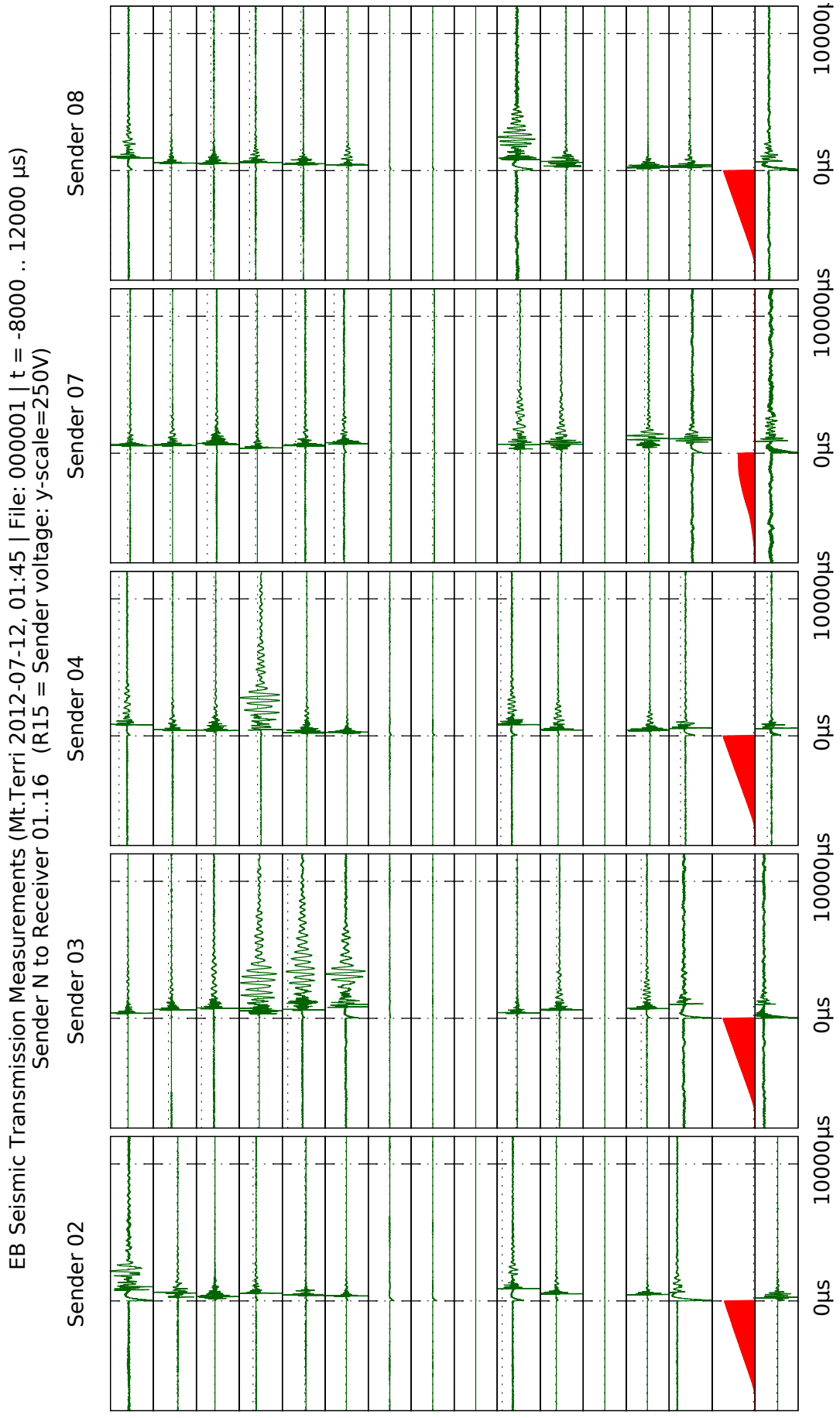

Abbildung 1: Durchschallungsstrecken incl. Sendesignal (rot), t=20ms

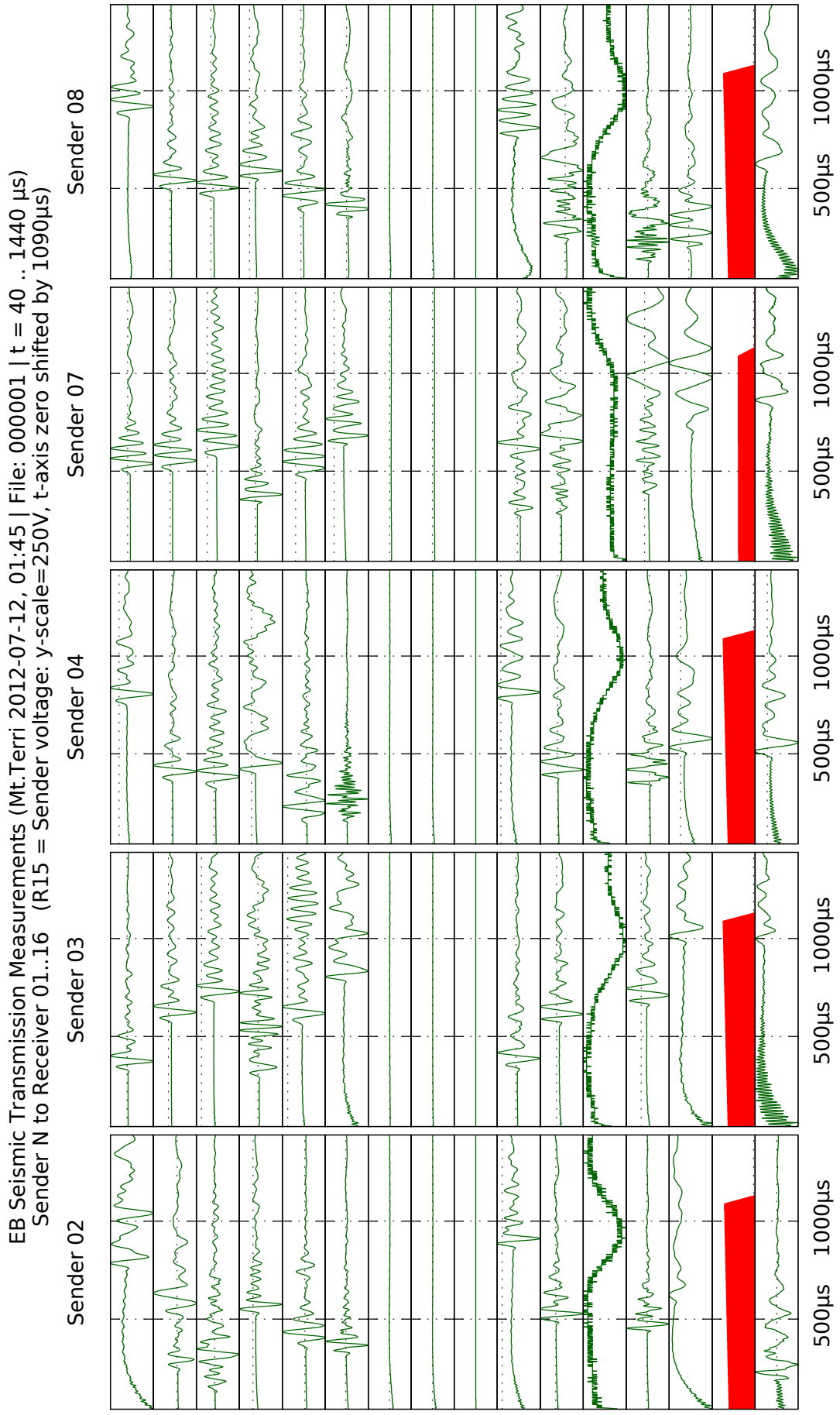

Abbildung 2: Durchschallungsstrecken incl. Sendesignal (rot), t=1.4ms

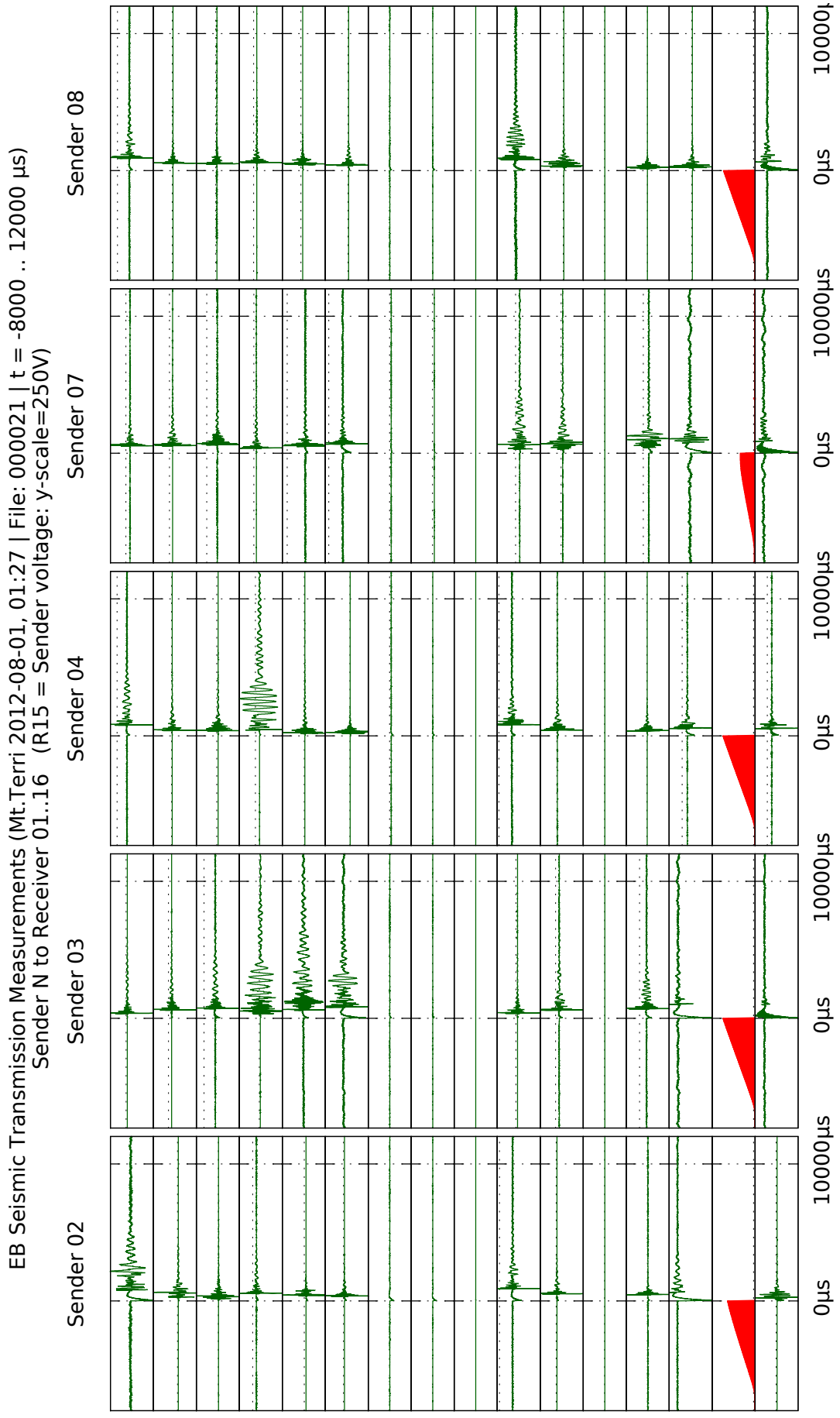

Abbildung 3: Durchschallungsstrecken incl. Sendesignal (rot), t=20ms

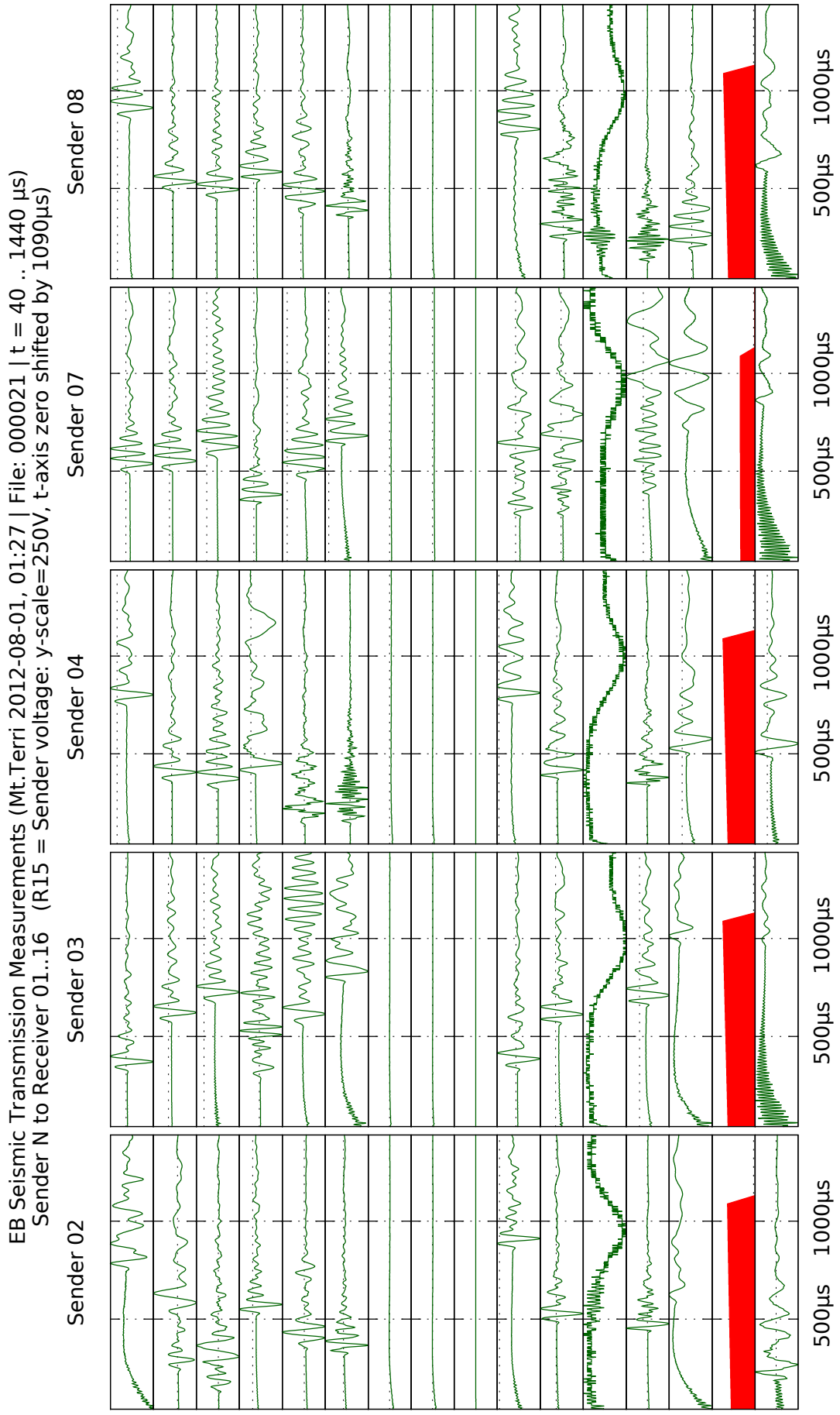

Abbildung 4: Durchschallungsstrecken incl. Sendesignal (rot), t=1.4ms

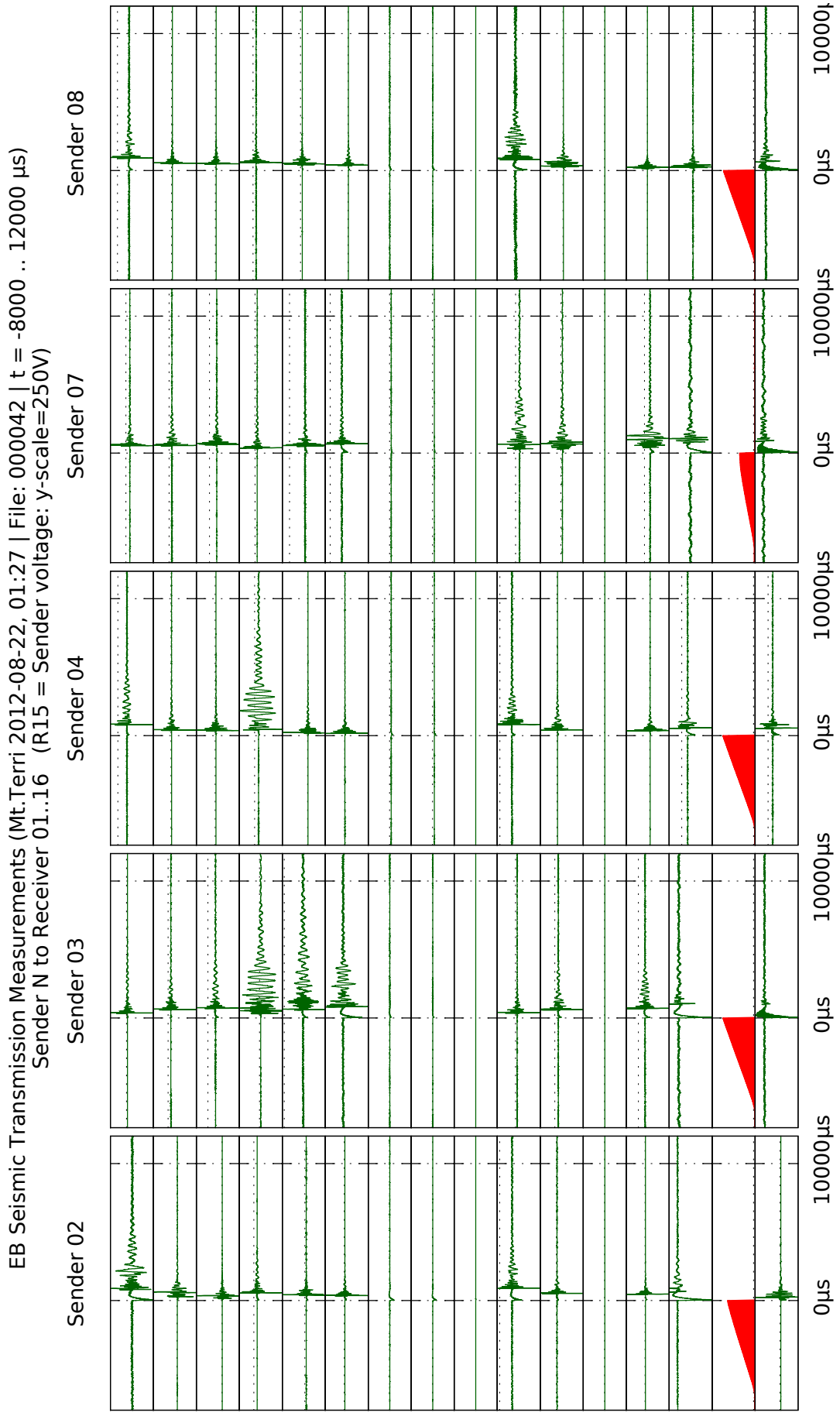

Abbildung 5: Durchschallungsstrecken incl. Sendesignal (rot), t=20ms

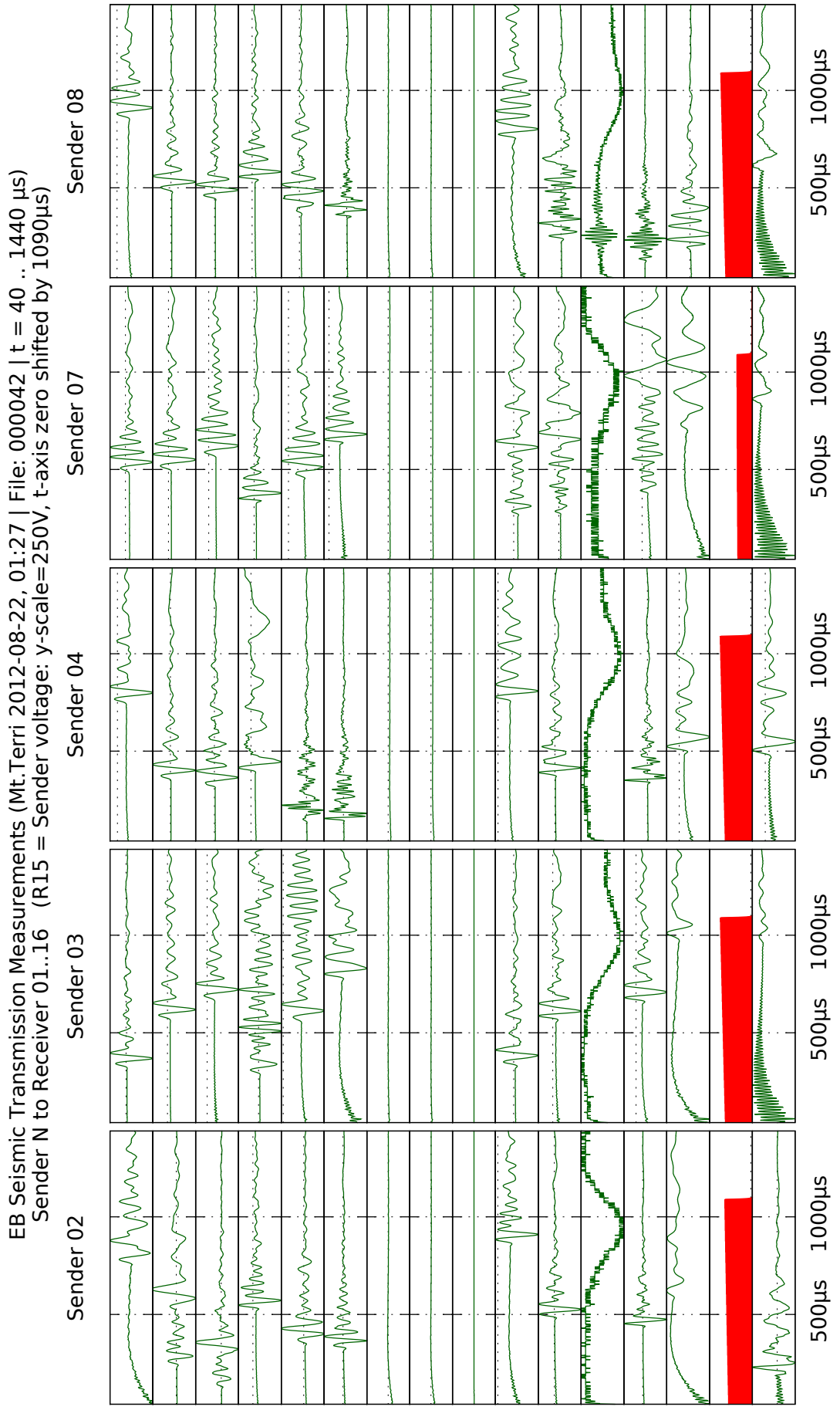

Abbildung 6: Durchschallungsstrecken incl. Sendesignal (rot), t=1.4ms